



Technische Universität München
TUM School of Engineering and Design

Enabling a Scalable Wet Coating Process for the Production of Sulfide-Based All-Solid-State Batteries

Célestine Singer

Vollständiger Abdruck der von der TUM School of Engineering and Design der Technischen
Universität München zur Erlangung einer

Doktorin der Ingenieurwissenschaften (Dr.-Ing.)

genehmigten Dissertation.

Vorsitz: Prof. Dr.-Ing. Markus Lienkamp

Prüfende der Dissertation:

1. Prof. Dr.-Ing. Rüdiger Daub
2. Prof. Dr. Jürgen Janek
3. Prof. Dr.-Ing. Arno Kwade

Die Dissertation wurde am 04.06.2024 bei der Technischen Universität München eingereicht
und durch die TUM School of Engineering and Design am 03.02.2025 angenommen.

Editor's Preface

In times of global challenges, such as climate change, the transformation of mobility, and an ongoing demographic change, production engineering is crucial for the sustainable advancement of our industrial society. The impact of manufacturing companies on the environment and society is highly dependent on the equipment and resources employed, the production processes applied, and the established manufacturing organization. The company's full potential for corporate success can only be taken advantage of by optimizing the interaction between humans, operational structures, and technologies. The greatest attention must be paid to becoming as resource-saving, efficient, and resilient as possible to operate flexibly in the volatile production environment.

Remaining competitive while balancing the varying and often conflicting priorities of sustainability, complexity, cost, time, and quality requires constant thought, adaptation, and the development of new manufacturing structures. Thus, there is an essential need to reduce the complexity of products, manufacturing processes, and systems. Yet, at the same time, it is also vital to gain a better understanding and command of these aspects.

The research activities at the Institute for Machine Tools and Industrial Management (*iwb*) aim to continuously improve product development and manufacturing planning systems, manufacturing processes, and production facilities. A company's organizational, manufacturing, and work structures, as well as the underlying systems for order processing, are developed under strict consideration of employee-related requirements and sustainability issues. However, the use of computer-aided and artificial intelligence-based methods and the necessary increasing degree of automation must not lead to inflexible and rigid work organization structures. Thus, questions concerning the optimal integration of ecological and social aspects in all planning and development processes are of utmost importance.

The volumes published in this book series reflect and report the results from the research conducted at *iwb*. Research areas covered span from the design and development of manufacturing systems to the application of technologies in manufacturing and assembly. The management and operation of manufacturing systems, quality assurance, availability, and autonomy are overarching topics affecting all areas of our research. In this series, the latest results and insights from our application-oriented research are published, and it is intended to improve knowledge transfer between academia and a wide industrial sector.

Rüdiger Daub

Gunther Reinhart

Michael Zäh

Preface

The process of writing this dissertation has been both intellectually engaging and personally meaningful. My interest in all-solid-state batteries developed during my studies at the Technical University of Munich, where I became increasingly drawn to the production technology aspects of batteries. This dissertation is the result of years of research, analysis, and dedication, and I appreciate the opportunity to contribute to this field. Throughout this process, I have encountered numerous challenges, from conceptual hurdles to practical setbacks. However, each obstacle has provided valuable lessons and has deepened my understanding of the subject matter. The support and encouragement of many individuals have made this journey possible, and I would like to take this opportunity to express my sincere gratitude.

First and foremost, I extend my deepest appreciation to my supervisor, Prof. Dr.-Ing. Rüdiger Daub, for his unwavering guidance, insightful feedback, and constant encouragement. His expertise and patience have been instrumental in shaping this dissertation. Further, I would like to thank Prof. Dr.-Ing. Gunther Reinhart and Prof. Dr.-Ing. Michael Zäh for their support and tireless commitment to create a great atmosphere and scientific framework at *iwb* also for future generations. Additionally, I would like to thank Prof. Dr. Jürgen Janek and Prof. Dr.-Ing. Arno Kwade for acting as co-advisors to this dissertation and Prof. Dr.-Ing. Markus Lienkamp for taking the chair of my thesis defense.

I am also grateful to my colleagues and peers at *iwb*, whose stimulating discussions and constructive criticism have greatly enriched my work. I want to acknowledge especially Sandro Stock, Lucas Hille and Lovis Wach for being great discussion partners, reviewers and friends. A significant contribution to this dissertation came also from the many hours of dedicated work by students, either through their theses or as research assistants, whom I had the privilege of supervising.

I would like to thank my family and friends for their unwavering support, patience, and understanding throughout this demanding endeavor. Their belief in me has been a source of strength and motivation.

Finally, this dissertation would not have been possible without the resources and support provided by TUMint. Energy Research GmbH. This company and research cluster has been invaluable in supporting and improving my research. A special thank you goes to Fabian Schatz.

While this work represents a significant milestone, I recognize that research is an ongoing process. I hope that this dissertation will serve as a foundation for further exploration and inspire future contributions to the field of all-solid-state batteries.

Table of Contents

List of Abbreviations.....	III
List of Symbols	IX
1 Introduction	1
1.1 Motivation and Thematic Scope.....	1
1.2 Objective and Framework	2
1.3 Scientific Approach	3
1.3.1 Subgoals.....	3
1.3.2 Research Methodology and Structure of the Work	4
2 Fundamentals.....	5
2.1 Functional Principle of All-Solid-State Batteries.....	5
2.2 Materials and Cell Formats of All-Solid-State Batteries.....	8
2.2.1 Cathode Materials.....	8
2.2.2 Anode Materials	9
2.2.3 Solid Electrolyte Materials	11
2.2.4 Cell Formats	14
2.2.5 Potential and Challenges	16
2.3 Electrode Production Process and Characteristics of Lithium-Ion Batteries	17
2.3.1 Mixing	18
2.3.2 Wet Coating.....	21
2.3.3 Drying.....	23
3 State of the Art.....	28
3.1 Laboratory-Scale Fabrication of Sulfide-Based All-Solid-State Batteries.....	28
3.2 Concepts for Process Chains in the All-Solid-State Battery Production.....	33
3.3 Electrode Production of Conventional Lithium-Ion Batteries.....	34
3.3.1 Wet Coating Process.....	35
3.3.2 Drying Process.....	35
3.3.3 Adhesion Measurements.....	37

3.4	Derivation of Need for Action and Objective	40
4	Results.....	43
4.1	Research Approach and Assignment of the Publications.....	43
4.2	Cumulative Overview of the Related Publications	45
4.2.1	Publication I: Scalable Processing Routes for the Production of All-Solid-State Batteries—Modeling Interdependencies of Product and Process.....	45
4.2.2	Publication II: Plant Technology for the Industrial Coating Process for Sulfide-Based All-Solid-State Batteries	47
4.2.3	Publication III: Hydrolysis of Argyrodite Sulfide-Based Separator Sheets for Industrial All-Solid-State Battery Production	48
4.2.4	Publication IV: Influence of the Slurry Composition on Thin-Film Components for the Wet Coating Process of Sulfide-Based All-Solid-State Batteries.....	50
4.2.5	Publication V: Fundamental Investigation on Drying Rates of Cathodes and Separators for Sulfide-Based All-Solid-State Batteries.....	52
4.2.6	Publication VI: Drying Process of Sulfide-Based All-Solid-State Battery Components—Investigation on Adhesion Strength and Microstructural Changes.....	53
4.2.7	Publication VII: Insights Into Scalable Technologies and Process Chains for Sulfide-Based Solid-State Battery Production	55
4.3	Qualification of the Roll-To-Roll Coating Machinery	56
4.3.1	Production Concept	56
4.3.2	Machine Design.....	58
4.3.3	Initial Parameter Set for Pilot-Scale Experiments.....	59
5	Discussion of Results	61
5.1	Contribution to the Industrialization of Sulfide-Based All-Solid-State Batteries	61
5.2	Transferability of Results and Critical Reflection.....	63
6	Summary and Outlook.....	65
6.1	Summary.....	65
6.2	Outlook.....	66
7	Bibliography.....	69
8	Appendix.....	85
A.	Publication List.....	85
B.	Overview of Supervised Student Theses	86

List of Abbreviations

ALD	Atomic layer deposition
Al	Aluminum
ASR	Area-specific resistance
ASSB	All-solid-state battery
C	Carbon
CAM	Cathode active material
CDA	Compressed dry air
Cl	Chlorine
ClO ₄	Perchlorate
CMC	Carboxymethyl cellulose
Co	Cobalt
CRP	Constant rate period
CVD	Chemical vapor deposition
DOR	Degree of removal
DPO	Dried powder on surface method
DRM	Design research methodology
e ⁻	Electron
EC	Ethylene carbonate
EDS	Energy dispersive X-ray analysis
EIS	Electrochemical impedance spectroscopy
F	Fluorine

Fe	Iron
FRP	Falling rate period
H ₂ S	Hydrogen sulfide
HDR	High drying rate
HE-NMC	High-energy nickel manganese oxide ($x\text{Li}_2\text{MnO}_3(1-x)\text{LiMO}_2$ (M = Ni, Co, Mn))
HNBR	Hydrogenated nitrile butadiene rubber
<i>iwb</i>	Institut für Werkzeugmaschinen und Betriebswissenschaften (engl.: Institute for Machine Tools and Industrial Management)
LATP	Lithium aluminum titanium phosphate ($\text{Li}_{1.3}\text{Al}_{0.3}\text{Ti}_{1.7}(\text{PO}_4)_3$)
LCO	Lithium cobalt dioxide (LiCoO_2)
LDR	Low drying rate
LFP	Lithium iron phosphate (LiFePO_4)
LGPS	Lithium germanium phosphorus sulfide
Li	Lithium
Li ⁺	Lithium-ion
Li ₂ S	Lithium sulfide
Li ₂ ZrO ₃	Lithium zirconiate
LIB	Lithium-ion battery
LiM	Lithium metal
LiMeO _x	Lithium metal oxide
LiNbO ₃	Lithium niobate
LiPAA	Lithium polyacrylate
LISICON	Lithium superionic conductor
LLTO	Lithium lanthanum titanium oxide ($\text{Li}_{0.34(1)}\text{La}_{0.51(1)}\text{TiO}_{2.94(2)}$)
LLZO	Lithium lanthanum zirconium oxide ($\text{Li}_7\text{La}_3\text{Zr}_2\text{O}_{12}$)

LMO	Lithium manganese spinel (LiMn_2O_4)
LNMO	High-voltage spinel ($\text{LiNi}_{0.5}\text{Mn}_{1.5}\text{O}_4$)
LNO	Lithium nickel oxide
LPS	Lithium phosphorus sulfide (Li_3PS_4)
LPSCI	Lithium phosphorus sulfide chlorine ($\text{Li}_6\text{PS}_5\text{Cl}$)
LTO	Lithium titanium oxide
MeO_x	Metal oxide
Mn	Manganese
N	Nitrogen
Nb	Niob
NBR	Acrylonitrile butadiene rubber
NCA	Nickel cobalt aluminum oxide ($\text{LiNi}_{0.8}\text{Co}_{0.15}\text{Al}_{0.05}\text{O}_2$)
Ni	Nickel
NiS	Nickel sulfide
NMC111	Nickel manganese oxide ($\text{LiNi}_{0.33}\text{Co}_{0.33}\text{Mn}_{0.33}\text{O}_2$)
NMC622	Nickel manganese oxide ($\text{LiNi}_{0.6}\text{Co}_{0.2}\text{Mn}_{0.2}\text{O}_2$)
NMC811	Nickel manganese oxide ($\text{LiNi}_{0.8}\text{Co}_{0.1}\text{Mn}_{0.1}\text{O}_2$)
NMP	N-methyl-2-pyrrolidone
$\text{N}(\text{SO}_2\text{CF}_3)_2$	Bistriflimide
O_2	Oxide
PAN	Poly(acrylonitrile)
PC	Propylene carbonate
PEC	Poly(ethylene carbonate)
PEO	Polyethylene oxide

PEP-MNB	Poly(ethylene-co-propylene-co-5-methylene-2-norbornene)
PEVA	Poly(ethylene vinyl acetate)
PF ₆	Hexafluorophosphate
PIB	Polyisobutylene
PLD	Pulsed laser deposition
PMMA	Poly(methyl methacrylate)
P	Phosphorus
PPC	Poly(propylene carbonate)
PVC	Polyvinyl chloride
PVD	Physical vapor deposition
PVDF	Polyvinylidene fluoride
S	Sulfide
SBR	Styrene butadiene rubber
SBS	Styrene butadiene styrene copolymer
SE	Solid electrolyte
SEBS	Styrene ethylene butylene styrene copolymer
SEI	Solid electrolyte interface
SEM	Scanning electron microscope
Si	Silicon
SiO ₂	Silicon dioxide
SOFC	Solid oxide fuel cells
SPACE ²	Sulfidic Cell Production Advancement Center
SPS	Spark plasma sintering
STEL	Short-term exposure limit

SysML	Systems modeling language
Ta	Tantalum
Te	Tellurium
THF	Tetrahydrofuran
TiS ₂	Titanium disulfide
TRL	Technology readiness level
TWA	Time-weighted average
Zr	Zirconia

List of Symbols

Greek symbols	Unit	Description
a_G	$\text{m}^2 \text{s}^{-1}$	Thermal diffusivity of the atmospheric gas
a_s	-	Activity of the solvent
$\alpha_{S,G}$	$\text{W m}^{-2}\text{K}^{-1}$	Heat transfer coefficient
$\beta_{S,G}$	m s^{-1}	Mass transfer coefficient between dispersion and environment
δ	m	Film thickness
γ	-	Shear
$\dot{\gamma}$	s^{-1}	Shear rate
$\dot{\gamma}_c$	s^{-1}	Coating shear rate
$\dot{\gamma}_w$	s^{-1}	Wall shear rate
γ_1	N m^{-1}	Surface energy of material 1
γ_{12}	N m^{-1}	Interfacial energy between phases 1 and 2
γ_2	N m^{-1}	Surface energy of material 2
$\tilde{\gamma}_{S,\infty}$	-	Molar distribution of the solvent in the drying environment
$\tilde{\gamma}_{S,Ph}$	-	Molar distribution of the solvent at the surface of the dispersion to the surrounding gas
η	Pa s	Shear viscosity
θ	°	Equilibrium contact angle at the three-phase contact point
λ_G	W K^{-1}	Thermal conductivity of the gas
μ	Pa s	Viscosity of the binder solution
π	-	Pi (value of 3.1415926)
$\tilde{\rho}_G$	mol m^{-3}	Molar density of the atmospheric gas
ρ_G	kg l^{-1}	Density of the atmospheric gas
ρ_P	kg m^{-3}	Density of the particle

LIST OF SYMBOLS

ρ_S	kg l ⁻¹	Density of the solvent
σ	Pa	Shear stress
σ_f	Pa	Fracture stress
σ_{ST}	N m ⁻¹	Surface tension
ψ	-	Plastic and viscoelastic deformations
ψ_i	-	Molar fraction of component <i>i</i>
Latin symbols	Unit	Description
<i>A</i>	m ²	Surface area
<i>b</i>	m	Slot width
<i>Ca</i>	-	Capillary number
<i>c_{p,G}</i>	J K ⁻¹	Heat capacity of the gas
<i>D</i>	m ² s ⁻¹	Diffusion coefficient of the solvent in the gas atmosphere
<i>E</i>	MPa	Effective modulus of elasticity
<i>E_R</i>	m s ⁻¹	Evaporation rate
<i>F</i>	N	Force
<i>F_A</i>	N	Adhesion force
<i>G</i>	N m ⁻¹	Fracture energy
<i>G_w</i>	m	Gap width
<i>G_w[*]</i>	-	Dimensionless gap width
<i>g</i>	m s ⁻²	Gravitational acceleration (value of 9.81 m s ⁻²)
<i>G₀</i>	N m ⁻¹	Substitute term for adhesive work (<i>W_A</i>) and cohesive work (<i>W_C</i>)
<i>H</i>	m	Wet film thickness
<i>h</i>	m	Height of liquid film layers
<i>h_{cg}</i>	m	Height of coating gap
<i>h_s</i>	m	Slot length

k	J K^{-1}	Boltzmann constant (value of $1.380658 \times 10^{-23} \text{ J K}^{-1}$)
k_{crit}	$\text{MPa } \sqrt{\text{m}}$	Material-dependent critical stress intensity factor
l	m	Length of the critical crack leading to fracture
Le	-	Lewis number
M_i	kg mol^{-1}	Molar masses of component i
m_i	kg	Mass of the component i
\tilde{M}_S	kg mol^{-1}	Molar mass of the solvent
\dot{m}_s	kg s^{-1}	Mass flow rate
n	-	Total number of moles
n_i	kg	Amount of substance of the component i
N_S	-	Sedimentation number
p_a	Pa	Ambient pressure
Pe	-	Peclet number
p_G	Pa	Pressure of the atmospheric gas
$p_v(T_{\text{Dis}})$	Pa	Vapor pressure of the solvent at the temperature of the dispersion
Q	$\text{m}^3 \text{ s}^{-1}$	Volumetric flow rate
R	m	Particle radius
R_m	$\text{J mol}^{-1} \text{ K}^{-1}$	Universal gas constant (value of $8.134 \text{ J mol}^{-1} \text{ K}^{-1}$)
T_D	$^{\circ} \text{C}$	Drying temperature
T_G	$^{\circ} \text{C}$	Temperature of the atmospheric gas
U	m s^{-1}	Roll speed
U_0	$\text{m}^2 \text{ s}^{-1}$	Stokes' sedimentation rate
v	m s^{-1}	Coating speed
W_A	N m^{-1}	Adhesive work
W_C	N m^{-1}	Cohesive work
x	m	Displacement of layers in liquid films

1 Introduction

The energy transition has emerged as a global challenge driven by the urgent need to address climate change and lessen reliance on fossil fuels. To take the role of a pioneer in sustainable energy policies, Germany has set ambitious targets to transition towards a low-carbon economy (UMWELTBUNDESAMT 2023). Central to this transformation is the intensified share of renewable energy sources in the national grid and the electrification of the mobility sector. The enhanced dedication to electromobility is mainly driven by technological progress, leading to significant changes in the transport systems and the power unit of vehicles. At present, the lasting implications are seen in the automotive sector. As part of this, the electrification of the global automotive market is advancing, and estimates predict a massive increase in the required amount of electrical energy storage over the next decade. (STAMPATORI ET AL. 2020)

In this context, lithium-ion batteries (LIBs) have emerged as a game-changing technology, providing a versatile and scalable means of energy storage. (BMWK 2023) The LIB is currently the most common type of energy storage with a highly increasing demand for electric vehicles. Therefore, Europe's LIB production capacity is estimated to grow from 124 gigawatt hours to 1.5 terawatt hours between 2022 and 2030, with the highest share in Germany (WEYMANN & LEIDERBERGER 2022). This technology's market growth affects industries worldwide, leading to new opportunities and challenges for the future development of the automotive branch.

1.1 Motivation and Thematic Scope

Significant effort has been devoted to state-of-the-art LIBs to electrify the transportation sector worldwide and attain customer acceptance of electrically driven vehicles. The LIB technology has made significant progress in the last decade, aiming at higher energy and power density as well as lower costs. (GAO ET AL. 2018) However, LIBs are restricted in performance due to the applied electrode materials and the cell design. Additionally, the liquid electrolyte used to obtain ionic conductivity in LIBs is flammable, causing serious safety concerns. (CHEN ET AL. 2018a). For these reasons, innovative battery technologies are being examined to overcome performance limitations and increase safety in future applications. (JANEK & ZEIER 2016)

Amongst those, the all-solid-state battery (ASSB) attracted much attention as the technology offers high energy densities, long-term stability, and a non-flammable solid electrolyte (SE) (FAN ET AL. 2018). Furthermore, applying metal anodes, e.g., pure lithium metal (LiM), to enhance energy and power density is feasible using a dense and mechanically stable SE (WANG ET AL. 2018). This technology has significantly succeeded due to years of material research. However, the production of ASSBs is currently limited to the laboratory scale, impeding entry into an industrial mass market. (BIRKE ET AL. 2022) Three main material classes are investigated as suitable SEs: polymers, oxides, and sulfides. The latter fulfills the most crucial

property: a high ionic conductivity and sufficient mechanical stability for good processability. (JANEK & ZEIER 2016) Therefore, sulfide-based ASSBs are researched by numerous groups and startups. However, the market entry of sulfide-based ASSBs is still prevented due to limited knowledge about electrochemical aspects and missing experience in the industrial production processes of ASSB cells. (TAN ET AL. 2022)

Laboratory research suggests that applying conventional production processes for LIBs is feasible for sulfide-based ASSBs. Hence, the process steps of mixing, wet coating, drying, densifying, and the cell assembly would remain the same. However, the usage of similar process technologies, e.g., doctor blade coating, and the transferability of process parameters remains to be proven. (SCHNELL ET AL. 2018) To avoid the need for entirely new machinery or Gigafactories for ASSB production, a focus should be on the qualification of available technologies to the requirements of novel sulfide-based materials. In addition to electrochemical challenges and material concerns regarding hydrogen sulfide (H₂S) formation, the main task is to gain knowledge about processability (TAN ET AL. 2022). Establishing ASSBs and realizing their potential is only achieved by upscaling to an industrial level. Using existing production capacities could accelerate the path to mass production. The goal of future ASSB research is to focus on the development of upscaled production processes and the identification of suitable parameter sets to enable high-throughput technologies.

1.2 Objective and Framework

Sulfide-based ASSBs contain new materials throughout every cell component, along with unknown requirements and challenges for production processes. Even if technologies used in LIB production can be applied, many challenges are associated with using sulfide-based materials, thus requiring a combined product-process study design. Therefore, this thesis aims to develop a holistic approach to planning, concepting, analyzing, and validating the production of sulfide-based composite cathodes as well as SEs based on theoretical and empirical studies.

Throughout the production process of LIBs, the first steps are decisive for the properties of electrodes. Therein, the mixing, coating, and drying processes are responsible for defect-free coating with high performance. As up to date, limited knowledge is available on the processing of ASSBs, these three process steps will be the focus of the present dissertation. The input material for the wet coating process is the slurry, a dispersion of powders, additives, and solvents, which is fabricated in the preliminary mixing step. Therefore, the boundaries of this work are set to include the characterization and optimization of the slurry to align required input parameters for the coating process but exclude further investigations on the mixing procedure. The frame of this thesis is set to the end of the drying process, which has a dry film with substrate as the outcome product. Figure 1-1 shows the scope of this dissertation with a focus on wet coating and drying, including the intermediate products slurry, wet, and dry film. The overall goal is to enable a scalable wet coating process for the production of sulfide-based ASSBs.

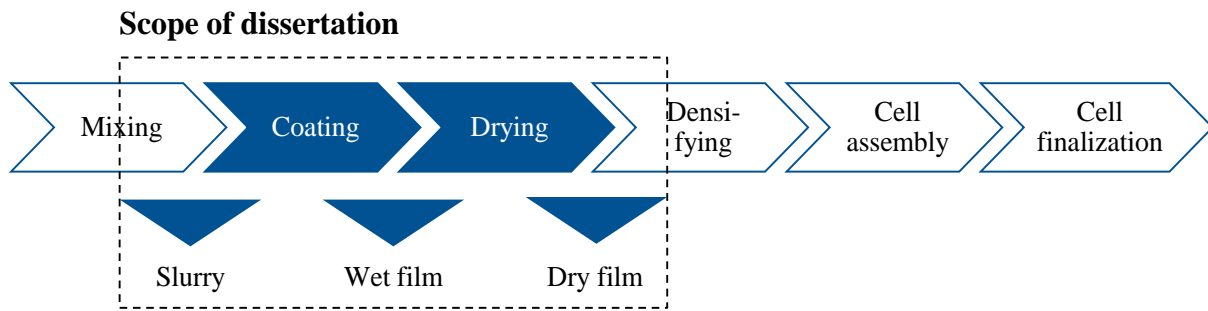


Figure 1-1: Scope of this dissertation along with the relevant processes in battery cell production.

The transfer of knowledge from the laboratory to the pilot scale and the initiation of the pilot-scale machinery is the goal of this thesis. Therefore, it aims to bridge the gap between technology readiness levels (TRL) three (coin cells), four (small prototype), and five (large prototype) (FRITH ET AL. 2023) to pave the way for pilot-scale production. The initial stage involves evaluating different process strategies and technologies for material and cost suitability. In addition, the selected processes are planned by establishing a machine concept and characterizing methods for a roll-to-roll process. In the following, a detailed experimental study of the structure-product-process relationships is initiated to analyze the behavior of the sulfide-based slurries and films during processing. The results will enable the implementation of a new roll-to-roll coater at *iwb* and the derivation of initial slurry recipes and process parameters for the pilot machinery.

1.3 Scientific Approach

The scientific procedure is described, and the research methodology is explained in this section to present the structure of this work including four subgoals.

1.3.1 Subgoals

To follow the objective outlined in Section 1.2, this research thesis is guided by Subgoals 1–4 (cf. Table 1-1). The overall objective will only be obtained by combining and realizing all subgoals. The fundamentals (Chapter 2) and state of the art (Chapter 3) further develop the subgoals to build the frame for the publications in Chapter 4. In Section 4.1, a detailed explanation of the incorporation of the subgoals into the overall developed method and published papers is given.

Table 1-1: Description of the four subgoals within this dissertation.

Subgoal 1	Modeling of process strategies and development of characterization methods in the production of sulfide-based components
Subgoal 2	Identification of material-specific requirements for process technologies and plant engineering
Subgoal 3	Experimental identification of structure-product-process relationships
Subgoal 4	Qualification of the pilot-scale plant and derivation of the initial parameter sets

1.3.2 Research Methodology and Structure of the Work

The dissertation's structure is strongly connected with the design research methodology (DRM) (BLESSING & CHAKRABARTI 2009) pictured in Figure 1-2. Chapters 1 and 2 concentrate on the motivation and clarification of the objective to formulate a research goal and present fundamental knowledge from the literature on battery technologies and their processing steps, mixing, coating, and drying. In Chapter 3, the state of the art is presented by analyzing selected research publications on ASSB fabrication, approaches to the identification of process chains for ASSBs, and process analyses of the industrial wet coating and drying processes of LIBs. This chapter is the first descriptive study of a DRM (BLESSING & CHAKRABARTI 2009) to better understand the existing state of the art in literature. After deriving the need for action, the results of Publications I to VII are summarized, forming the prescriptive study. Since the publications contain descriptive elements with empirical data, both study types are presented in Chapter 4. Publication VII and Section 4.3 represent the validation by transferring knowledge from experimental data to develop a roll-to-roll machinery. This part of the dissertation and Chapter 5, in which results will be critically analyzed, form the descriptive study II (BLESSING & CHAKRABARTI 2009). The dissertation ends with a summary and outlook of this thesis in Chapter 6.

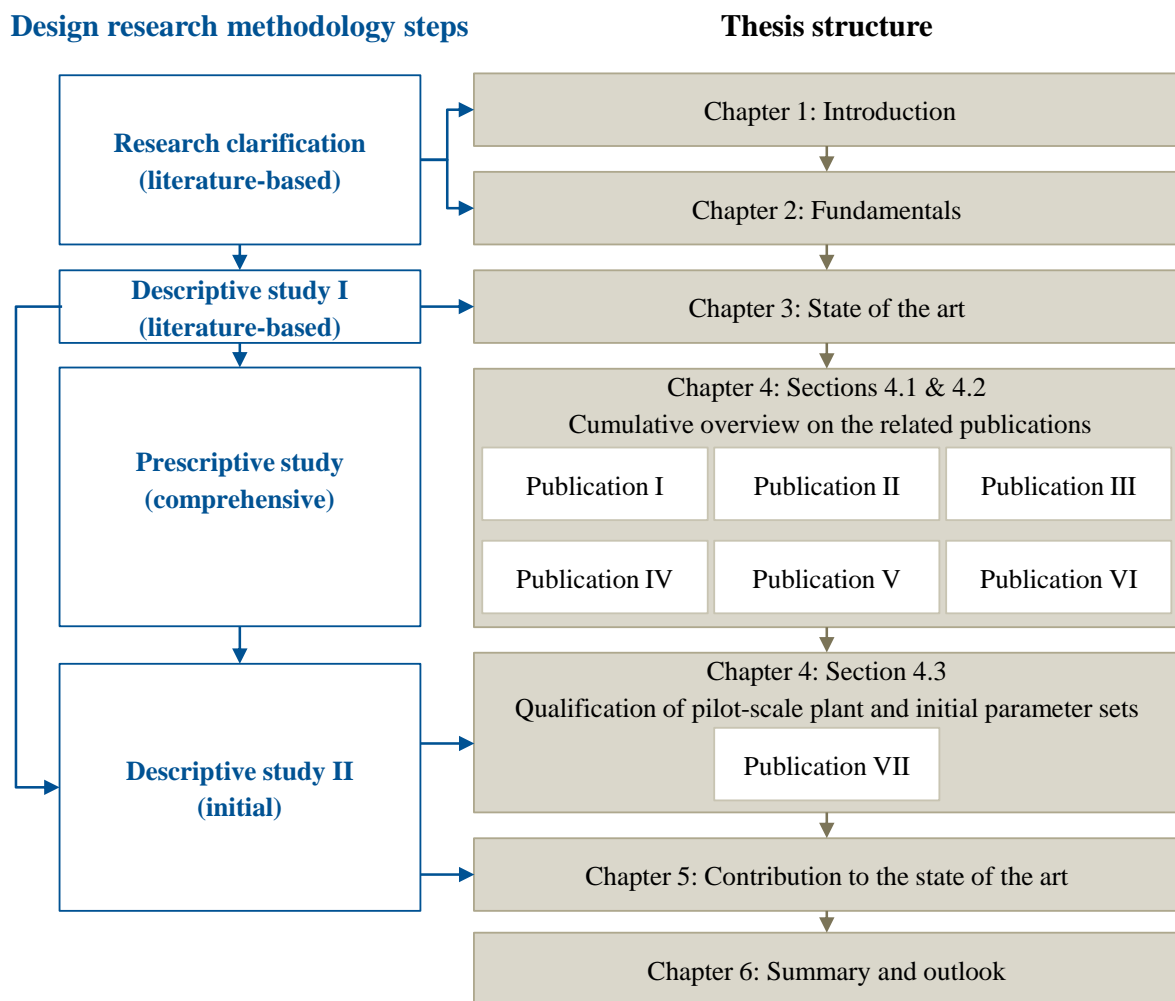


Figure 1-2: Design and research methodology, along with the structure of the thesis. According to BLESSING & CHAKRABARTI (2009).

2 Fundamentals

This chapter provides fundamental knowledge on ASSBs as well as the principles of processing and characterization methods for LIBs. Terminology is introduced to explain relevant concepts and clarify correlations between ASSB components. First, the functional principle and the composition of ASSBs are discussed (cf. Section 2.1). Besides cathode and anode materials, a strong focus is on SE materials and their properties (cf. Section 2.2). Relevant cell set-ups and research work correlated to this field are presented in Subsection 2.2.4, leading to the discussion of potentials and challenges (cf. Subsection 2.2.5). The following gives in-depth fundamentals of characteristic properties in the mixing, coating, and drying process of LIB electrodes. The chapters contain battery-specific aspects such as rheology, binder migration, and adhesion strength (Subsections 2.3.1, 2.3.2, 2.3.3).

2.1 Functional Principle of All-Solid-State Batteries

The electrochemical operation principle of an ASSB cell is very similar to that of a LIB cell. In both cases, it is a secondary (rechargeable) battery. Energy conversion from chemical to electrical energy occurs during discharge, and reverse energy conversion happens during charging. (KARABELLI & BIRKE 2022) An ASSB consists of two electrodes, a solid electrolyte (SE) separator, and current collectors. The cathode is applied onto a current collector (positive in case of discharge). Here, the cathode of the ASSB is a so-called composite cathode, as it contains SE material in addition to the typical cathode materials (active material, conductive carbon, and binder) (cf. Figure 2-1). The SE particles fill voids inside the cathode to create a consistent ionic conductivity throughout the cathode. The composite cathode is electrically isolated from the anode by an ion-conducting SE. Accordingly, the SE takes the role of the LIB liquid electrolyte and the separator, in which a charge exchange can occur between the anode and cathode. The solid separator is isolating to electrons and thus prevents a short circuit between the anode and cathode. (VARZI ET AL. 2016, p. 2) On the other side of the SE is the anode coated onto a second current collector (negative in case of discharge). In a bipolar design, only one single collector may be applied between a cathode and an anode, leading to a serial connection of single cells instead of a typical parallel connection. This cell design is discussed in Subsection 2.2.4.

The existence of ion transport in solids has been known for decades (RICKERT 1978). The first investigations of ion transport mechanisms in solids occurring at the atomic level can be traced back to Joffé, Frenkel, Schottky, and Wagner (FRENKEL 1926).

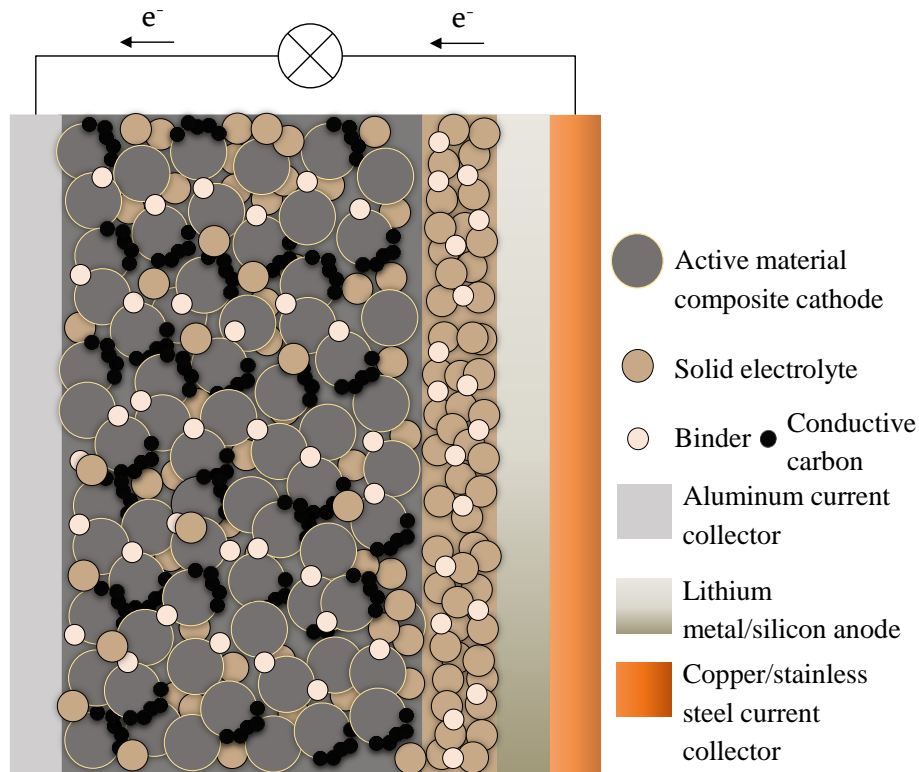


Figure 2-1: Schematic ASSB cell with aluminum current collector, composite cathode, SE, LiM or silicon anode, and a copper or stainless-steel current collector. External current flow is pictured for the discharge process.

In contrast to liquid electrolytes, the ion transport phenomenon within SEs appears to be notably more intricate. The modes of ion transport are described as either an interstitial or void mechanism. (GRUNDMANN 2016; KUMAR & YASHONATH 2006) Point defects within the solid state exhibit diverse manifestations. The Frenkel and Schottky defects are frequently discussed in the context of ionic conduction within SEs. Both defects encompass combinations of lattice imperfections that often arise (cf. Figure 2-2).

Schottky defects denote vacancies where the number of absent ions in the anionic lattice mirrors that in the cationic lattice. Ion conduction occurs within Schottky defects by exploiting these vacancies for ion migration between crystal structures. (GRUNDMANN 2016, pp. 81–88) In Frenkel defects, the underlying mechanism governing ion transport involves the diffusion of ions through the crystal lattice of a SE by occupying interstitial sites (GAO ET AL. 2018). Interstitial sites are spaces within the crystal lattice of a SE between the regular lattice ions. When an ion, i.e. a mobile cation or anion, enters the crystal lattice and positions itself in one of these interstitial sites, it is referred to as an interstitial ion. This ion is not a part of the regular lattice structure. The interstitial ion is not bound to a specific lattice position like the regular ones. It can move within the crystal lattice by hopping from one interstitial site to another. This movement is known as diffusion. The interstitial ions must overcome an energy barrier to move from one interstitial site to another. This barrier depends on the forces between the ion and the surrounding lattice ions. Higher temperatures typically provide the energy to surmount this barrier, facilitating ion mobility. The movement of interstitial ions within the crystal lattice contributes to ion conduction. (GRUNDMANN 2016)

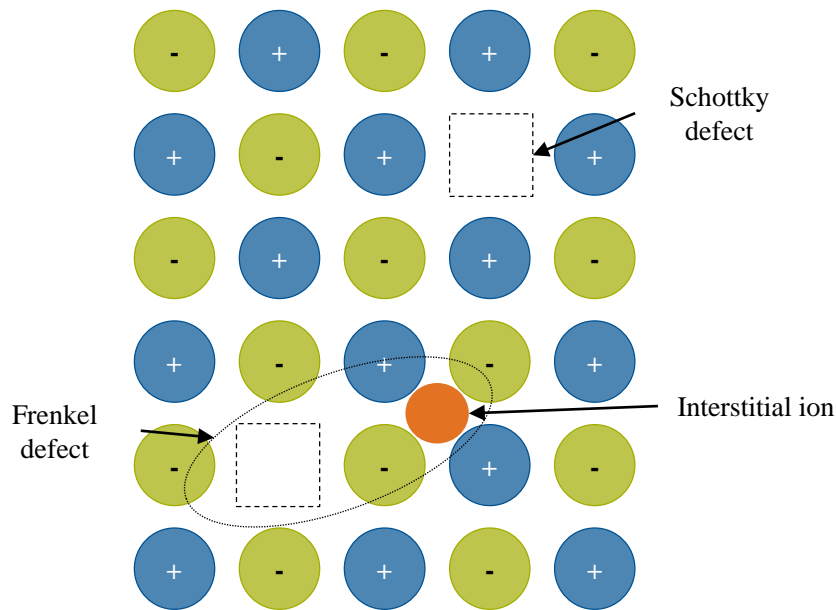


Figure 2-2: Schottky- und Frenkel-defect in a SE grid. Replicated from GAO ET AL. (2018).

When an external electric field is applied, these mobile ions can move in response to the field, contributing to the overall electrical conductivity of the SE. The electrons flow via the consumer when the battery cell is discharged and via the charging source when it is charged. When discharging the battery cell, the electrons e^- move from the negative electrode (anode) to the positive electrode (cathode), as shown in Figure 2-1. The positive current direction is traditionally opposite to the electron direction (DOPPELBAUER 2020, p. 135).

During charging and discharging, oxidation and reduction reactions occur in the electrodes, which are shown in Equations (1) to (2) for the case of a battery cell with a lithium-based anode and a metal oxide cathode (KORTHAUER 2019).

In the charged state, the active anode material (lithium Li in this case) is in a chemically reduced state. During discharge an oxidation reaction takes place and lithium-ions Li^+ are de-intercalated and electrons e^- are released (KORTHAUER 2019):



At the cathode, a reduction reaction takes place during discharge. The Li^+ are intercalated into the active material, e.g. a layered metal oxide MeO_x , and form a lithium metal oxide $LiMeO_x$:



Total reaction when discharging the battery cell is shown in Equation (3):



These reactions are reversed when charging the battery cell.

2.2 Materials and Cell Formats of All-Solid-State Batteries

As described above, electrochemical reactions in ASSBs differ from the conventional LIB due to the point contacts at the interfaces of the SE and electrode particles. Thus, the composition of the individual layers becomes the central factor for the electrochemical behavior (HWANG 2017, p. 7796). A deficient combination of cell materials plays an equally important role in the manufacturing processes and cycling performance of the cells. The most significant materials for every cell component are presented in the following.

2.2.1 Cathode Materials

A cathode in an ASSB is a composite of active material, SE, and additives, i.e., conductive carbon and binder. (KARABELLI & BIRKE 2022). The choice of active material for the cathode depends on several factors. On the one hand, a sufficient energy density must be achieved, claiming the suitability of cathode active materials with high capacities. On the other hand, the active material must be compatible with the SE, not only by shape and particle size distribution but also by electrochemical stability windows. (STRAUSS ET AL. 2018) Here, a trade-off between high ionic or electronic conductivities might be necessary (BIELEFELD ET AL. 2020).

In general, active materials, which are already known from LIB cathodes, are eligible. Hence, the distinction into layered oxides, spinels, and phosphates is applicable (GRAF 2018, pp. 29–41). Cathode materials for use in an ASSB mainly belong to the layered oxides group, except lithium iron phosphate LiFePO_4 (LFP). Olivine lattices, such as LFP, allow linear mobility of lithium-ions (Li^+). The advantages of olivine lattices include high safety, cycling stability, and low cost. The disadvantages of olivine grids are the low specific capacity and voltage. Layered structures are characterized by two-dimensional ion mobility and offer a high specific capacity. Representatives are lithium cobalt dioxide, LiCoO_2 (LCO), nickel manganese oxide, $\text{LiNi}_{0.33}\text{Co}_{0.33}\text{Mn}_{0.33}\text{O}_2$ (NMC), $\text{LiNi}_{0.8}\text{Co}_{0.15}\text{Al}_{0.05}\text{O}_2$ (NCA), or the high-voltage spinel $\text{LiNi}_{0.5}\text{Mn}_{1.5}\text{O}_4$ (LNMO). Most recently, high-energy NMC of the formula $x\text{Li}_2\text{MnO}_3(1-x)\text{LiMO}_2$ ($M = \text{Ni}, \text{Co}, \text{Mn}$) (HE-NMC) attracted attention as a cathode material for the automotive industry because it has high specific capacities (about 300 mAh g^{-1}). The disadvantage of layered structures is the cost compared to the other two structure types. Another structure type is spinel lattices, i.e., lithium manganese spinels and LiMn_2O_4 (LMO), characterized by high specific capacity and moderate costs. (KURZWEIL & DIETLMEIER 2018, pp. 189–204) ASSBs currently predominantly contain layered Ni-rich oxides of NMC-type (NMC111, NMC622, or NMC811). Moreover, LCO and LFP are represented in the literature. (RANDAU ET AL. 2020)

In contrast to LIBs, where the liquid electrolyte provides excellent ionic conductivity by filling the pores of the porous cathode and anode, in solids, the close contact of the particles is in focus (cf. Section 2.1). This contact should be realized at the interface between the electrolyte and electrode and inside the electrode (JANEK & ZEIER 2016, p. 3) to avoid a substantial increase in resistances and to guarantee high power densities (YU ET AL. 2017, p. 7). High resistances within the cell lead to decreased Li^+ transport properties (LUNTZ ET AL. 2015, p. 4600; VARZI ET AL. 2016, p. 17265). Moreover, stress at the interfaces can occur due to the volume changes

of the cathode during cycling, which results in loose contact of particles or separation of the interfaces (YAO ET AL. 2016, p. 9; GUO ET AL. 2023). Solutions to these cathode-related challenges are chemo-mechanical and include the reduction of particle sizes and a surface coating of active material with thin films (TATSUMISAGO ET AL. 2013, p. 22; SUN ET AL. 2017, p. 376). Typical materials for coatings are, e.g., Li_2ZrO_3 (STRAUSS ET AL. 2020) or LiNbO_3 (KIM ET AL. 2019a). Moreover, production-related aspects, such as the mixing of starting material with SE particles, the introduction of heat during production, and the targeted construction of an interfacial layer between cathode and electrolyte, are considered (LUNTZ ET AL. 2015, p. 4603; XU ET AL. 2018, p. 6014).

2.2.2 Anode Materials

In conventional LIBs, graphite with a specific capacity of 372 mAh g^{-1} is most commonly used as anode material. The material offers a layered structure that embeds the Li^+ and exhibits good properties, i.e., high capacity retention over many charge cycles (WURM ET AL. 2018). Another advantage is the ease of processing (KIM ET AL. 2015, p. 301). However, the use of graphite in ASSBs does not offer a decisive advantage for the volumetric energy density (JANEK & ZEIER 2016, p. 3) since the specific capacity is low and graphite would need to be mixed with SE particles (PLACKE ET AL. 2017, p. 1953). Furthermore, graphite offers little optimization possibilities regarding energy density since it has reached the theoretical limit of its properties (THIELMANN ET AL. 2017, p. 44).

Further materials have been investigated, but amongst them, pure LiM has the highest theoretical specific capacity of 3860 mAh g^{-1} , a low electrochemical potential of -3.040 V (vs. standard hydrogen electrode), and a low density of 0.53 g cm^{-3} at room temperature (KIM ET AL. 2021). These properties make LiM the optimal anode material in terms of energy density. LiM anodes were initially used for secondary batteries, but due to severe challenges, they are currently only applied in thin-film batteries (KRAUSKOPF ET AL. 2020, p. 7746). The difference with graphite is that Li^+ do not intercalate in the LiM anode. Instead, the Li^+ are deposited as metallic lithium (KRAUSKOPF ET AL. 2019, p. 7746; LEE ET AL. 2019, pp. 21–22).

For the usage of LiM anode in ASSBs, challenges regarding safety and cycling stability must be overcome (LIN ET AL. 2017, p. 194). These challenges include the formation of a solid electrolyte interface (SEI), the constant volume change of the battery during operation, and the growth of lithium dendrites. (WURM ET AL. 2018) Due to the low redox potential of LiM, a SEI forms at the LiM interface with any electrolyte. The advantage of a SEI is that it allows the cell to operate with the highly reducing LiM and increases the voltage window. The disadvantage of the SEI is its inhomogeneous distribution, which reduces ionic conductivity (LIN ET AL. 2017, pp. 194–195).

The volume change of the LiM anode is theoretically infinite since it has no host lattice. Practically, the thickness of the LiM anode changes by tens of micrometers depending on the initial amount of lithium. (LIN ET AL. 2017, p. 196) The interfacial contact between the LiM and the SE is constantly mechanically stressed by the volume change that can also cause the SEI to crack and expose fresh LiM, which reacts with the SE. As a result, the thickness of the SEI

increases. A thick SEI leads to a high charge transfer resistance and thus reduces cell operation efficiency. Fractures in the SEI also promote dendrite formation that poses a safety hazard. (VARZI ET AL. 2020, p. 2)

Lithium dendrites are pointed, branched deposits of the LiM anode that grow toward the cathode (KURZWEIL & DIETLMEIER 2018, p. 172). These local deposits accelerate lithium dendrite growth during the cell's initial cycling (LEE ET AL. 2019, p. 22). If they reach the cathode, they lead to a short circuit of the cell. Dendrites preferentially grow through defects at the surface of the SE, such as pores or vacancies between particles (LEE ET AL. 2019, p. 22). Strategies to prevent dendrite growth include the reduction of the current density, stabilizing the LiM anode surface by interlayers (TIKEKAR ET AL. 2016), and reducing the operating pressure (BANERJEE ET AL. 2020, p. 40). To prevent damage to the battery and ensure contact between the electrodes and electrolyte, a pressure device is used in ASSBs to apply variable or fixed pressure during the cell operation (DOUX ET AL. 2020b, p. 1).

Alternatives to pure LiM as the ASSB anode are lithium alloys or "anode-free" batteries (BONNICK & MULDOON 2022, p. 1848). In the latter, the SE is assembled directly onto the negative current collector. Li^+ are released from the intercalation cathode and deposited on the negative current collector during the charging process. This layer represents the anode in battery operation. During the discharge process, the Li^+ move back into the cathode. (KARABELLI & BIRKE 2021, p. 2) The advantage of this cell design is the reduction of costs and challenges associated with handling pure LiM in production (WANG ET AL. 2020, p. 7). WANG ET AL. (2020) demonstrated the function of anode-free cells with oxidic SE over fifty cycles. The film thickness of the anode formed in the charging process was approx. 20 μm . In ASSBs with LiM anode, YE & LI (2021) found that a very thin LiM anode leads to a higher cycling performance than an anode-free battery during the discharge process.

Besides LiM, silicon is emerging as a future anode material and has been used in several publications to build ASSBs (WANG ET AL. 2023). The material has a similar high capacity (3590 mAh g^{-1}) as pure lithium and a lithiation potential of 0.4 V (vs. Li^+/Li), leading to increased energy densities and a minor risk of lithium plating than other lithium alloys (FRANCO GONZALEZ ET AL. 2017). Thicknesses for the silicon anodes of about 6–8 μm are sufficient to provide a lithium reservoir for ASSB cells but depend on the cathode. They are achieved by either fabrication in a wet coating step known from conventional LIBs or a vapor deposition process. (HUO & JANEK 2022) However, silicon also poses significant production challenges, which still have to be overcome in the future. One major challenge is the silicon's immense expansion and shrinkage during charging and discharging (TAN ET AL. 2021). Moreover, the choice of binder in a wet coating step is crucial since the combination of binder-solvent solutions is currently limited to polar solvents, which induce side reactions with sulfide-based SEs (SHIN ET AL. 2022). Further, the cycling stability was successfully proven in some publications (TAN ET AL. 2021). However, high pressures (over 100 MPa) are needed to provide sufficient interface contact between the silicon anode and the SE separator (HUO & JANEK 2022).

2.2.3 Solid Electrolyte Materials

The classification of SEs according to VARZI ET AL. (2016) is shown in Figure 2-3. There are organic polymer electrolytes and inorganic SEs. Based on their aggregate state, polymers can be divided into conventional SEs and gel electrolytes. Inorganic SEs can be distinguished by either their structure or their composition. In this chapter, the distinction of inorganic SEs based on their composition is chosen. Inorganic SEs are characterized by a high ionic conductivity compared to organic SEs and robustness regarding lithium dendrites (VARZI ET AL. 2016, p. 17257). Representatives of inorganic SEs maintain their operational functionality at temperatures starting at $-50\text{ }^{\circ}\text{C}$ up to $200\text{ }^{\circ}\text{C}$ (FAMPRIKIS ET AL. 2019, p. 1). In the following, polymer-, oxide-, and sulfide-based SEs are characterized based on their advantages and disadvantages. This work does not discuss nitride- and halide-based SEs since their use in ASSBs is not as advanced (MANTHIRAM ET AL. 2017). Oxide- and sulfide-based SEs are abbreviated as oxides and sulfides in the following.

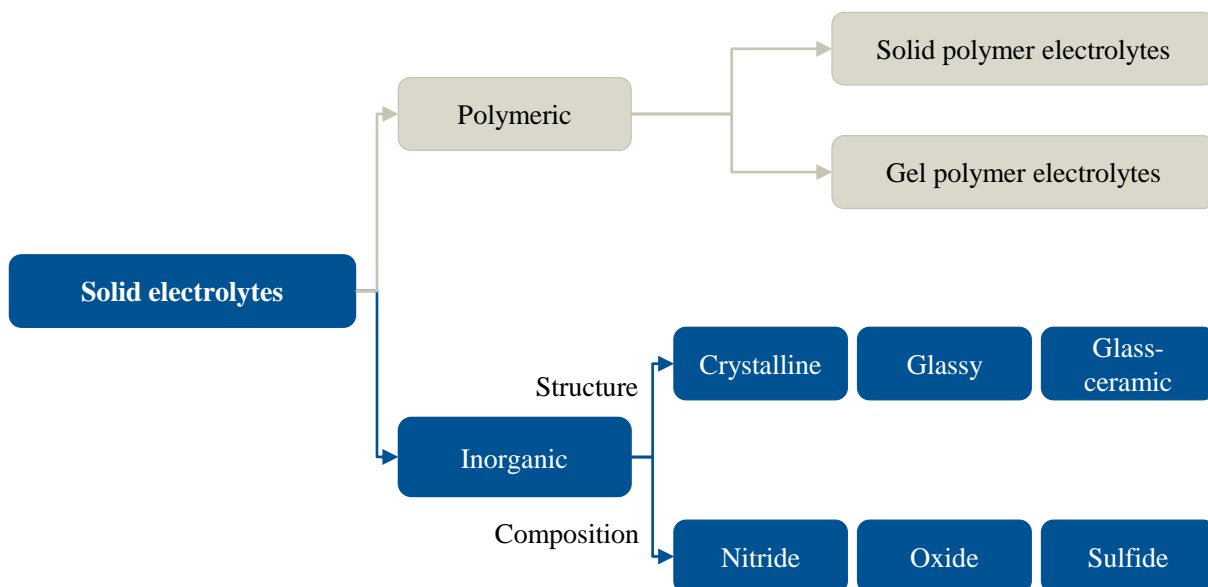


Figure 2-3: Schematic classification of SEs based on VARZI ET AL. (2016).

Polymers

Solid polymer electrolytes, known as dry polymer SEs, consist of a polymer matrix containing alkali metal salt (KURZWEIL & DIETLMEIER 2018, p. 219). The most common matrix material is polyethylene oxide (PEO), where the conducting salt is a lithium salt (LiX , $\text{X} = \text{ClO}_4$, PF_6 , or $\text{N}(\text{SO}_2\text{CF}_3)_2$) (VARZI ET AL. 2016, p. 17253). Moreover, commonly used polymer electrolytes are poly(acrylonitrile) (PAN), poly(methyl methacrylate), polyimide, or cellulose, which are also used as a polymer membrane (DIRICAN ET AL. 2019; KIM ET AL. 2020). The ionic conductivity of polymeric SEs is typically lower than for inorganic SEs and in a range of 10^{-5} S cm^{-1} but can be increased up to $1.4 \times 10^{-4}\text{ S cm}^{-1}$ by modification with the help of inorganic fillers such as SiO_2 nano powder. In other studies, polymers are more commonly used as stabilizers and added to inorganic SEs, forming hybrid materials (ZHENG ET AL. 2019; PERVEZ ET AL. 2019).

The stability of the polymer is not entirely given against cathodes with a voltage higher than 4 V or LiM anodes because a passivation layer is formed. The elastic and plastic deformation of the material has advantages, such as compensation for the change in volume of the cell (JANEK & ZEIER 2016, p. 1). Furthermore, the material is more accessible to process, which could reduce manufacturing costs compared to inorganic materials (MANTHIRAM ET AL. 2017, p. 6). Disadvantages include interfacial instability, poor mechanical stability, and the high operating temperature of the cells for sufficient ionic conductivity. These operating temperatures can be realized when applied in electric vehicles, but the energetic expense of these temperatures could be more efficient for use in series production vehicles (ZHANG ET AL. 2004). However, polymer electrolytes were used in one of the first ASSB-powered vehicles developed by the company Blue Solutions, claiming high energy densities of 380 Wh l⁻¹ at cell level at an operation temperature of -30 °C to +60 °C (BOLLORÉ GROUP 2023).

Adding liquid plasticizers such as propylene carbonate (PC) or ethylene carbonate (EC) reduces the crystalline structure of polymer electrolytes. This modification turns a solid polymer into a gel-like polymer (FERGUS 2010). This improves ionic conductivity, but the compatibility with LiM concerning dendrite growth is reduced (VARZI ET AL. 2016, p. 17254).

Oxides

Oxides belong to the group of inorganic SEs. The advantage of oxides over sulfides is their high chemical stability concerning LiM, as they have a higher oxidation potential. Young's modulus of oxides is 100–200 GPa and, therefore, much higher than that of sulfides (10–20 GPa) (KIM ET AL. 2021). Materials with high Young's modulus are brittle and non-flexible. For this reason, oxides are unsuitable for mechanically demanding applications (WOLFENSTINE ET AL. 2018). Oxides must be sintered at high temperatures above 800 °C to achieve low porosity and high ionic conductivity, which makes production more complex and expensive. Among oxides, materials with crystalline structures are most suitable as SEs for ASSBs (KIM ET AL. 2021). Crystalline oxides include lithium superionic conductor (LISICON, Li₁₄ZnGe₄O₁₆) (KAMMAMPATA & THANGADURAI 2018), perovskites, and garnet-structured lithium lanthanum zirconium oxide (LLZO) (MURUGAN ET AL. 2007). Lithium aluminum titanium phosphate (LATP), a NaSICON structure, has a moderate bulk conductivity of 10⁻³ S cm⁻¹ at room temperature (WOLFENSTINE ET AL. 2018). INAGUMA ET AL. (1993) were the first to experiment with the chemical compound lithium lanthanum titanium oxide (LLTO, Li_{0.34(1)}La_{0.51(1)}TiO_{2.94(2)}). They demonstrated ionic conductivities of up to 10⁻³ S cm⁻¹ (bulk) and total conductivities of 2 × 10⁻⁵ S cm⁻¹ at room temperature. The disadvantage of this material is its instability towards pure LiM (THANGADURAI & WEPPNER 2006, p. 91; JIA ET AL. 2020).

MURUGAN ET AL. (2007) first discovered the garnet-structured LLZO (Li₇La₃Zr₂O₁₂), considered one of the most promising oxide materials. With ionic bulk conductivities of 10⁻³–10⁻⁴ S cm⁻¹ and the best electrochemical stability towards metallic lithium, it exhibits high intrinsic stability and safety compared to other oxides (KIM ET AL. 2021). However, according to the literature, complete stability to LiM has not been demonstrated here either (KASEMCHAINAN & BRUCE 2018, p. 178). For example, lithium dendrites have been found at

grain boundaries in garnet-structured electrolytes with a density of over 99.5 % (KASEMCHAINAN & BRUCE 2018, p. 178; WOLFENSTINE ET AL. 2018, p. 1275). Total conductivity can be substantially increased by adding other elements. SONG ET AL. (2018) substituted Zr_{4+} with Gd_{3+} , reaching an ionic conductivity of $2 \times 10^{-4} \text{ S cm}^{-1}$ at room temperature. Higher values are documented at $10^{-3} \text{ S cm}^{-1}$ (HAN ET AL. 2012) by adding Ta and $1.02 \times 10^{-3} \text{ S cm}^{-1}$ with Te (DEVIANNAPOORANI ET AL. 2013). The disadvantage of LLZO and other oxides is a required sintering temperature over $1000 \text{ }^\circ\text{C}$ (KIM ET AL. 2021).

Sulfides

Replacing oxygen ions with sulfur ions in the chemical formulas of the oxide materials leads to the material group of sulfides. Due to the lower binding energy between sulfur ions and Li^+ , the Li^+ can move more freely, resulting in the high conductivity of sulfides, similar to those of liquid electrolytes (CHEN ET AL. 2018b, p. 58). They have a glass structure, are glass-ceramic or crystalline (cf. Figure 2-3), and exhibit high plasticity.

WANG ET AL. (2021) distinguish three groups of sulfidic SEs based on the number of their chemical starting materials: pseudo-binary, -ternary, and -quaternary sulfides. The more chemical starting materials a sulfide contains, the higher its ionic conductivity. Pseudo-binary systems were investigated in the 1980s and have an ionic conductivity of up to $10^{-3} \text{ S cm}^{-1}$ at room temperature. A well-known representative of this group is lithium phosphorus sulfide Li_3PS_4 (LPS). Pseudo-ternary systems have an ionic conductivity of about $10^{-2} \text{ S cm}^{-1}$ at room temperature. Argyrodites (Li_6PS_5X , $X = Cl, Br, I$) and sulfidic LISICON structures, i.e., lithium germanium phosphorus sulfide (LGPS) belong to the group of pseudo-ternary systems. Li_6PS_5Cl (LPSCl) belongs to the class of argyrodites, which exhibit high ionic conductivities between 10^{-2} and $10^{-3} \text{ S cm}^{-1}$ at room temperature (WENZEL ET AL. 2018, p. 103). Studies have successfully demonstrated the electrochemical cycling of argyrodite using various cathode and anode materials (RANDAU ET AL. 2020). Argyrodites are more stable to LiM than other sulfides (YE & LI 2021, p. 218). When in contact with LiM, argyrodites form a kinetically stable SEI. The ionically conducting Li_2S dominates this SEI and prevents further decomposition of the adjacent phases (KASEMCHAINAN & BRUCE 2018, p. 178). Li_2S has a relatively low ionic conductivity and significantly determines the conductivity of the SEI (WENZEL ET AL. 2018, p. 104).

Besides their high ionic conductivity, sulfides are characterized by their elastic deformation behavior (MCGROGAN ET AL. 2017). The material properties of sulfides allow cold pressing, which is favorable compared to sintering due to less energy consumption (KIM ET AL. 2021, p. 6). Consequently, the grain boundary resistances are less prominent than in oxide materials. (TAKADA 2013, p. 391). The ductility and ease of deformation of sulfides are advantageous for the manufacturing process, as neither cracking nor pore formation leads to increased resistance (SEINO ET AL. 2014, p. 628).

Sulfides have a low reaction and thermodynamic stability towards LiM and the range of the electrochemically stable window is narrow (XIAO ET AL. 2020). If the potential of an electrode is outside this stability range, the sulfidic SE reacts with electrode components and forms an SEI on the surface. (ZHOU ET AL. 2020, p. 647) Moreover, sulfides undergo reduction or

oxidation reactions earlier than oxides (KIM ET AL. 2021, p. 19). A decomposition through oxidation is the main reason for a high capacity loss in the first cycle of an ASSB (XIAO ET AL. 2020).

With regard to scalable production, wet coating processes have already been applied in numerous publications to produce thin-film sheets, posing an enormous advantage in comparison to other SEs (NAM ET AL. 2018; OH ET AL. 2017; TAN ET AL. 2019; SAKUDA ET AL. 2017). The main hurdle of applying sulfidic materials in production is the instability towards water in the atmosphere where hydrogen sulfide (H₂S) is formed (CHEN ET AL. 2022). Therefore, processing should be executed in an inert gas or extremely dry atmosphere. (HATZELL & ZHENG 2021, p. 34; CHEN ET AL. 2022).

To summarize, Figure 2-4 overviews of the important properties of polymer, oxide, and sulfide SEs (MANTHIRAM ET AL. 2017). Besides (electro-)chemical properties, processing aspects are also compared. Sulfide materials are pictured as advantageous due to their good mechanical properties and reasonable processing costs, paired with their high ionic conductivity and thermal stability. However, various SEs are the subject of research, and more material classes will likely be enabled for use in ASSBs. The realization of potential advantages in large-scale cells remains to be proven. (NIKODIMOS ET AL. 2022)

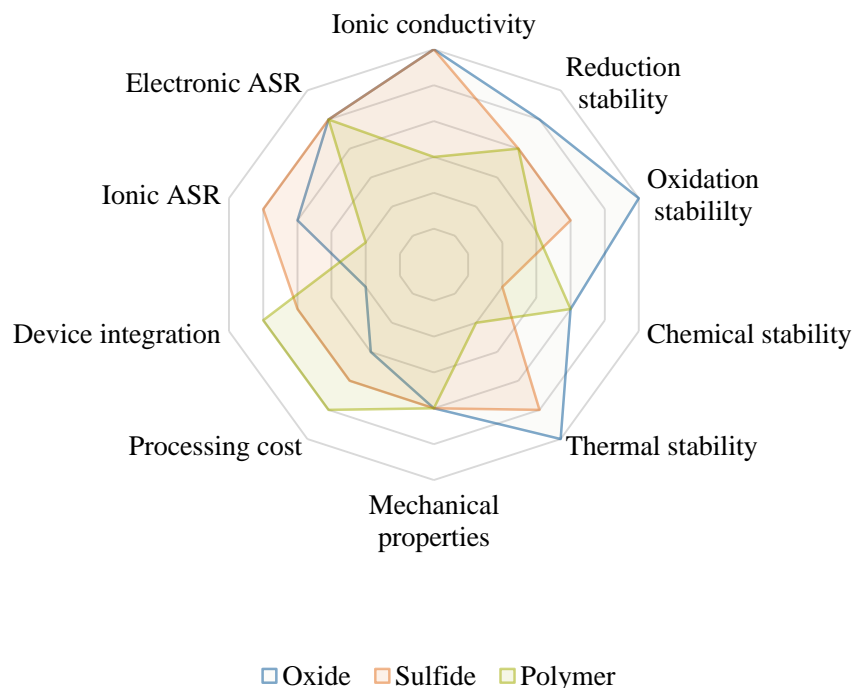


Figure 2-4: Comparison of SE properties for polymers, oxides, and sulfides. ASR: area-specific resistance. Replicated from MANTHIRAM ET AL. (2017).

2.2.4 Cell Formats

In literature, two cell types of ASSB are distinguished. On the one hand, there are thin-film batteries. They consist of electrodes, whose film thickness is usually less than 10 μm, and an electrolyte film of a few 100 nm (SAKUDA ET AL. 2017, A2474). The disadvantage of these

batteries is the costly manufacturing processes for producing the thin films, e.g., sputtering, pulsed laser deposition (PLD), atomic layer deposition (ALD), chemical vapor deposition (CVD), or spark plasma sintering (SPS) (KAZYAK ET AL. 2018; CHEN ET AL. 2017; BAEK ET AL. 2014). Due to the small electrode thickness, the ratio of active to inactive materials is low, resulting in a limited volumetric energy density.

On the other hand, literature shows that most fabricated ASSB cells are so-called bulk-type cells. (KATO ET AL. 2016; JUNG ET AL. 2015) They consist of composite electrodes containing both active material and electrolyte particles and a SE separator. Bulk-type cells are manufactured by compressing the components as pellets. The thicknesses of each component are relatively large (several 100 μm) since producing a thin and homogeneous film is impossible with technologies such as mechanical milling, sintering, and compaction (KIM ET AL. 2015, p. 303). Only sheet-type batteries are suitable for overcoming energy and power density limitations and aiming at automotive applications. The energy densities of these batteries are documented as 184 Wh kg^{-1} in an early research article (NAM ET AL. 2018) because the dimensioning of the SEs is too high compared to the electrodes in currently manufactured batteries. A complete overview of ASSB cells published in 2020 shows that most cells contain a specific energy density below 200 Wh kg^{-1} (RANDAU ET AL. 2020). Considering current energy densities for LIBs in the region of 250–300 Wh kg^{-1} , a significant gap becomes apparent. The technological advancement of sheet-type batteries reveals manufacturing at a laboratory scale with mostly single-layer pouch cells.

Starting with the sheet-type cell designs, developing new design variations produced by scalable and low-cost manufacturing technologies is required to compete with the specific energy densities of conventional LIBs. Hence, sheets with active material must be thicker, providing enough active material. At the same time, the SE separator should be as thin as possible to shorten the ion transportation ways and reduce ionic resistances at interfaces (LUNTZ ET AL. 2015, p. 4600). In SCHNELL ET AL. (2018), two possible cell designs with a structure for large-scale series production were presented. One is the cathode-supported cell, in which the cathode is the thickest component supporting the cell and is coated with a thin electrolyte. The other one is a three-layer matrix structure (trilayer) made of electrolyte material, in which a thin, dense SE separator is located between two porous SE separators. The cathode and anode particles are respectively placed in these porous structures. This approach originates from producing solid oxide fuel cells (SOFC) and is mainly suitable for producing oxidic ASSB cells (SCHNELL ET AL. 2018, p. 172). According to a Patent US11417870B2, a 5–40 μm thickness is targeted for the dense SE, while the porous sheets range between 20–200 μm . Stacking the SE cells, including the collectors, leads to the entire galvanic cell. In a conventional LIB, the positive electrode is coated onto an aluminum collector and the negative electrode onto a copper collector. The individual sheets are connected in parallel. One advantage of the ASSB is the possible use of a bipolar collector (CAO ET AL. 2022). In this case, a cathode and an anode are on each side of the collector (Patent US 20170/263981 A1; GAMBE ET AL. 2015). The cells are connected in series and achieve an increased voltage. The substitution of the liquid electrolyte allows a more compact design, where a single-cell unit consists of the cathode, the SE separator, the anode, and the bipolar collector. This allows the weight and volume of the battery to be

reduced and the specific energy density to be increased (HU 2016, p. 2). Furthermore, smaller lateral dimensions and higher inherent cell voltages are achieved (PLACKE ET AL. 2017, p. 1955). Nevertheless, aspects such as the compatibility of collector materials with both anode and cathode, electrode balancing, and outer layer contact remain challenging (SCHNELL ET AL. 2018, p. 164). Moreover, cells in a bipolar design cannot be monitored individually as in a parallel stack, leading to a high risk of (dis-)overcharge (HOMANN ET AL. 2020).

2.2.5 Potential and Challenges

Increased safety is one of the most essential advantages of an ASSB over a conventional LIB. Due to substituting the organic liquid electrolyte, the flammability of the cells is reduced (TAKADA 2013, p. 767; XU ET AL. 2018; MAUGER ET AL. 2019). Furthermore, using a SE enables the potential use of a LiM anode, as some materials have the necessary chemical and mechanical properties to pair with elemental lithium (MURUGAN ET AL. 2007, p. 7778). Moreover, SEs offer wide electrochemically stable windows against high voltage (over 5 V) cathodes (e.g., LNMO) (XU ET AL. 2016, p. 235; XU ET AL. 2018, p. 6008), favoring long life cycles (DUAN ET AL. 2018, p. 45). Li^+ and anions are mobile in liquid electrolytes, causing concentration gradients. In inorganic SEs, only Li^+ can move, which suppresses this phenomenon. As a result, higher power densities and, thus, shorter charging times for ASSBs are possible due to higher cell currents (JANEK & ZEIER 2016). More efficient use of the installation space is achieved through a bipolar cell structure (JUNG ET AL. 2019; HOMANN ET AL. 2020). Further advantages can be seen in a simplified battery structure. The cell can be operated at higher temperatures by eliminating the liquid electrolyte, so the cooling system at the battery pack level can be obsolete (TAKADA 2013, p. 767).

However, ASSBs pose challenges due to the change in physical and chemical properties. One of the biggest hurdles is the reduced ionic conductivities in solids compared to liquid materials. As previously described, there is no continuous contact between the electrolyte and electrode particles (JANEK & ZEIER 2023). The low ionic conductivities are accompanied by high ohmic polarization and poor bonding of particles at the electrode-electrolyte interface due to high internal resistances (VARZI ET AL. 2016). FAMPRIKIS ET AL. (2019) described that the mechanical properties of an ASSB majorly influence cell performance. The solid electrolyte and its interfaces mainly affect the cell's cycling behavior; however, the mechanisms behind this correlation are poorly understood. The surface adhesion describes the tendency of two surfaces to keep together and resist delamination (cf. 2.3.3). Therefore, the adhesion between the solid electrolyte and the electrode in an ASSB is directly correlated to the interfacial resistance. Due to electrochemical reactions in the electrode, local stress can be induced, leading to failures such as fractures, delamination of surfaces, or loss of contact between particles. This phenomenon is controversial to LIB reactions, where the liquid electrolyte builds a hydrostatic pressure and can be homogeneously distributed within the voids of delamination or cracks. For these reasons, the material combinations of electrode and electrolyte and the manufacturing process at this interface are essential (TAN ET AL. 2022). From a mechanical perspective, using LiM or silicon anode materials leads to high volume changes in the cell that need to be controllable during operation (DOUX ET AL. 2020a). The role of external pressure during the

fabrication and operation of ASSBs is crucial for the functionality of the cells. The cycling stability remains to be investigated (ZHANG ET AL. 2017, p. 28542). According to JANEK & ZEIER (2023), the following aspects need to be deepened to guarantee the successful deployment of ASSBs:

- Thick cathode architectures with a low SE fraction
- SEs with effective conductivities in the composite greater than 10 mS cm^{-1}
- A high-performance anode, which is stable at high current densities and during fast charging
- Lower lithium content in SEs
- Cost-efficient industrial material processing and cell fabrication

The latter bullet point refers to the as-yet immature processes for manufacturing ASSBs. This aspect is another obstacle to the widespread application of ASSBs (TAN ET AL. 2022). From a production engineering perspective, it is essential to determine cell's corresponding product requirements and properties at an early stage to pave the way for mass production (SCHNELL ET AL. 2018, p. 162).

2.3 Electrode Production Process and Characteristics of Lithium-Ion Batteries

The following subsections explain the fundamentals of the mixing, coating, and drying of the electrode production processes. Moreover, characteristic properties of the battery slurry, e.g., rheology, and the dry film, e.g., binder migration and adhesion strength, are described. The focus is on relevant correlations, mostly known from LIBs, to build a basis for the results on sulfide-based ASSBs in Chapter 4. All processes examined belong to the first part of electrode manufacturing (cf. Figure 2-5, blue). The process of calendaring, the cell assembly, and the cell finalization are not in the scope of this thesis (cf. Figure 2-5, brown).

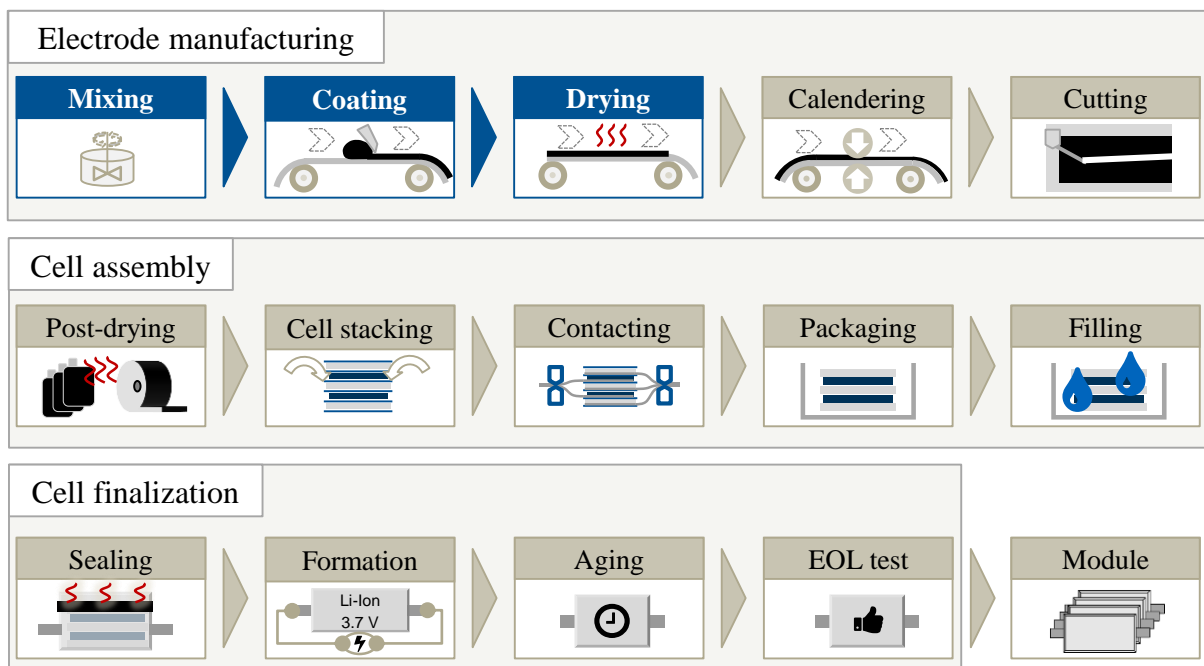


Figure 2-5: Schematic processes in the LIB production divided into electrode manufacturing, cell assembly, and cell finalization. According to KORTHAUER (2019).

2.3.1 Mixing

In the first process of battery production, various materials in a solid or liquid state are mixed to form a battery slurry. Usually, a dry and a wet mixing step is differentiated. Electrodes contain an active material and additives, conductive carbon, and binder (dry mixing), which form a dispersion with suitable solvents (wet mixing) (BITSCH ET AL. 2014). As the battery slurry is the first intermediate product in the battery process chain, it decisively influences the final microstructure of the electrodes in a wet and dry state (GUTOFF ET AL. 2006, p. 44). Requirements for the slurry and resulting electrode coating include:

- Homogeneous distribution of active material
- Prevention of agglomerates
- Formation of an electrically conductive network of additives
- High mass ratio of active materials compared to inactive materials (binders and conductive additives) to increase the energy density

Moreover, the morphology of particles (size, shape) is decisive for the mixing procedure. Since the electrode processing directly affects the electrode performance, it is important to understand the characteristics of a battery slurry when measuring and adjusting it to the process requirements. (KRAYTSBERG & EIN-ELI 2016) The first step of implementing new materials into battery electrodes is to align the rheology and accelerate the downstream process development by predicting coating properties. This can be achieved by using the rheological data for quality control and adjusting the mixing and subsequent coating process to ensure uniform coatings. (REYNOLDS ET AL. 2022)

The flow behavior is a highly influencing variable in the coating process, which is responsible for the formation of defects. (KAISER ET AL. 2014) Fundamental aspects of the central property, the viscosity, and characteristics of battery slurries are highlighted in the following.

Shear Rates and Viscosity

Shear in a liquid film occurs when the upper layer moves at a greater velocity than the lower layer, causing them to shift against each other (SCHETZ & FUHS 1999). If the resulting shear γ is derived as the ratio between displacement x and height h with respect to time, the shear rate $\dot{\gamma}$ is obtained as the change in shear deformation with time according to Equations (4) and (5):

$$\gamma = \frac{x}{h} \quad (4)$$

$$\dot{\gamma} = \frac{dy}{dt} \quad (5)$$

To achieve this deformation, a force F needs to be applied to a surface A , resulting in the shear stress σ in Equation (6):

$$\sigma = \frac{F}{A} \quad (6)$$

The dynamic viscosity η , as a proportionality coefficient between the shear stress σ and shear rate $\dot{\gamma}$ occurs as damping or loss of kinetic energy due to internal fluid frictional resistances defined in Equation (7):

$$\eta = \frac{\text{shear stress}}{\text{shear rate}} = \frac{\sigma}{\dot{\gamma}} \quad (7)$$

The dynamic viscosity as a material-dependent property is determined as a function of the shear rate. Depending on its course, four different behaviors of fluids are distinguished (GUTOFF ET AL. 2006, p. 46):

1. Newtonian fluids: Constant viscosities independent of the shear rate. A characteristic linear correlation between shear stress and shear rate is given.
2. Pseudoplastic or shear-thinning behavior: The viscosity decreases with an increasing shear rate.
3. Dilatant or shear-thickening behavior: The viscosity increases with an increasing shear rate.
4. A Bingham solid with yield-stress behavior: The fluids start to flow after the shear stress exceeds a finite value.

The viscosity is usually measured offline in viscometers with either a constant or variable shear. (REYNOLDS ET AL. 2022) Viscometers with a constant shear rate offer only a single-point measurement or a small, limited range of shear rates below 300 s^{-1} , whereas variable shear viscometers are more flexible with a wide range of shear rates that cover high values, which are usually required to characterize shear-thinning fluids. (GUTOFF ET AL. 2006, p. 47) A viscometer can only determine the fluids' flow or viscosity curve, while a rheometer determines many more rheological parameters. Moreover, the measuring principle can be divided into rotational and oscillation tests. Oscillatory tests are executed to characterize the viscoelastic behavior of fluids (MEZGER 2020).

Slurry Rheology

The electrode slurry behavior is central to the production process and is determined by the raw material ratio, mixing procedure, and mixing sequence (BITSCH ET AL. 2014). State-of-the-art mixing procedures implement technologies such as planetary mixers or dispersers with differing mixing principles to create a homogeneous slurry (LIU ET AL. 2014). Besides the process parameters, the composition and the interplay among individual constituents within the mixture are highly influencing. For instance, incorporating new materials or additives aims at improved dispersion of elements. (DRAKOPOULOS ET AL. 2021)

The dispersions used in LIB production typically exhibit a shear-thinning character, with two plateaus occurring for the zero-shear viscosity and the infinite shear viscosity. (BAUER & NÖTZEL 2014) This is characterized by a strongly decreasing course of viscosity with increasing shear rates, which can be attributed to a microstructural alignment. For example, particles in dispersions align with the flow, polymer chains in polymeric solutions disentangle and become

stretched, and aggregations of smaller particles break up. Plotted twice logarithmically, high shear rates usually result in a plateau called infinite shear viscosity η_{∞} (cf. Figure 2-6). This is where the most prominent alignment and, thus, the lowest viscosity is reached. It is mainly determined by the solvent viscosity. (KAISER ET AL. 2014) In most cases, shear-thinning media also exhibit a plateau at low shear rates, referred to as shear zero viscosity η_0 (cf. Figure 2-6), often several orders of magnitude above η_{∞} . It results from particles and molecules that maintain their disordered structure at low shear rates, which results from the preserved Brownian molecular motion. (MEWIS & WAGNER 2012)

Figure 2-6 shows an example of the viscosity of a water-based anode dispersion and an N-methyl-2-pyrrolidone-based (NMP) cathode dispersion measured over the shear rate. Both exhibit structural viscosity and thus shear-thinning character. Moreover, the constant shear zero viscosity can be determined in the range of low shear rates, which is responsible for the sedimentation behavior, contour fidelity at the coating edge, and dewetting at substrate defects. Here, the anode dispersion shows a high shear zero viscosity of about 300 Pa s, whereas the cathode dispersion has a viscosity of 10 Pa s. While shear rates of 1000–30000 s^{-1} are typical for slot dies, shear rates less than 100 s^{-1} occur in the slower doctor blade coating process. (KAISER ET AL. 2014) However, in literature, shear rate ranges differ between 20–40000 s^{-1} for doctor blades and 3000–100000 s^{-1} for slot dies (REYNOLDS ET AL. 2022). A suitable viscosity should be set to achieve a good film application with homogeneous films and high web speeds in the subsequent wet coating process. On the one hand, a high solvent content results in good flowability in the coating process and easy degassing of trapped air. On the other hand, this increases the raw material costs, the process duration, and the cost for the drying process. A trade-off between these adjusting levers must be pursued in every process engineering study. (KAISER ET AL. 2014)

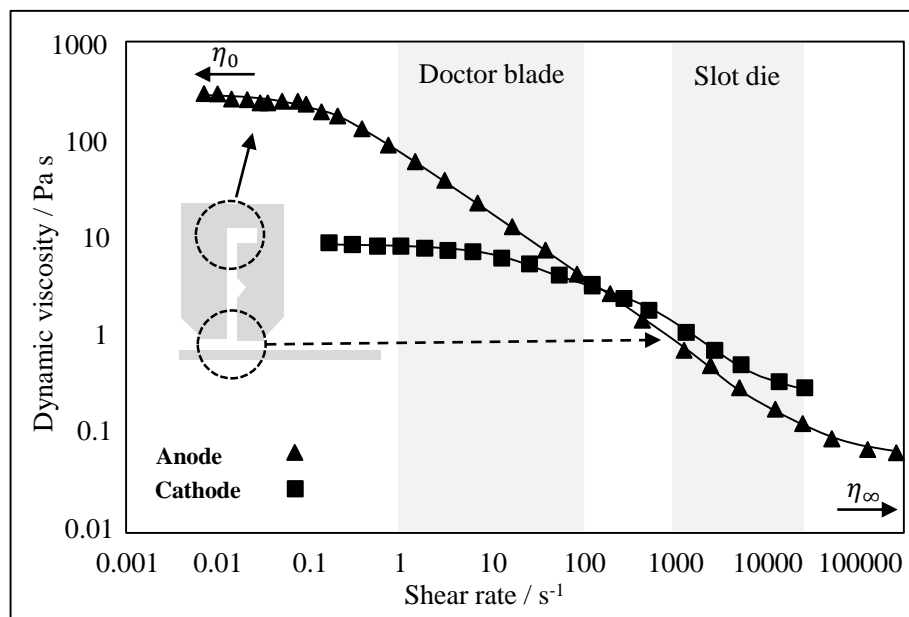
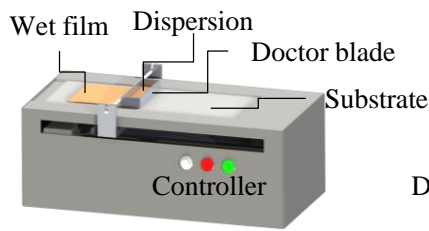


Figure 2-6: Viscosity of anode and cathode dispersion in conventional LIB production as a function of shear rate determined by rotational rheometer. Replicated from KAISER ET AL. (2014).

2.3.2 Wet Coating

After mixing, the slurry is applied to a substrate with a defined film thickness in a wet coating process. Different application tools are used to achieve this. While the doctor blade method is usually established on a laboratory or pilot scale, the slot die is considered state-of-the-art in industrial battery production. (KAISER ET AL. 2014) In a doctor blade process, the slurry is poured into a reservoir in front of the blade. Depending on the dispersion's viscosity, different blade shapes are applied. (GUTOFF ET AL. 2006) The dispersion is then spread onto a substrate with a particular coating velocity while the doctor blade is stationary. On a laboratory scale, the doctor blade is moved manually or by an automated laboratory coater (cf. Section 3.1). In contrast, on an industrial scale, the doctor blade is fixed, and the substrate (web) is moved along rolls with a specific web tension and coating velocity (cf. Figure 2-7). The result is a wet film, which is thinner than the coating gap, depending on the surface tension of the dispersion. (BERNI ET AL. 2004) As shown in Figure 2-7, the drying occurs immediately after coating (cf. Subsection 2.3.3.)

Laboratory scale



Prototype/Industrial scale

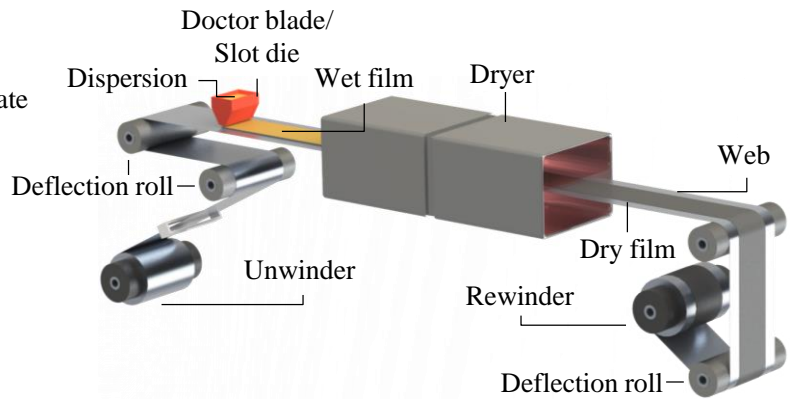


Figure 2-7: Schematic principle of laboratory-scale (left) and prototype/industrial-scale (right) doctor blade coating.

Considering the application of a coating process for LIBs, the shear rate during coating $\dot{\gamma}_c$ inside a doctor blade can be described by Equation (8) with the coating speed v and the coating gap h_{cg} (MEZGER 2020):

$$\dot{\gamma}_c = \frac{v}{h_{cg}} \quad (8)$$

The advantages of the slot die in comparison to the doctor blade are higher coating speeds, the application of large viscosity ranges, and the closed system, which prevents contamination. The rheological properties of the dispersion influence the flow condition in the nozzle. (KAISER ET AL. 2014) Therefore, the coating shear rate $\dot{\gamma}_c$ in Equation (8) and a wall shear rate $\dot{\gamma}_w$ (Equation (9)) apply during slot die coating:

$$\dot{\gamma}_w = \frac{6Q}{b \times h_s^2} \quad (9)$$

Q is the volumetric flow rate of the material, b is the slot width, and h_s is the slot length. Both shear rates are important to characterize the battery slurry. (REYNOLDS ET AL. 2022) In addition to viscosity, DING ET AL. (2016) highlight surface tension, gap height, vacuum pressure, volume flow, and web speed as relevant process parameters concerning the possible operating range in slot die coating. Further coating methods such as roll coating, rod coating, or curtain coating are well known and can be used to create a thin film (GUTOFF ET AL. 2006), but do not play a significant role in the industrial manufacturing of battery coatings and are not regarded further.

Coating Window and Defects

In order to obtain a high-quality and homogeneous film, it is important to find the optimum process window depending on the slurry and the coating technology. In the wet coating process of LIBs, the process properties can be described by the capillary number Ca as a function of the dimensionless gap width G_w^* . These two parameters are defined in Equations (10) and (11) with η as the dynamic viscosity, U the roll speed, σ_{ST} the surface tension, G_w the gap width and H the wet film thickness:

$$Ca = \frac{\eta \times U}{\sigma_{ST}} \quad (10)$$

$$G_w^* = \frac{G_w}{H} \quad (11)$$

As described in Subsection 2.3.1, the slurry of LIB electrodes has a shear-thinning behavior. Therefore, the viscosity is dependent on the parameter U and G_w . (SCHMITT ET AL. 2013) According to viscocapillary models, the quality of the applied wet film is limited by the minimum wet film thickness and respective maximum coating velocity (HIGGINS & SCRIVEN 1980; CARVALHO & KHESHGI 2000). As a result, a coating process can be considered robust if there is more capillarity to hold the coating fluid in place between slot die and substrate than viscosity to move the substrate. Defects in the form of longitudinal streaks in the coating occur when the viscous forces exceed the stabilizing capillary forces. As the coating speed increases, the air entrained by the substrate will also destabilize the menisci in the coating gap. This results in the formation of air inclusions in the film, which cause characteristic defects at right angles to the direction of the coating. (KAISER ET AL. 2014)

Moreover, a homogeneous slurry can form surface defects by changing the coating parameters (SCHMITT ET AL. 2013). For example, a change in the surface tension of the coating can lead to craters in the surface at isolated points, regardless of the materials used (GUTOFF ET AL. 2006, p. 164). Agglomerates and larger particles in the slurry can also lead to streaks in the film surface (KAISER ET AL. 2014). Typical defects are heavy edges formed at either intermediate coatings (DIEHM ET AL. 2020b) or super elevated edges in stripe and pattern coatings (SCHMITT ET AL. 2014). A complete overview of common coating defects can be found in further literature (GUTOFF ET AL. 2006; MOHANTY ET AL. 2016).

2.3.3 Drying

After wet coating, the subsequent drying process evaporates the solvents, resulting in the final dried film. During drying, the homogeneity of particles can be influenced depending on parameters such as the drying temperature and duration. The mass flow rate \dot{m}_s of the solvent from the dispersion layer to the atmosphere is called the drying rate. In order to clarify the terms and relation of parameters in the drying process, the most relevant equations are explained in the following.

The drying rate depends on the molar mass of the solvent \tilde{M}_S , the molar density of the atmospheric gas $\tilde{\rho}_G$, the mass transfer coefficient $\beta_{S,G}$ between the dispersion and the environment, the molar distribution of the solvent in the drying environment $\tilde{\gamma}_{S,\infty}$, and the molar distribution of the solvent at the surface of the dispersion to the surrounding gas $\tilde{\gamma}_{S,Ph}$. (KUMBERG ET AL. 2019, p. 1) The relation is shown in Equation (12):

$$\dot{m}_s = \tilde{M}_S \times \tilde{\rho}_G \times \beta_{S,G} \times \ln \frac{(1 - \tilde{\gamma}_{S,\infty})}{(1 - \tilde{\gamma}_{S,Ph})} \quad (12)$$

To determine the molar mass of the dispersion \tilde{M}_S directly after coating, the molar fractions ψ_i and molar masses M_i of components i are needed, as can be seen in Equation (13) (BAEHR & STEPHAN 2008, p. 76):

$$\tilde{M}_S = \sum_i \psi_i M_i \quad (13)$$

The molar fraction ψ_i of a component is calculated from the amount of substance n_i of the component and the total number of moles n (compare Equation (14)) (BAEHR & STEPHAN 2008, p. 75). n is the sum of the amounts of substances n_i of each component, which is determined from the mass of the component m_i and its molar mass M_i as described in the following Equation (15) (BINNEWIES ET AL. 2016, p. 7):

$$\psi_i = \frac{n_i}{n} \quad (14)$$

$$n_i = \frac{m_i}{M_i} \quad (15)$$

The molar density $\tilde{\rho}_G$ in Equation (16) is calculated by the general gas equation from the pressure of the atmospheric gas p_G and the temperature T_G . R_m is the universal gas constant with a value of $8.134 \text{ J mol}^{-1} \text{ K}^{-1}$ (VDI E.V. 2013):

$$\tilde{\rho}_G = \frac{p_G}{R_m \times T_G} \quad (16)$$

As shown in Equation (17), the mass transfer coefficient $\beta_{S,G}$ depends on the diffusion coefficient D of the solvent in the gas atmosphere and the film thickness δ (BAEHR & STEPHAN 2008, p. 9):

$$\beta_{S,G} = \frac{D}{\delta} \quad (17)$$

Since δ is often unknown, it is recommended to reference on cases that have been recorded in respective literature (BAEHR & STEPHAN 2008, p. 91). An alternative is the determination by the Lewis analogy, describing the relationship between the heat transfer coefficient $\alpha_{S,G}$ and the mass transfer coefficient $\beta_{S,G}$ via the heat capacity of the gas $c_{p,G}$, the density of the atmospheric gas ρ_G , the Lewis number Le , and the flow type, where n is 0.3 for laminar flow and 0.4 for turbulent flow (Equation (18)):

$$\beta_{S,G} = \frac{\alpha_{S,G}}{c_{p,G} \times \rho_G \times Le^{1-n}} \quad (18)$$

$\alpha_{S,G}$ is calculated using different formulas depending on whether free or forced convection prevails (KUMBERG ET AL. 2019; BAEHR & STEPHAN 2008). Le is calculated according to Equation (19) as a function of the thermal diffusivity a_G of the atmospheric gas and the diffusion coefficient D , which for the present combination of solvent and ambient gas can be taken, for example, from empirically determined diffusion tables (BAEHR & STEPHAN 2008, 394):

$$Le = \frac{a_G}{D} \quad (19)$$

a_G is calculated according to Equation (20) as a function of the heat capacity of the gas $c_{p,G}$, the thermal conductivity of the gas λ_G and the density of the gas ρ_G (BAEHR & STEPHAN 2008):

$$a_G = \frac{\lambda_G}{c_{p,G} \times \rho_G} \quad (20)$$

To calculate the mass flow rate \dot{m}_s , the molar distribution of the solvent in the drying environment $\tilde{\gamma}_{S,\infty}$ and the molar distribution of the solvent at the surface of the dispersion to the surrounding gas $\tilde{\gamma}_{S,Ph}$ need to be defined as well. For $\tilde{\gamma}_{S,Ph}$ Equation (21) holds as a function of the vapor pressure of the solvent $p_v(T)$ at the temperature of the dispersion (T_{Dis}), the activity a_s of the solvent, and the ambient pressure p_a :

$$\tilde{\gamma}_{S,Ph} = \frac{p_v(T_{Dis}) \times a_s}{p_a} \quad (21)$$

a_s can be assumed with the value 1, except for a low solvent loading. For $\tilde{\gamma}_{S,\infty}$, the value zero can be assumed in a dry environment without circulating air. (KUMBERG ET AL. 2019)

Binder Migration

The drying rate influences the phenomenon of binder migration, which causes inhomogeneous binder distribution inside of coatings. The resulting local accumulations affect the mechanical and electrochemical properties of the battery cell (FONT ET AL. 2018). Studies on LIB electrodes have shown that high drying rates lead to accumulations of binder on the evaporation surface and the bearing surface towards the substrate (MÜLLER ET AL. 2017). The study of CHOU ET AL.

(2014) on electrodes showed that binder migration significantly influences the battery cell's cycle stability. To enforce different binder distributions for their study, MÜLLER ET AL. (2017) dried electrodes at different temperatures and drying rates.

LIM ET AL. (2013) stated that the three physical influences on binder migration are evaporation, sedimentation, and diffusion. Evaporation describes the evaporation of the solvent, supported by capillary action during drying in the resulting pores. Sedimentation is the downward movement of particles caused by gravity and density differences between the components of a dispersion. Diffusion effects are caused by temperature and concentration differences. At high drying rates, diffusion processes cannot compensate for binder migration toward the surface of the coating caused by evaporation (FONT ET AL. 2018). LIM ET AL. (2013) described the relationship between evaporation, sedimentation, and diffusion by the Peclet number Pe and the sedimentation number N_S . Pe depends on the drying rate (evaporation rate) E_R of the solvent, the wet film thickness H , and the diffusion coefficient D and is calculated according to Equation (22) (LIM ET AL. 2013, p. 6):

$$Pe = \frac{(E_R \times H)}{D} \quad (22)$$

D according to Equation (23) depends on the drying temperature T_D , the particle radius R , the viscosity μ of the binder solution, and the Boltzmann constant k (BINNEWIES ET AL. 2016):

$$D = \frac{k \times T_D}{6\pi \times \mu \times R} \quad (23)$$

N_S is calculated from the Stokes' sedimentation rate U_0 and E_R , as shown in Equation (24) (LIM ET AL. 2013):

$$N_S = \frac{U_0}{E_R} \quad (24)$$

The sedimentation velocity U_0 depends on the particle radius R , the gravitational acceleration g , the density of the particle ρ_p , the density of the solvent ρ_s , and the viscosity of the binder solution μ . If Pe is significantly greater than one, evaporation is the dominant effect, and binder migration occurs at the top of the film. When Pe is much smaller than one, diffusion dominates, resulting in a homogeneous distribution. If the sedimentation number N_S is much smaller than one, sedimentation is negligible compared to the other two effects. (LIM ET AL. 2013)

Adhesion Strength

The adhesion strength is one of the main characteristics of LIB electrodes in the dried state. To understand this property and its value, the complex mechanism behind it is explained in more detail.

The intercalation and deintercalation processes of electrodes cause a change in volume in the active materials, which results in mechanical stress on the components. Moreover, during the production of the batteries, the cell components are exposed to mechanical stress, e.g., bending in a roll-to-roll process (BILLOT ET AL. 2020; BILLOT ET AL. 2021). This can lead to a partial or

complete delamination of the coating from the substrate resulting in a reduced functionality. (HASELRIEDER ET AL. 2015; MEYER ET AL. 2020) Therefore, adhesion measurements are conducted after drying to evaluate the bond between the coating and the substrate.

For an adhesion bond to break, energy must be supplied. As soon as the bond fails, two new surfaces are formed. This energy required to form new surfaces is the so-called surface energy. When the failure occurs at the interface between phase 1 and phase 2, this energy corresponds to the work of adhesion W_A . The work of adhesion is the decrease in Gibbs free energy per unit area when an interface is formed from two individual surfaces. It depends on the surface energy γ_1 of the first material, γ_2 of the second material, and the interfacial energy γ_{12} between the phases 1 and 2. The work of adhesion is calculated according to Equation (25) (DA SILVA ET AL. 2011, 2018), and can be described as the change in adhesion force F_A over strain dx (MITTAL 1976, p. 24) in Equation (26):

$$W_A = \gamma_1 + \gamma_2 - \gamma_{12} \quad (25)$$

$$W_A = \int F_A dx \quad (26)$$

In the case of an adhesion failure of battery component, the electrode is delaminated from the substrate and the maximum adhesion strength of the electrode can be measured (cf. Figure 2-8, middle).

If one of the two materials does not fail at the interface, there is no adhesion failure but a cohesion failure (MITTAL 1976, p. 24; RICKERBY 1988, p. 542; DA SILVA ET AL. 2018, p. 14). In case of a cohesion failure, the adhesion of the coating to the substrate is higher than within the coating, leading to particle fractions (cf. Figure 2-8, left). Equation (27) describes the cohesive work W_C for the failure of material 1 (DA SILVA ET AL. 2011, p. 14, 2018):

$$W_C = 2 \gamma_1 \quad (27)$$

In practice, the fracture energy G is often significantly larger than W_A and W_C . In the following, W_A and W_C , respectively, will be referred to as G_0 . During a fracture, other energy-absorbing processes occur in addition to G_0 , such as plastic and viscoelastic deformations. In Equation (28), these processes are summarized in the term ψ (DA SILVA ET AL. 2018):

$$G = G_0 + \psi \quad (28)$$

The two terms G_0 and ψ are coupled to each other, so G_0 cannot be omitted simplistically, even if ψ is usually significantly larger (DA SILVA ET AL. 2018). Similar considerations apply to the fracture stress σ_f as to the fracture energy G . The two quantities depend on each other, as seen in Equation (29). Here, k_{crit} is the material-dependent critical stress intensity factor, l is the length of the critical crack leading to fracture, and E is the effective modulus of elasticity (DA SILVA ET AL. 2018):

$$\sigma_f = k_{\text{crit}} \times \sqrt{\frac{E \times G}{l}} \quad (29)$$

The third fracture scenario is the failure of adhesive, where the compound of electrode, substrate, and adhesive is delaminated off the test fixture, resulting in an invalid test result. (HASLRIEDER ET AL. 2015) The cohesiveness of the adhesive must be greater than the adhesion between the coating or substrate and the adhesive. (MITTAL 1976)

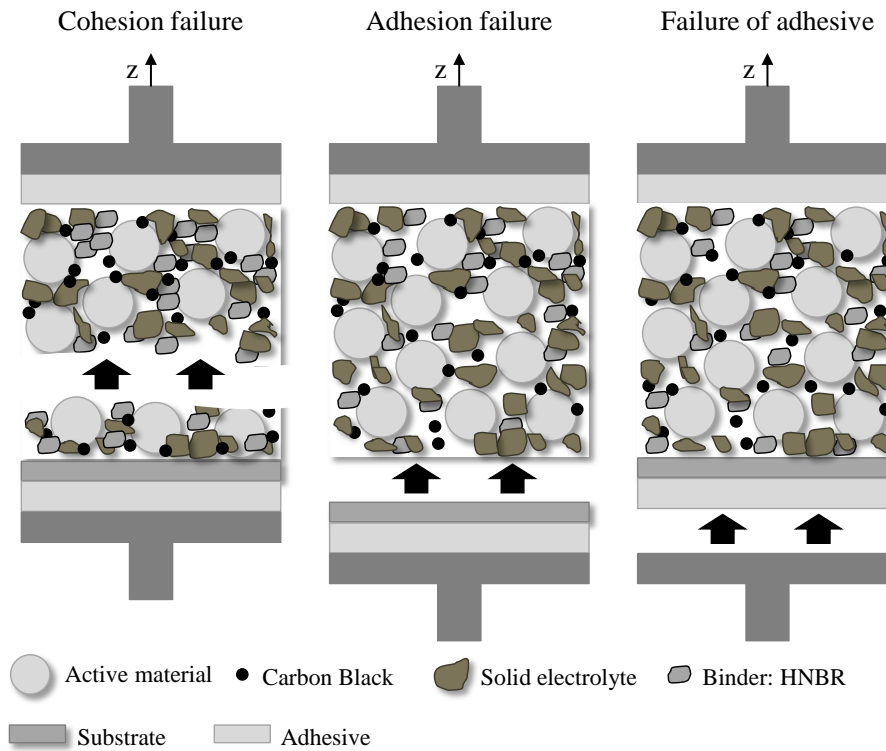


Figure 2-8: Schematic differentiation of fracture scenarios during experimental adhesion measurements in a z-tensile strength test adapted for ASSB materials. Left: cohesion failure, middle: adhesion failure, right: failure of adhesive. Replicated from HASLRIEDER ET AL. (2015).

3 State of the Art

Chapter 2 builds the foundation for the further description of the state of the art. Detailing the functions and materials of ASSBs, the fundamental principles of rheology, the wet coating and the drying process, and the adhesion strength is part of the literature-based research clarification described in Figure 1-2. In Chapter 3, relevant publications and dissertations from the state of the art are presented and discussed. To derive the need for action, three major topics regarding the most important literature are chosen and examined to clarify the objective of this dissertation. Therefore, laboratory-scale tests for wet coating of sulfide-based components are summarized in the beginning (cf. Section 3.1), followed by concepts for scaling up ASSB production (cf. Section 3.2). To bridge the gap to already applied scalable processes, industrial wet coating and drying processes of LIBs are discussed afterward (cf. Section 3.3). The chapter is closed by deriving the need for action to enable the scalable wet coating process for sulfide-based ASSBs (cf. Section 3.4).

3.1 Laboratory-Scale Fabrication of Sulfide-Based All-Solid-State Batteries

In laboratory-scale fabrication, the SE and composite cathode are often produced using techniques such as cold pressing to form thick pellets with a thickness of over 300 μm (XU ET AL. 2021, p. 5). For industrial mass production of high-performance ASSBs, thinner film thicknesses below 100 μm are required for high energy densities compared to LIBs (MCCLOSKEY 2015). Thin film thicknesses below 50 μm can compensate for the comparatively lower energy density of inorganic SEs, which have a higher density than liquid electrolytes (SCHNELLE ET AL. 2018). Small and thin sulfide-based sheets can be realized due to the flexibility of the material, but larger films tend to have low mechanical strength compared to thick pellets and might fracture while bending. At the laboratory level, it is possible to accurately check the density and surface area of small pellets and the occurrence of internal defects. In contrast, methods for inspecting large and thin SE separators are limited, so defects are not detected internally or on the surface. (XU ET AL. 2021, p. 9)

On a laboratory scale, processes for sulfide-based ASSBs are similar to those of LIBs described in Section 2.3 despite the addition of the SE as an extra component and as an addition to the cathode. The schematic process chain of the wet mixing route for sulfide-based ASSBs is shown in Figure 3-1. Compared to LIBs, two separate strands are needed to fabricate the SE and composite cathode (parallel or sequential). A mixing step is conducted to create a composition of SE with a binder pre-mixed in a solvent. For the composite cathode, the active material is mixed with a SE, a binder, and a conductive additive. The next step is the coating procedure. Depending on the application tool, e.g., the doctor blade, the slurry is spread onto a substrate with a certain gap height, resulting in a wet film followed by a drying step to evaporate the

solvent from the pores inside the films. Afterward, the residual porosity needs to be decreased. Components of ASSBs need to be densified more than LIBs, down to zero percent porosity – although this is a theoretical value, which is hardly reached in a heterogenous system such as the composite cathode. The produced sheets are then handled in the final cell assembly, where the anode is added to build a full ASSB cell. These process steps are suitable for the laboratory scale, while for industrial mass production, the sequence and techniques that can be used to produce the cathode and the SE vary. Since the scope of this dissertation is on component manufacturing, relevant literature in this field is summarized in the following.

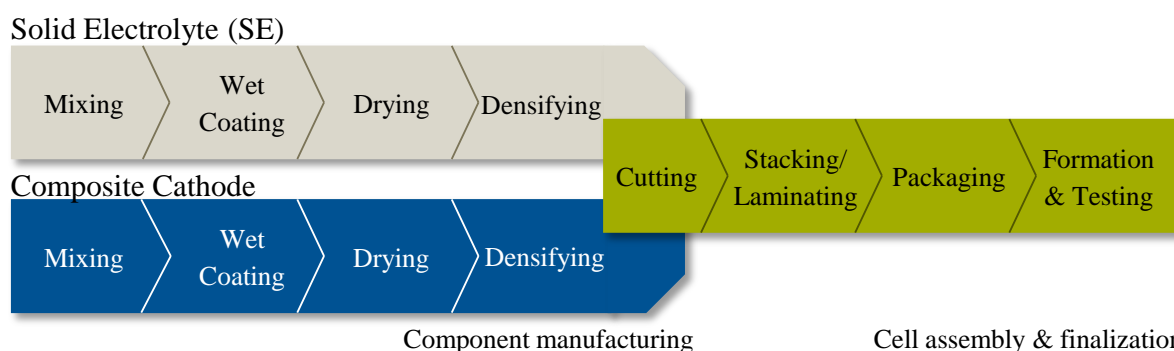


Figure 3-1: Schematic processes for laboratory-scale fabrication of sulfide-based ASSBs. The SE (grey) and composite cathode (blue) component manufacturing is similar. The cell assembly and finalization are pictured in green. The anode processing is not considered in this figure. Adapted from BATZER ET AL. (2022a).

In 2015, NAM ET AL. reported the first bendable and free-standing sulfide-based SE using the glass-ceramic Li_3PS_4 and $\text{Li}_{10}\text{GeP}_2\text{S}_{12}$ in a toluene solution. Films were coated via the doctor blade method on a nickel foil and then cold pressed with a mechanically compliant poly(paraphenylene terephthalamide) nonwoven scaffold to create a $70\ \mu\text{m}$ thick compound. The SE separator was reinforced to gain free-standing, stackable sheets with flexibility and mechanical strength at the same time. Afterward, cells were built with an LCO cathode, the SE film, and an LTO anode. The resulting energy density was $44\ \text{Wh kg}^{-1}$.

KIM ET AL. (2017) focused on producing composite cathodes using infiltration. The porous structure of conventional LIB cathodes with LCO as active material was infiltrated with $\text{Li}_6\text{PS}_5\text{Cl}$ -ethanol solution or $0.4\text{LiI}-0.6\text{Li}_4\text{SnS}_4$ in methanol. The cathode was produced by using dip coating and was suggested to be scalable by applying methods such as spray coating in the future. Subsequently, the solvent was evaporated by drying the cathodes at $180\ ^\circ\text{C}$ under vacuum and densified by cold-pressing. High reversible capacities of $141\ \text{mAh g}^{-1}$ for the cathodes and $364\ \text{mAh g}^{-1}$ for the graphite anode were achieved.

KIM ET AL. (2019a) also reported this infiltration method, producing composite silicon anodes with $\text{Li}_6\text{PS}_5\text{Cl}$ -ethanol solution. The electrodes were produced using a dipping method followed by solvent evaporation and vacuum drying at $180\ ^\circ\text{C}$. The densification was achieved by cold-pressing under $550\ \text{MPa}$. Especially the effects of the silicon's particle size and choice of polymeric binders (polyvinylidene fluoride (PVDF) vs. polyacrylic acid/carboxymethyl cellulose) were examined. The silicon electrodes infiltrated with $\text{Li}_6\text{PS}_5\text{Cl}$ showed reversible capacities over $300\ \text{mA h g}^{-1}$ at $30\ ^\circ\text{C}$. The assembled ASSB with an LCO cathode exhibited an energy density of $338\ \text{Wh kg}^{-1}$ at $0.14\ \text{mA cm}^{-2}$ and $30\ ^\circ\text{C}$. KIM ET AL. (2020) focused on thin

and flexible SE membranes made of $\text{Li}_6\text{PS}_5\text{Cl}_{0.5}\text{Br}_{0.5}$ and polyimide as a mechanical stabilization.

In SAKUDA ET AL. (2017), a solvent-based process route was applied for a composite cathode using NMC111, $75\text{Li}_2\text{S}-25\text{P}_2\text{S}_5$, acetylene black with two binder systems, styrene-butadiene-based binder (SBS) in combination with anisole and styrene ethylene butylene styrene copolymer (SEBS) with heptane. The slurry was prepared in a planetary centrifugal mixer and coated onto an aluminum foil. Sulfide-based separators containing Li_3PS_4 were prepared using SBS binder and anisole as a solvent in a slurry coating process. The substrate was a release sheet, and a subsequent drying step was conducted at $25\text{ }^\circ\text{C}$. After pressing the SE films at 330 MPa or 410 MPa, they were exfoliated from the copper foil. Composite anodes were fabricated using the same materials as the cathode but with graphite as the active material. The full cells had dimensions of $20 \times 20\text{ mm}^2$ or $22 \times 22\text{ mm}^2$, showing a reversible capacity of 1.5 mAh cm^2 and an energy density of 155 Wh kg^{-1} .

OH ET AL. (2017) investigated the fabrication of composite electrodes consisting of an active material (NMC622, graphite), the carbon additive *Super C65*, the SE Li_3PS_4 (LPS), and a polymeric binder (acrylonitrile butadiene rubber (NBR) or polyvinyl chloride (PVC)) by using the doctor blade method. The solvent used was tetrahydrofuran (THF). First, the active material, additives, and components of LPS were dissolved in THF and stirred at room temperature. The coating was applied to aluminum or nickel foil in the next step using the doctor blade method. The film was then dried at $140\text{ }^\circ\text{C}$ under vacuum. The dry thickness of the coatings was $70\text{ }\mu\text{m}$. The particle size of the produced electrodes was examined by scanning electron microscopy (SEM). The assembled full cell had a reversible capacity of 131 mAh g^{-1} at 0.1 C and $30\text{ }^\circ\text{C}$, which relates to an energy density of 241 Wh kg^{-1} .

NAM ET AL. (2018) reported ASSB cells with 184 Wh kg^{-1} using composite cathodes (NMC622, LPSCl, NBR, carbon additives) fabricated by doctor blade method and subsequent heating at $120\text{ }^\circ\text{C}$ under vacuum overnight. The wet-coated cathodes were mixed with NBR, while the dry-mixed cathodes contained no binder. Aspects such as the SE share and mass loading varied. Pouch cells in $80 \times 60\text{ mm}^2$ format were built and cycled. The separator was coated directly onto a graphite anode, and thin films with thicknesses of $88\text{ }\mu\text{m}$ (cathode) and $30\text{ }\mu\text{m}$ (separator) were produced. The presence of binder and lower SE shares led to poorer ionic contacts between the active material and SE, which resulted in lower capacities and poorer rate capabilities than the dry-mixed cathodes.

BATZER ET AL. (2022b) systematically evaluated the fabrication of sulfidic composite cathodes and SE separators. The cathode active material was NMC622 with an LNO coating. LPS was used as a SE in two varieties with different particle size distributions: one in the sub-micrometer range and one with approx. $70\text{ }\mu\text{m}$. Therein, two different binder systems, HNBR and PIB, are used, and p-xylene was chosen as a solvent. Under variation of the contents of each component, cathodes were fabricated by a sequential dry mixing step in a 3D shaker mixer and a subsequent wet mixing step in a dissolver. The slurry was applied by doctor blade on an aluminum foil on a heated metal plate. The coating was dried for 15 min at $70\text{ }^\circ\text{C}$. The sulfidic separator was only mixed in the dissolver and coated similarly. No subsequent drying step was applied here.

Electrochemical and mechanical tests of the samples were conducted, focusing on electrochemical impedance spectroscopy (EIS). The performance of the components was then tested in cells with indium as anode, resulting in a low rate capability with capacity retentions of 86.9 % in the first cycle and 42.5 % in the tenth cycle.

Further procedures were reported in similar studies, using binder-solvent systems to coat either thin composite cathodes or SE separators based on sulfidic materials in combination with suitable binder and solvent systems (JIMÉNEZ ET AL. 2016; CHOI ET AL. 2017; LEE ET AL. 2017; RIPHAUS ET AL. 2018; ZHANG ET AL. 2018; YAMAMOTO ET AL. 2018; TAN ET AL. 2019; OH ET AL. 2019; ZHAO ET AL. 2023). Besides wet coating and infiltration, dry coating of composite cathodes is widely researched but still in an early stage (BATZER ET AL. 2022a). An overview of challenges regarding all three types of processing paths was presented by CAO ET AL. (2020), highlighting the necessity of thin and stable separators. Further, the effects of different binders and carbon additives in the highly complex system of composite cathodes are discussed. To summarize the most important aspects, Table 3-1 presents all parameters available in the literature mentioned above.

Table 3-1: Summary of laboratory-scale wet coating and drying processes for sulfide-based components in literature.

Cathode active material	Solid electrolyte (SE)	Binder	Conductive additive	Solvent	Substrate	Coating tool	Drying temperature in °C	Drying time in h	Sheet area	Sheet thickness in μm	Source
-	Li_3PS_4 , $\text{Li}_{10}\text{GeP}_2\text{S}_{12}$	-	-	Toluene	Nickel	Doctor blade	-	-	1.5×1.5 cm^2	70; 90	Nam et al. 2015
LCO	$\text{Li}_6\text{PS}_5\text{Cl}$	PVDF	-	Ethanol; NMP	Al	Infiltration	180 (vacuum)	-	-	-	Kim et al. 2017
NMC622	Li_3PS_4	NBR, PVC	Super C65	THF	Al	Doctor blade	140	-	20×20 mm^2	70	Oh et al. 2017
MC111 + LiNbO_3	Li_3PS_4	SEBS, SBS	Acetylene Black	Heptane, Anisol	Al	Doctor blade	25	-	20×20 mm^2	70–100	Sakuda et al. 2017
NMC811	$75\text{Li}_2\text{S} \cdot 25\text{P}_2\text{S}_5$	NBR	Denka black	p-Xylene	Al	Doctor blade	RT; 60	1; 24	-	-	Lee et al. 2017
NMC622+ LiNbO_3	LPSI	PEP-MNB	Super P	Heptane	Al	Doctor blade	-	-	-	-	Choi et al. 2017
NMC622	$\text{Li}_6\text{PS}_5\text{Cl}$	NBR	SuperC65	Xylene	Al	Doctor blade	120	Over night	Pellets: $\phi 13$ mm, Pouch: 80×60 mm^2	SE: 30; Cathode: 88	Nam et al. 2018
-	LSPS	PIB, SBR, HNBR, PMMA, PEVA	-	Toulene	Mylar	Doctor blade	RT	13	-	20–40	Ripphaus et al. 2018
NMC811 + LiNbO_3	$\text{Li}_6\text{PS}_5\text{Cl}$	Ethyl cellulose	Carbon black	Ethanol	Al	Doctor blade	80	Over night	-	-	Zhang et al. 2018
NMC111 + LiNbO_3	$75\text{Li}_2\text{S} \cdot 25\text{P}_2\text{S}_5$	PEC, PPC	Acetylene black	1,2-dichloroethane, anisole	Al	Doctor blade	225 (vacuum)	0.5	-	200–300	Yamamoto et al. 2018
-	$\text{Li}_7\text{P}_3\text{S}_{11}$	SEBS	-	Xylene	Al, Teflon	Doctor blade	RT; 60	1; 6	200×50 mm^2	50	Tan et al. 2019
NMC622	Li_3PS_4	PIB, Oppanol	Super C65, VGCF	Toulene	Al, Mylar	Doctor blade	RT	Over night	SE: 1.13 cm^2 Cathode: 0.76 cm^2	SE: 20 Cathode: 30	Ates et al. 2019
-	$\text{Li}_6\text{PS}_5\text{C}$	NBR	Super C65	DBM	Al	Doctor blade	60; 120 (vacuum)	-	-	-	Oh et al. 2019
-	$\text{Li}_6\text{PS}_5\text{Cl}$	PVDF	-	Ethyl-Acetat	-	-	-	-	Pellet	100–120	Wang et al. 2020
NMC622	Li_3PS_4	HNBR; PIB	Super C65	p-Xylene	Al	Doctor blade	70	0.25	-	-	Batzler et al. 2022
-	$\text{Li}_{0.88}\text{GeP}_{1.96}\text{S}_{11.88}\text{Cl}_{0.12}$	-	-	Toluene	-	Doctor blade	-	-	-	8	Zhao et al. 2023

3.2 Concepts for Process Chains in the All-Solid-State Battery Production

Besides literature about experimental doctor blade coating and small-scale fabrication, numerous publications are considering potential upscaling scenarios theoretically. The most significant ones are discussed in the following.

HU (2016) was one of the first to address the difference between laboratory-scale and industrial-scale fabrication of ASSBs, pointing out the advantage of wet coating processes to produce thin films compared to cold pressing. It was stated that a subsequent laminating step can be applied to form bipolar electrodes. This publication concludes that LIB processes are suitable for upscaling and controlled production. A further consideration of processes was not detailed.

In 2017, a detailed description considering diverse production paths was published by KERMAN ET AL. The focus was on oxide SEs and their challenges, highlighting the necessity of dense and thin films with minimal defects, such as cracks or microscopic grain boundaries. Therefore, a process flow diagram showing different techniques to form a dense oxidic SE was presented. Accordingly, oxidic precursors can be further processed by either creating a melt, dissolving them into liquid solvents, homogenizing a mixture by mechanical or thermal treatment, or growing a film by techniques such as PVD or CVD. Sulfide-based materials were considered, given the advice of a controlled atmosphere concerning H₂S development in ambient atmospheres and the advantage of cold pressing for dense small pellets. Not all suggested technologies for oxides are also applicable to sulfides.

The idea of identifying different paths for the production of ASSBs was further elaborated by SCHNELL ET AL. (2018). Therein, two types of cell designs were distinguished: the cathode-supported design and the three-layer-matrix structure derived from solid oxide fuel cells. Based on the cell design, the SE and requirements for upscaling, process chains for the SE separator, the composite cathode, and the anode were derived. An example of the SE separator fabrication is shown in Figure 3-2. For sulfide-based ASSBs, the forecast was made that LIB production processes can be adapted to the material in contrast to oxides, where processes from fuel cell production will be required. For both components, SE separator and composite cathode, multiple other technologies might be suitable for upscaled production, e.g., dry coating processes such as extrusion or powder-based technologies or aerosol deposition. In further work, the costs of oxide-based ASSB fabrication were calculated (SCHNELL ET AL. 2019), and the financial comparison to the production of LIBs in a bottom-up calculation was presented (SCHNELL ET AL. 2020). The work was summarized in the dissertation of SCHNELL (2020), including a methodology for strategic technology planning for ASSBs. Within the dissertation, possible technology chains for customized ASSB production scenarios were generated and evaluated from a technical and economic perspective.

FAMPRIKIS ET AL. (2019) emphasized the identification of suitable processing routes as one of the key issues in gaining fundamental knowledge of inorganic SEs. The suggested path in the publication contained a three-step fabrication of bulk solid-state batteries, divided into synthesis, densification, and integration. A further division was made to fabricate pellets by,

e.g., sintering and the coating route for sheet-type cells. However, no specific technologies were proposed.

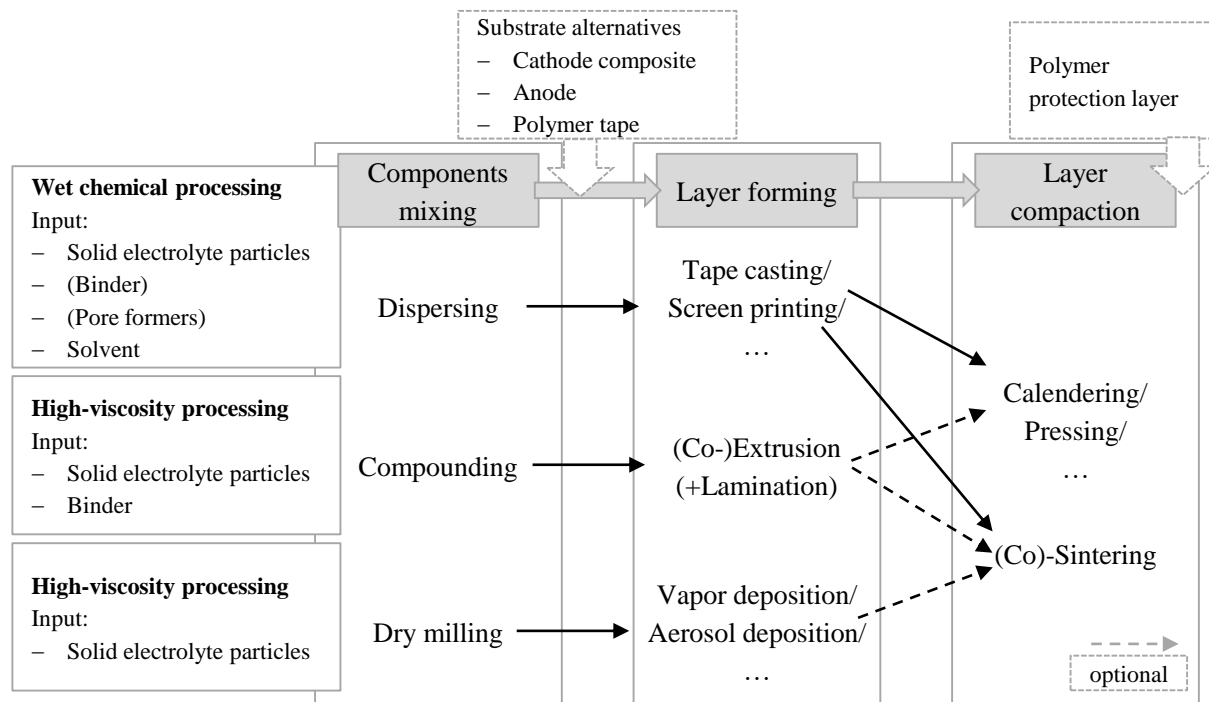


Figure 3-2: Schematic process chains for the SE separator fabrication. Replicated from SCHNELL ET AL. (2018).

DUFFNER ET AL. (2021) reviewed several post-LIB cell concepts and their compatibility for fabrication in a LIB production infrastructure. Therein, solid-state LiM batteries, lithium-sulfur, and lithium-air batteries were discussed. The battery technology chains were compared along the whole electrode production, cell production, and conditioning. While sodium-ion batteries were shown to have the identical processing route to LIBs, new manufacturing equipment is required for every post-LIB cell technology, at least in a few process steps.

TAN ET AL. (2022) provided a perspective on different aspects of the upscaling process for sulfidic solid-state batteries. Besides costs for the SEs and their synthesis, summaries of current fabrication scenarios and requirements for the upscaling from laboratory to pilot scale were given. An outlook on the electrode and SE separator production, as well as cell assembly strategies, was discussed. Future challenges were pointed out and underlined with experimental results.

Further reviews on scalable processes were given in the literature (HUANG ET AL. 2021; LEE ET AL. 2021; KIM ET AL. 2022). To bridge the gap to technologies already scaled up for LIB production, an overview of process studies for the wet coating and drying process is presented in the following section.

3.3 Electrode Production of Conventional Lithium-Ion Batteries

Conventional LIB electrodes are manufactured in a continuous roll-to-roll process. The aim of this industrial process is to produce homogeneous, defect-free electrode sheets with the desired

electrochemical properties and a defined morphological structure (cf. Section 2.3). In order to ensure this, the influence of the process parameters on the properties of the cell must be determined and then measured and controlled during the subsequent production process. (KAISER ET AL. 2014; GÜNTHER ET AL. 2016) Therefore, the following subsections introduce relevant literature on process-product correlations for LIB components. The literature on the mixing procedure is not analyzed as it is out of the scope of this dissertation (cf. Section 1.2).

3.3.1 Wet Coating Process

In 2013, SCHMITT ET AL. published a study focusing on characterizing the process window for slot die coating. The goal was to identify stable coating conditions with increasing velocities up to 60 m min^{-1} without inducing defects for lithium-ion graphite anodes. Changes in the surface were characterized by using an in-line laser scanner. As a result, they presented that large particles and agglomerates cause film break-ups at small film thicknesses independent of the coating velocity. In the following publication, SCHMITT ET AL. (2014) investigated edge effects in stripe and pattern coatings with a water-based anode by varying the coating gap, speed, and wet film thickness and keeping the geometrical and rheological parameters constant. In their conclusion, they stated that minimizing the dimensionless gap ratio G_w^* (Equation (11)) was beneficial to coating an optimized edge. Moreover, it was shown that the variation in the coating speed did not influence the edges. However, the investigation of the viscoelastic slurry behavior, the surface tension, or the shear thinning behavior was recommended to be conducted in further studies.

The formation of edges in intermitted coatings in water-based anodes was further analyzed by DIEHM ET AL. (2020b). The focus was on the coating speed and the wet-film thickness as influencing parameters on the shape and length of falling and rising edges. Again, it was proven that the coating speed had no influence on the edge formation.

DAVID ET AL. (2018) classified defects that arise during coating into four categories: agglomerates, pinholes, line defects, and metal particle contamination. To simulate coating defects resulting from a slot die process, these types of defects were induced into a cathode coating with the subsequent cycling of full cells to investigate the impact on the degradation of LIB cells according to the defect. As a result, line defects were shown to have a significant impact on the cell degradation. A detailed review of the coating process for LIBs was published by REYNOLDS ET AL. (2021).

Most of the available studies on the wet coating process are considering the slot die as favored technology to produce industrial-scale LIB electrodes. However, general observations might help the development of a suitable coating process for ASSB components.

3.3.2 Drying Process

The drying process for LIBs has been intensively studied and further developed. Relevant literature is discussed in detail in the following.

WESTPHAL ET AL. (2014) investigated the impact of convection drying on electrode performance of the graphite anodes. A pilot-scale roll-to-roll dryer with three sections was used to analyze the influence of the drying process on the elasticity, electrical volume resistivity, and adhesion strength in a temperature range of 80 °C–130 °C. Besides the temperature and drying time, the nozzle speed and airflow were varied to gain insights in the demixing of components inside the anode coatings. Gradients in the binder distribution were influenced by a combination of driving force intensity and time to mobilize particles.

In 2016, JAISER ET AL. investigated the drying process of LIB electrodes using two conveying blowers, one operating at 100 % of the blower frequency (high drying rate, HDR) and the second at 25 % (low drying rate, LDR). With this test setup, the drying behavior was investigated by varying the drying rate as a function of the convection. The weight of the samples was determined gravimetrically before and after additional drying for 12 hours at 76.5 °C in a vacuum oven. This allowed the solvent loading of the sample to be calculated. Furthermore, the adhesion of each sample was measured using a 90 ° peel test device detaching the film from the copper foil. Further investigations were carried out using energy-dispersive X-ray analysis (EDS), revealing the binder content at the top and bottom surfaces of the samples. The results presented that heavy binder distribution gradients were induced by high drying rates based on the two fundamental processes of capillary action and diffusion. Moreover, the characteristic stages of film shrinkage were defined, showing a top-down film consolidation. Interestingly, the binder migration was found to proceed after the termination of the film shrinkage.

This field of study was extended by a publication of the same group trying to aim for industry-related electrode production (JAISER ET AL. 2017). The heat transfer coefficient α comprised 75 W m⁻² K⁻¹, and the drying rate was set to 1.17 g m⁻² s⁻¹ for one minute. This experimental setup allowed quasi-isothermal solvent evaporation. The microstructure of the film was examined during the drying process using a cryogenic SEM. It was shown that small pores have a higher degree of saturation than large pores, which could be attributed to the capillary pressure-driven transport of the liquid phase from larger to smaller pores. The finding that the saturation of the pores is higher at the surface than in the sub-stratified region also supports the theory that capillary pressure-driven transport plays a significant role in the drying process.

MÜLLER ET AL. (2017) researched the drying of graphite anodes. The electrodes were coated with the doctor blade method, resulting in an average dry thickness of 70 µm and thicker samples of 400 µm for binder distribution investigations. Copper foil served as the substrate. Drying rate variations were induced by adjusting temperature and fan speed in a convective dryer. Cross-sections of electrode films were created using an ion beam cutter to study the binder distribution. However, SEM investigations showed that the polymer binder degraded due to the electron beam. Hence, samples were examined for the same duration for comparability. EDS analysis revealed the fluorine fraction, indicating binder distribution. Higher drying rates increased the fluorine concentration of the PVDF binder at the surface but decreased towards the current collector.

The analysis of drying conditions on the segregation in graphitic anodes was further researched by WESTPHAL & KWAVE (2018). Besides the influence of the drying temperature on the adhesion strength and relative resistance of the anodes, the PVDF binder concentration was traced by its fluorine share by EDS measurements along a cross-section. A much higher fluorine concentration at the top of the samples was found that increases with the amount of heat, proving binder migration.

KUMBERG ET AL. (2019) conducted experiments using water-based anodes on copper foil to identify different phases of solvent evaporation and wet film shrinkage. Isothermal drying conditions were achieved using a periodically moving hot plate and a slot nozzle dryer. The drying temperature was selected to correspond to a specific drying rate at a defined air flow rate and the drying air's water content. Drying curves for four different areal-loaded anodes were generated by weighing the remaining solvent content. Results in this publication showed that the drying process was dominated by the pore size distributions, especially at the end of film shrinkage. Afterward, the drying rate was constant, while the capillary network is mandatory for the evaporation of solvents. This hypothesis was proven for thin electrodes, while thicker electrodes showed a different behavior due to their higher complexity of the pore network. In the following, the mass ratio of solvent to solid content was determined, indicating the point at which no further volume change occurred during drying, signifying the end of the wet film shrinkage. Moreover, it was shown that drying rates up to $15 \text{ g m}^{-2} \text{ s}^{-1}$ can be applied without significantly cracking of the electrode coating.

In summary, the presented literature reveals the depth of research for the drying process of LIB components. A lot of prevailing phenomena are based on fundamental aspects such as capillary forces and diffusion. Although no study on sulfide-based ASSBs was conducted so far, the knowledge of LIBs can support the initial test set ups and result interpretations of ASSBs.

3.3.3 Adhesion Measurements

The adhesion between the components of a battery cell significantly influences the cycle life (cf. Subsection 2.3.3). In the following the most important studies are described.

WESTPHAL ET AL. (2014) investigated the influence of drying parameters on the electrochemical and mechanical properties of anodes. The anode was fabricated by roll coating on a $10 \mu\text{m}$ thick copper foil. The dried anodes had a composition of 91 m% graphite, 3 m% PVDF binder, and 6 m% conductive carbon black. The coatings were convectively dried at different temperatures. A material testing machine from was used for the adhesion strength measurements. When investigating the influence of the drying temperature, the temperature was varied between $80 \text{ }^\circ\text{C}$, $110 \text{ }^\circ\text{C}$, and $130 \text{ }^\circ\text{C}$. A higher temperature led to a decreasing adhesion strength. As the adhesion force decreased, also an increase in electrical resistance was observed. WESTPHAL ET AL. (2014) proved in their study that drying parameters highly influence the electrical conductivity and the adhesion strength between electrode and substrate. Accordingly, segregation of the binder in the electrode can occur during the drying process, leading to binder migration. The results indicate a mass-loading dependent drying temperature profile to maximize the adhesion strength.

HASELRIEDER ET AL. (2015) investigated adhesion forces between electrodes and substrate materials using the same experimental setup as in WESTPHAL ET AL. (2014). Cathodes (NM111, PVDF, carbon black) and anodes (graphite, PVDF, carbon black) were fabricated with NMP as a solvent for the experiments, and the adhesion force was measured. In addition to the adhesion force, the degree of electrode area removed from the substrate (DOR) was recorded, indicating the fracture type (cf. Figure 2-8). According to WESTPHAL ET AL. (2014), a DOR greater than 95% is dominated by adhesive fracture; partial to complete cohesive fracture may be present below that. The DOR was determined by taking images of the samples after the adhesion measurement, which were examined by pixel analysis. The sampling rate, compression force, compression speed, compression dwell time, and peel speed were varied in the experiments. Cathodes with a mass loading of 90 g m^{-2} and a film thickness of $65 \mu\text{m}$ were used for these studies. The adhesion forces between the cathodes and the aluminum substrate ranged from 1000 kPa to 1400 kPa. For the anodes, adhesion forces between 160 kPa and 480 kPa were measured at mass loadings between 85 g m^{-2} and 95 g m^{-2} for binder contents of 5 to 8 m%, respectively.

KUMBERG ET AL. (2019) investigated the drying of anodes produced on copper foil using a doctor blade process. The dispersion was prepared by dissolving graphite, conductive carbon black, and a binder system of SBR and carboxymethyl cellulose binder (CMC) in water. Drying was performed with a hot plate and a slot nozzle dryer. Adhesion measurements were made using a 90° peel test fixture that the measured force in N/m. The reference specimens had an average adhesion force of 16.2 N m^{-1} during the mass loading tests. A decrease in adhesion force was observed with increasing mass loading. One reason for this was suggested to be the increasing length of the diffusion paths. Due to the capillary action in the pores formed during the drying of an electrode, binder migration occurs, as described in Subsection 2.3.3. With increasing thickness, the capillary network becomes longer and more complex, which means that the diffusion compensation of the binder requires more time. Thus, with thicker anodes, there is less binder at the bottom surface than in thinner anodes, so the adhesion force is lower.

MEYER ET AL. (2020) investigated the influence of densified cathodes on the adhesion force between the two components. The doctor blade coating process used a dispersion with a solid content of 65 m% and the solvent NMP. With increasing mass loading between 79 g m^{-2} and 283 g m^{-2} , the adhesion force between the cathode and current collector decreased from 1500 kPa to 1000 kPa. With decreasing porosity by increasing compactness using a hydraulic press, a decrease in adhesion force was observed for NMC specimens with drying temperatures of 25°C , 60°C , and 90°C at a mass loading of 79 g m^{-2} .

BILLOT ET AL. (2020) varied process parameters to investigate the relationship between the manufacturing process of LIB anodes and their adhesion strength. Copper foil was used as the substrate material for the experiments. The anodes were prepared from a dispersion consisting of 45 m% NMP as a solvent and a 55 m% solid content of graphite and binder (PVDF). The binder content in the solid was varied between 5 m%, 7 m%, and 9 m%. The coating was carried out using a doctor blade process. The coatings were dried using an infrared dryer at 55°C , 75°C , or 95°C . Adhesion force measurements were performed using a tensile tester. A

decrease in adhesion force was observed with increasing copper surface roughness. The high particle size of graphite compared to the surface roughness of the copper foil explained these results. Accordingly, the graphite particles were able to form fewer mechanical anchorage points with the rough substrate than with smooth current collector foil. The surface tension was increased by electrical discharge pretreatment of the copper foil. Thus, the surface polarity was increased, which affects the adhesion ability in connection with polarizing binders. A decrease in adhesion strength was measured with increasing coating thickness. This could be explained by binder migration, capillary action, and back diffusion of the binder during the drying process described by (KUMBERG ET AL. 2019). The film thickness variation due to calendaring resulted in a decrease of the adhesion force with decreasing film thickness. This resulted from the flow of the electrode material to the side during the densification process. In this process, shear stresses occur at the interface due to the different material expansion properties of the anode and substrate, which reduces the adhesion force.

One of the first publications on the systematic evaluation of the adhesion strength for sulfide-based ASSB components was shown by BATZER ET AL. (2022b). Composite cathodes were fabricated with NMC622 (coated and uncoated), LPS, *Super C65*, and HNBR or PIB as binders. The binder was dissolved in p-xylene. It was coated onto aluminum foil and heated at 70 °C during coating and an additional 15 min after. The SE fabrication was done in the same way, but no heat was applied during coating. In the following, the binder, SE, and their amount inside the composite cathode, as well as the carbon black share, were varied. Only the type of binder and their share were changed for the SE separator. As a result, it was presented that HNBR and higher binder contents led to a higher adhesion strength than PIB and lower binder contents.

In summary, several publications on the adhesion measurements of LIB electrodes are available, highlighting the importance of this characterization method for evaluating the fabrication process. Moreover, the diversity of test setups and investigated process and product parameters show this research field's complexity. Therefore, the investigation of ASSB components concerning their adhesion strength is inevitable.

3.4 Derivation of Need for Action and Objective

The presented literature provides an overview of the current state of the art in three major research fields by examining relevant literature in a descriptive study. Currently, research on ASSBs primarily focuses on electrochemistry and laboratory-scale cell tests, as no publications or dissertations detail production techniques, making process knowledge unavailable. The film fabrication on a laboratory scale involves mixing, coating, and drying, focusing on coin or small single-layer pouch cells (cf. Section 3.1). However, more comprehensive and systematic studies must be conducted to evaluate the influence of production parameters on the final cell components. Moreover, implications coming from material requirements on the design of machinery on a large scale are omitted.

Numerous publications have attempted to theorize production routes for ASSBs (cf. Section 3.2). Although multiple process chains are presented, a critical omission lies in selecting decision criteria to choose process chains, which should ideally be based on empirical data. Additionally, these publications overlook the in-depth consideration of specific material properties, a crucial aspect of practical implementation.

Conversely, studies on the coating and drying processes for conventional LIBs have seen considerable progress over the past decade. These studies rely on experimental approaches and delve into analytical and data-driven methodologies, providing a more comprehensive understanding of the processes (cf. Subsection 3.3.1). These publications focus on slot die coating, the predominantly applied tool used in industrial coating lines. However, this dissertation focuses on doctor blade coating since ASSB slurries are at an early research stage. For this reason, the presented literature is only partly relevant to this thesis. Nevertheless, the impact of process parameters and defects on the coatings of a LIB cell is important to understand and might be transferable to ASSBs. In addition, doctor blades are often used on pilot lines in research institutes or small production lines instead of slot dies. However, literature on the mechanisms of doctor blades is scarce. Limited access to innovative materials such as sulfide-based SEs and small test amounts make it more feasible to use the doctor blade. Therefore, the experimental investigation of sulfide-based ASSBs with the doctor blade as coating technology supports the production research and can analyze the fundamental behavior of new recipes and parameters on roll-to-roll machinery.

For the drying process and adhesion tests, insights into the methodological approach and the analysis of LIB components from the literature help gather and investigate data on ASSB components (cf. Subsections 3.3.2 and 3.3.3). Since numerous detailed publications in this field are available, this knowledge can be used to describe similar phenomena and correlations in ASSBs.

By comparing the LIB and ASSB technology, a noticeable gap becomes apparent, highlighting the urgent need for process research on sulfide-based materials to accelerate the ramp-up in ASSB production. Bridging this gap from laboratory to pilot scale would require addressing the limitations in the current research, exploring new production techniques, and considering the unique material properties that distinguish ASSBs from conventional LIBs. Only through such

concerted efforts can the full potential of ASSBs be realized and effectively integrated into the market.

This dissertation endeavors to enable a scalable wet coating process for sulfide-based ASSBs with applicability in industrial production. The outcomes of this research are presented in seven publications, each of which will be succinctly summarized in the subsequent section.

4 Results

The present dissertation is a publication-based work containing seven publications addressing the four introduced subgoals in Section 1.3. These subgoals are further developed from the state of the art (Chapter 3) and detailed in Section 4.1. In Section 4.2, all publications of this thesis are summarized, and the author's contribution is given at the end. The individual publications on which this thesis is based have been produced in collaboration with other scientists under the leadership of the author of this thesis and have been published in highly recognized peer-reviewed journals. Lastly, Section 4.3 contains qualification aspects of the roll-to-roll coating machinery showing the complete production concept and machine design.

Considering the aspects of Subsection 2.2.3, sulfide-based materials show clear advantages over other SE materials, including the highest ionic conductivity, but even more importantly, the adaptability of industrially applied manufacturing processes in LIB Gigafactories. For this purpose, the investigation of scalable technologies for sulfide-based materials represents the central aspect of this work. Due to their advantageous properties, the materials LPSCl (cf. p. 11) and LPS ($\text{Li}_3\text{P}_7\text{S}_{11}$) are processed in the experimental investigations (cf. Subsections 4.2.3–4.2.7).

4.1 Research Approach and Assignment of the Publications

Based on the derivation of the need for action (Section 3.4), seven publications were published and assigned to the subgoals (Subsection 1.3.1) to build the frame for this dissertation (cf. Figure 4-1). The subgoals were elaborated based on Chapters 2 and 3 and are connected to one another as stated in the following.

Subgoal 1: Process Planning

Modeling of process strategies and development of characterization methods in the production of sulfide-based components

Subgoal 1 lays the foundation for all further investigations of this work. It includes modeling process strategies to evaluate the applicability of suitable production technologies to sulfide-based materials. The scalability of these technologies is highly important, and therefore, aspects such as cost-effectiveness and high throughput are considered. Further, the goal is to set up a holistic and expandable model, including all components of sulfide-based ASSBs (composite cathode, SE separator, and anode), technologies, and costs. As a second aspect, the material-specific requirements of sulfides (cf. Subgoal 2) are used to identify characterization methods since unique material properties lead to the need for new measuring methods in this field.

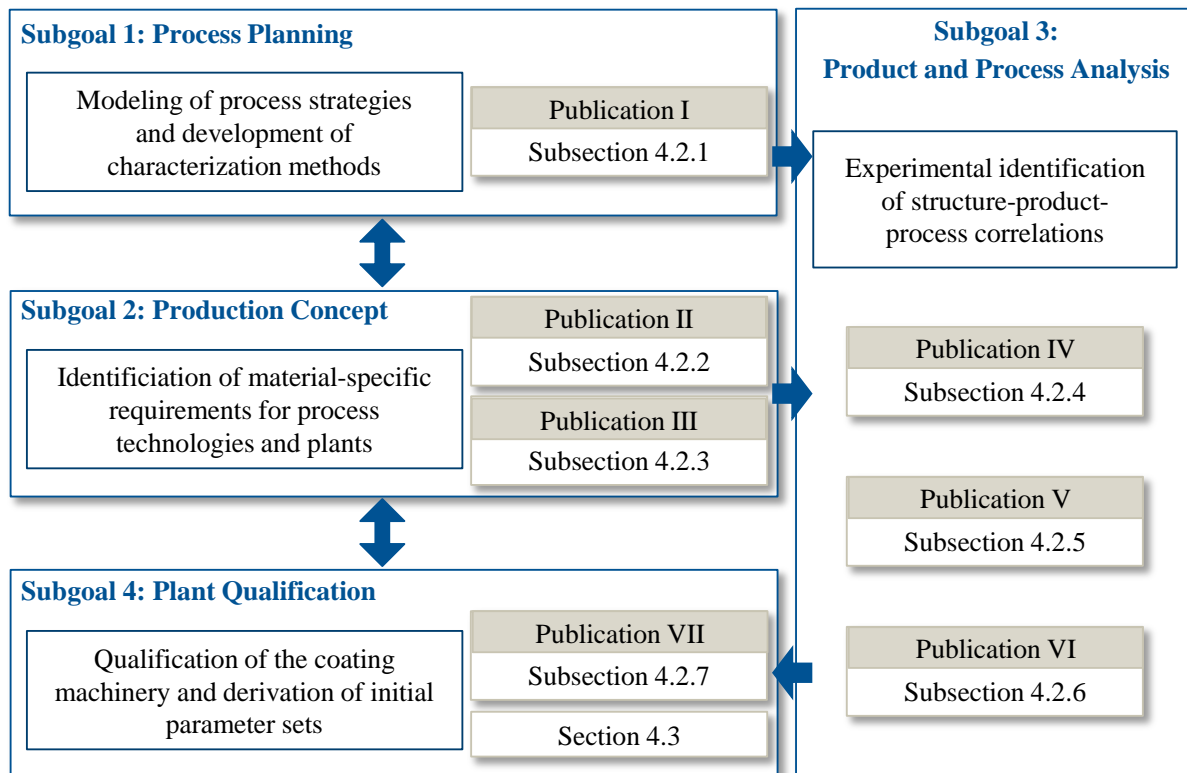


Figure 4-1: Overview of the structure of the subgoals and the respective publications in the presented dissertation.

Subgoal 2: Production Concept

Identification of material-specific requirements for process technologies and plant engineering

Subgoals 1 and 2 are strongly related to create a production concept including suitable techniques to fabricate the sulfide-based components. The requirements are, by implication, influenced by material-specific criteria, respective characterization methods, and their suitability to be integrated into industrial machinery. The goal is to create a pilot-scale machinery for the coating process of sulfide-based ASSBs. A sulfide-specific concept is designed by describing necessary changes to LIB machinery and comparing different production environments to prevent the formation of H_2S . To achieve this, the precise investigation of H_2S formation in dependence on the sulfidic material and the surrounding atmosphere needs to be examined. Since the material is present in different states (powder, wet film, dry film, densified film) along the process chain, the influence of this aspect is analyzed.

Subgoal 3: Product and Process Analysis

Experimental identification of structure-product-process relationships

Based on the first two subgoals, this dissertation's third part focuses on the product and process analysis. Subgoal 3 is based on experimental investigations with sulfide-based materials. The aim is to investigate structure-product-process correlations and gather empirical data. The focus lies on the wet coating process by doctor blade and the drying process as well as characteristic product features such as coating defects, binder migration, and adhesion strength, which describe the morphological structure. In order to analyze the scalability of these processes, the mixing process is scaled up to a certain amount of slurry and then considered constant to follow

the thesis frame discussed in Figure 1-1. The investigations feature theoretical and experimental approaches.

Subgoal 4: Plant Qualification

Qualification of the pilot-scale plant and derivation of the initial parameter sets

The last subgoal aims to transfer the previously obtained results of the structure-product-process correlations from the laboratory to the pilot scale. A summary of the researched process steps is given, evaluating the feasibility of LIB processes, i.e. wet coating and drying, for sulfide-based materials. Challenges and key aspects of upscaling are highlighted. The most important product and process parameters are used to design and construct the final coating roll-to-roll machinery. The setup and qualification of the roll-to-roll coating machinery at the *iwb* are conducted, and the initial parameter set to start the experiment on the pilot scale is derived.

4.2 Cumulative Overview of the Related Publications

The following publications address a holistic approach in which scalable processing routes, machinery, product requirements, and process parameters for sulfide-based ASSBs are researched and discussed according to Figure 4-1. The main aspects and findings of the publications are presented in the following subsections.

4.2.1 Publication I: Scalable Processing Routes for the Production of All-Solid-State Batteries—Modeling Interdependencies of Product and Process

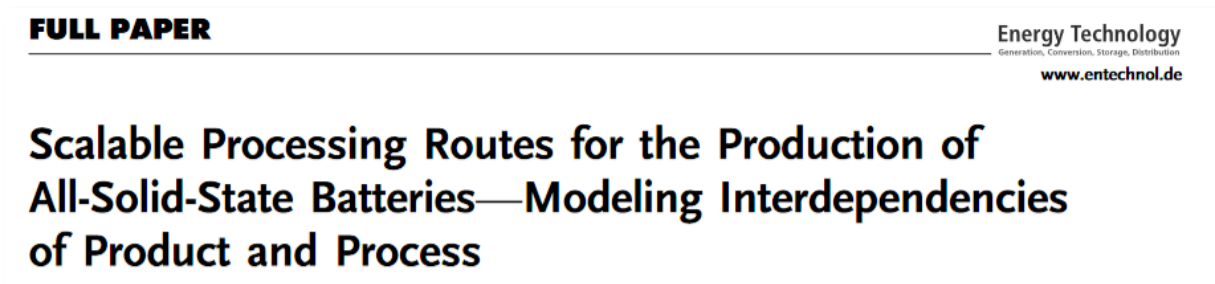


Figure 4-2: Header of Publication I published in the Journal Energy Technology.

The first publication of this cumulative dissertation focuses on describing the ASSB components, relevant production technologies for fabrication, and economic aspects in five system models, which are linked to each other. Therefore, a complete picture of the product and processes was drawn using the graphical modeling language *SysML*. The model was built from three blocks: system requirements, structure, and behavior. The last two blocks contained sub-models, where detailed information about every product variant, technology, and cost is stored. The model can be scaled to implement further information, new findings, and other products or production technologies.

Within the model, production technologies were connected to product- and process-relevant aspects. These served as input for an automated tool, which generated technology chains to fabricate each component in an ASSB cell. The user needed to give input about different frame

conditions, e.g., the annual capacity of the battery factory, cell format, cell type, materials, and a weighted focus on quality, time, or maturity of technologies. The user could optionally give more detailed input, e.g., determining the share of SEs in a composite cathode, the thickness of sheets, or the ratio of the cathode to anode capacity. Exemplarily, the generation of technology chains was conducted for sulfidic ASSBs. The key achievements and findings of the publication are as follows:

- Creation of a product model containing relevant information to derive requirements of ASSB components for their manufacturing process
- Description of the manufacturing process through technology functions, which pictured the task to be fulfilled by production technologies, e.g., materials mixing or layer fabrication
- Identification of numerous production technologies from differing fields, such as solid oxide fuel cells, used to fabricate components of ASSBs
- Collection of the technologies in a technology model, description of relevant process parameters, and linkage to essential characteristics of each technology
- Correlation between the five models of the system structure (product, technology functions, technology, technology chains, economics) and system behavior (technology identification, technology planning, technology assessment)
- Set up of an automated Excel tool to automatically find the most suitable technology chain according to the production task of the user's input
- Generation of relevant technology chains to manufacture sulfide-based ASSBs with a focus on high throughput, revealing that the wet coating process was the most suitable technology to fabricate thin films due to high maturity, low costs, and short production times

Contributions of the authors

Célestine Singer planned and created the method, the SysML model, and the automated Excel tool within her master's thesis. Joscha Schnell planned and coordinated the framework of the thesis. Célestine Singer analyzed the data and discussed the findings with Joscha Schnell. The manuscript was written by Célestine Singer and Joscha Schnell. It was edited by Gunther Reinhart. All authors commented on the results.

4.2.2 Publication II: Plant Technology for the Industrial Coating Process for Sulfide-Based All-Solid-State Batteries



Available online at www.sciencedirect.com

ScienceDirect

Procedia CIRP 104 (2021) 56–61



www.elsevier.com/locate/procedia

54th CIRP Conference on Manufacturing Systems

Plant Technology for the Industrial Coating Process for Sulfide-Based All-Solid-State Batteries

Figure 4-3: Header of Publication II published in the Journal Procedia CIRP 104.

The second publication described the plant technology for roll-to-roll machinery based on the requirements of sulfidic materials for the wet coating process. This study presented the initial investigation of the hydrogen sulfide (H₂S) formation during the hydrolysis process of sulfidic SEs. The primary focus was to address workers' occupational safety concerns in the production environment. Given the variation in workplace H₂S limits across different countries, the design of production facilities needed to be tailored to comply with local regulations. Therefore, the time-weighted average (TWA) exposure over a designated period (8–10 hours per day) was set to 5 ppm, and the short-term exposure limit (STEL), which restricts the H₂S concentration for a maximum duration of 15 minutes, was established at 10 ppm.

Furthermore, the study evaluated various housing concepts for machinery, considering their advantages and disadvantages. One such concept is a microenvironment, characterized by a system where the worker is completely isolated from the machine and can only interact with the inner components through gloves and locks. Incorporating different sensor types and data processing of their recorded values were also essential aspects of the research.

The publication concluded with an economic analysis considering using of different inert gases within the microenvironment and the associated costs of maintaining a dry room. These costs were compared by normalizing the machine's hourly rate over the water concentration in nitrogen, argon, and dry air. This comprehensive study aimed to contribute to the enhanced safety and efficiency of the production process, paving the way for further advancements in this field.

Key findings and results in this publication are summarized as follows:

- Identification of two aspects to describe the safety in production environments of sulfidic ASSBs concerning the H₂S formation, including occupational safety (depending on the legal regulation) and product quality (depending on the material)
- Derivation of the technical design for a scalable wet coating machinery from the safety aspects considering two significant aspects: the housing of the machinery and the sensor technology

- Discussion of three plant concepts: Dry room, known from conventional LIB production, mini-environment (the machine and the working places are housed), and microenvironment (only the machine is housed)
- Selection of the microenvironment concept due to the high significance of occupational safety and the protection of the coating over handling issues or the need for additional inertization systems
- Development of a concept for the microenvironment, including positioning considerations about sensors inside the housing and required access to the machine due to processing, handling, cleaning, or maintenance
- Choice of sensors according to limitations regarding the cross-contamination potential of solvents with H₂S sensors and their dew point and temperature limits
- Conduction of an economic calculation to evaluate different possibilities for the choice of gas inside a microenvironment with their respective volume flow through the system. The calculation was based on the machine's hourly rate as a function of the water concentration for nitrogen, argon, and dry air and the comparison to a dry room.
- The results showed that either the maximum volume flow of fresh gas inside the system is 0.6 m³ h⁻¹ or the water concentration has to be 4.6 ppm in nitrogen and 4.9 ppm in argon. Otherwise, using a dry room would be more cost-efficient. The importance of purification and reconditioning systems for microenvironments was highlighted. However, values for gas costs or electricity were considered in 2021 and might change the conclusion from a current point of view.

Contributions of the authors

Célestine Singer planned, coordinated, and executed the plant concept and economic calculation. Célestine Singer, Hans-Christoph Töpper, and Florian Günter discussed the findings. The manuscript was written by Célestine Singer and edited by Hans-Christoph Töpper, Florian Günter, and Gunther Reinhart. All authors commented on the results.

4.2.3 Publication III: Hydrolysis of Argyrodite Sulfide-Based Separator Sheets for Industrial All-Solid-State Battery Production



www.acsami.org

Research Article

Hydrolysis of Argyrodite Sulfide-Based Separator Sheets for Industrial All-Solid-State Battery Production

Figure 4-4: Header of Publication III published in the Journal ACS Applied Materials & Interfaces.

The third publication is intended to augment the safety aspects detailed in the second paper. A detailed experimental analysis was conducted to quantify the hazards from hydrolysis of the

sulfide-based SE. Therefore, the argyrodite LPSCl (cf. Section 2.2) was used to fabricate thin SE separator films with a thickness of 40–80 μm . First, a baseline was created to investigate the reaction velocity of water with the SE at different dew points. Afterward, different material states of the LPSCl, which would also occur in production, were exposed to dew points between $-50\text{ }^{\circ}\text{C}$ and $+10\text{ }^{\circ}\text{C}$ using raw powder, undensified, and densified sheets to measure the H_2S formation rate per area in $\text{ppm min}^{-1}\text{ cm}^{-2}$.

Moreover, the sheet area and the fan's speed, which distributes the air inside the desiccator, were varied to measure the influence. The effects of hydrolysis on the product quality were determined by measuring the ionic conductivity of the material and investigating changes in the microstructure of the SE. In the end, the publication revealed the implications of the reactivity of sulfidic materials for large-scale production along the processes of mixing, wet coating, drying, and calendering. Key results and conclusions of this publication are summarized in the following:

- Densified sheets showed a slower reaction of H_2S than uncompressed sheets, leading to the conclusion that the pore surface significantly influences the formation of H_2S . The thickness of the sheets, however, did not impact the H_2S concentration.
- The area of the sheets showed a high influence on the H_2S formation rate, while the fan's speed inside the desiccator did not cause a more pronounced H_2S formation.
- The most important aspect was the dew point, respectively the water concentration, in the production atmosphere. The formation rate was proven to be exponentially dropping in the same way as the water concentration over dew points from $+10\text{ }^{\circ}\text{C}$ down to $-50\text{ }^{\circ}\text{C}$. At $-40\text{ }^{\circ}\text{C}$, the H_2S formation rate decreases to zero, showcasing that these dew points might be low enough to prevent any formation of hazardous H_2S .
- SE sheets, which were exposed to an atmosphere with a dew point of $-49\text{ }^{\circ}\text{C}$, showed that compared to a pristine sample, the ionic conductivity decreases slowly but noticeably after 1–2 h exposure. This result led to the conclusion that even though no H_2S is measured at dew points around $-49\text{ }^{\circ}\text{C}$, hydrolysis was still taking place and influenced the most important quality parameter of the argyrodite. Storage or time-consuming processes, therefore, should not be conducted under dry air but inert gas.
- In the case of the LPSCl exposure to ambient air (dew point $+10\text{ }^{\circ}\text{C}$), a heavy reaction occurred. The formation rate was extremely high, and the material was undergoing a chemical reaction, where lithium chlorine was formed and visible in SEM pictures on the surface of SE sheets. These compounds were not ionic conductive, indicating a reason for lower ionic conductivity after the hydrolysis.
- As implications for industrial production, relevant product and process parameters were listed, influencing the hydrolysis reaction process during production.

Contributions of the authors

Célestine Singer planned, coordinated, and executed the experiments. Hans-Christoph Töpper and Tobias Kutsch supported the experimental execution. Célestine Singer analyzed the experimental data and discussed the findings with Hans-Christoph Töpper. The manuscript was

written by Célestine Singer and edited by Hans-Christoph Töpper, Tobias Kutsch, Robin Schuster, Raimund Koerver, and Rüdiger Daub. All authors commented on the results.

4.2.4 Publication IV: Influence of the Slurry Composition on Thin-Film Components for the Wet Coating Process of Sulfide-Based All-Solid-State Batteries

The following publications IV-VI focused on collecting and linking empirical data from the morphological structure, intermediate products, and process. These three experimental studies investigated the wet coating and drying process of sulfide-based components of ASSBs. A quantitative data set was created to support the further upscaling composite cathodes and SE separators with technologies known from conventional LIB production. The gap between laboratory scale and a roll-to-roll process was addressed because of the limited publications and knowledge on the processing aspects. Publication IV, therefore, aimed to reveal correlations between the slurry composition and the behavior of the slurry during the doctor blade coating process leading to the final wet film.



Figure 4-5: Header of Publication IV published in the Journal of Energy Storage.

In this publication, two sulfide-based materials, which have attracted significant attention in research, were investigated. LPS and LPSCl were mixed with HNBR binder to produce different slurries with varying compositions regarding the solid and binder content in a toluene solvent-based dispersion. Composite cathodes containing the active material NMC622, the SE LPSCl, the binder HNBR, and the conductive carbon Super C65 were produced. First, the viscosity as the main parameter of the mixing and coating step was analyzed. Therefore, various slurries were mixed, and rheological data was measured to compare them to known properties from conventional LIB cathodes. In the next step, five SEs, purchased from different suppliers were compared. They differentiated in their synthesis method, particle size distribution, and morphology. The aim was to show the differences between those materials, especially visible in the color and particle size distribution, even though they possessed the same chemical formula.

Moreover, the study revealed film thicknesses and respective areal weights according to the gap height of the doctor blade. A wet film thickness was theoretically calculated. In addition, the geometric homogeneity focusing on edge profiles and the influence of the coating velocity on the thicknesses of the films were analyzed. With regard to a scalable process and its challenges, the following key findings support the further process development:

- LPS slurries showed a steep decrease in viscosity over higher shear rates, implicating the known phenomena of shear-thinning dispersion. However, they form a plateau at higher shear rates above $5\text{--}10\text{ s}^{-1}$. This behavior was not observed for LIB slurries before.
- LPSCI slurries also showed a shear-thinning character, but no plateau was formed. In contrast, the viscosity decreased further with higher shear rates.
- Adapting the solid contents and binder contents of both SE materials, the viscosity was approximated to those of LIB cathode dispersions, leading to the conclusion that the material is applicable in a wet coating process with doctor blades.
- The composite cathode slurry was adapted by varying the solid content to show similar viscosities as LIB slurries. However, SE and cathode dispersions require lower solid contents than LIB materials, resulting in higher solvent shares and unwanted toxic materials in the production process. The reason for this phenomenon was found to be the SE. The smaller the particle size distribution, the more solvent and binder are needed to stabilize the dispersion and produce a coatable slurry. These results followed the investigation of five different SEs of the chemical formula LPSCI, revealing each material's most beneficial composition of solid and binder content.
- In order to influence the geometrical homogeneity of the films, a higher binder content was required to prohibit the formation of heavy edges at coated films.
- The coating velocity significantly influenced the thickness of these films, especially for the cathode. Herein, two different solid contents behave controversially at increasing velocities up to 8 cm s^{-1} . A 50 wt% slurry showed a decreasing thickness at elevated velocities, while a 60 wt% slurry led to an increasing dry film thickness. However, the standard deviation of both dry films was within the same range, which led to no clear conclusion, although the median proved differing behavior.
- In summary, the sulfidic material was enabled for the wet coating process with doctor blades known from LIB production. However, the addition of SEs into the composite cathode required a highly adapted slurry composition in correlation with the particle size distribution of the powder material.

Contributions of the authors

Célestine Singer planned, coordinated, and executed the experiments. Stefan Schmalzbauer supported the experimental execution within his semester thesis (supervised by Célestine Singer). Célestine Singer analyzed the experimental data and discussed the findings with Stefan Schmalzbauer. The manuscript was written by Célestine Singer and edited by Stefan Schmalzbauer and Rüdiger Daub. All authors commented on the results.

4.2.5 Publication V: Fundamental Investigation on Drying Rates of Cathodes and Separators for Sulfide-Based All-Solid-State Batteries



Figure 4-6: Header of Publication V published in the Journal Drying Technology.

Publication V was a combination of theoretical and experimental results for determining of drying rates for the porous wet films of ASSB components. The subsequent drying process of wet films is necessary when a wet coating procedure with solvents is applied. This process step has the highest energy consumption and costs in LIB production since temperatures between 70–150 °C are required in multiple dryer sections. The drying rate is the most important parameter in this process to define how much solvent or water is evaporated per area of the wet film and time. With Equation (12), the mass flow of the evaporating solvent can be quantified as the drying rate. Since it is majorly dependent on the properties of the solvent, this parameter changes for ASSBs using non- or weak-polar solvents in comparison to LIBs.

The study, therefore, contained composite cathode (NMC622, LPSCI, HNBR) and SE separator (LPSCI, HNBR) films with different mass loadings to gain insights into the influence of this product parameter. The slurry, based on the solvent toluene, was coated with the doctor blade and dried in a glovebox oven. Theoretical calculated values for the drying rate were compared with experimental results and discussed, considering published knowledge about LIB drying rates. The primary outcomes of this publication are described in the following:

- The theoretically calculated drying rates of the composite cathode were $0.196 \text{ g m}^{-2} \text{ s}^{-1}$ for a mass loading of 120 g m^{-2} and $0.190 \text{ g m}^{-2} \text{ s}^{-1}$ for a mass loading of 208 g m^{-2} .
- Based on the properties of the SEs, experimental values for the drying rates were lower than for the composite cathode. Films with a mass loading of 55 g m^{-2} showed drying rates of $0.161 \text{ g m}^{-2} \text{ s}^{-1}$ and $0.156 \text{ g m}^{-2} \text{ s}^{-1}$ for mass loadings of 80 g m^{-2} .
- Thinner components with a lower mass loading showed higher drying rates at the beginning of the drying process but faster-decreasing values at the end. Reasons for this behavior were drawn on the transition from the constant rate period (CRP) at the beginning of every drying process to the falling rate period (FRP) and the end of the film shrinkage.
- The measurement of drying rates at 50 °C and 100 °C showed that values for the evaporation of toluene in both the composite cathode and the SE separator are higher

than for LIB electrodes known from the literature. Therefore, the assumption that the higher evaporation number of toluene compared to NMP or water led to faster evaporation was experimentally proven. Although this phenomenon could lead to lower drying times and temperatures in industry, the implications on the microstructure of the components and the development of a pore network need to be considered.

Contributions of the authors

Célestine Singer planned, coordinated, and executed the experiments. Lorenz Kopp supported the experimental execution within his semester thesis and work as scientific associate. Célestine Singer analyzed the experimental data and discussed the findings with Lorenz Kopp. The manuscript was written by Célestine Singer and edited by Lorenz Kopp and Rüdiger Daub. All authors commented on the results.

4.2.6 Publication VI: Drying Process of Sulfide-Based All-Solid-State Battery Components—Investigation on Adhesion Strength and Microstructural Changes

RESEARCH ARTICLE

Energy Technology
Generation, Conversion, Storage, Distribution
www.entechol.de

Drying Process of Sulfide-Based All-Solid-State Battery Components—Investigation on Adhesion Strength and Microstructural Changes

Figure 4-7: Header of publication VI published in the Journal Energy Technology.

As identified in Publications IV and V, the solvent share in the slurry of composite cathodes and SE separators needs to be higher than in LIB slurries. Therefore, more and different solvent is contained in the wet film of both components, leading to a varying drying behavior compared to LIBs.

As a sequel publication to the investigation on drying rates (Publication V), the content of Publication VI follows up on the results presented above by analyzing the impact of the drying process. The focus was on the experimental investigation of structure-product-process relations detailing the impact of the drying process on the adhesion strength and changes in the microstructure of composite cathodes and SEs. The prepared slurries contained toluene as solvent and HNBR as a binder system in both cathodes (NMC622, LPSCI) and SE separators (LPSCI) and were coated using a doctor blade. First, the drying curves of wet film from composite cathodes and SE separators were measured for each of the two mass loadings and drying temperatures of 25 °C (room temperature), 50 °C, and 100 °C to validate the evaporation behavior of toluene. After drying, the same samples were analyzed in adhesion tests using a z-tensile strength test in a uniaxial testing machine. Herein, the influence of the mass loading and the drying temperature on the adhesion strength was analyzed and discussed. Further, the

microstructure of adhesion and cohesion failures (cf. Subsection 3.3.3) after the adhesion test was investigated using SEM and EDS analysis. The role of binder and other particle migration is discussed within the publication. A summary of decisive results and findings is described in the following and valid for both the composite cathode and the SE:

- With increasing mass loading, the adhesion strength was decreasing, contrary to results known from LIB electrodes. However, the porosity of the films was not constant since a higher mass loading leads to less porosity. This observation was deduced from the fact that higher gap heights in the doctor blade lead to less shear, and, therefore, particles were not stressed as much as in smaller gap heights. Results herein revealed the strong correlation of porosity to gap height and adhesion strength to respective porosities.
- The adhesion strength was decreasing majorly at higher drying temperatures. This phenomenon is already known from LIB electrodes. However, thinner samples (with lower mass loading) were less sensitive than thicker samples since the decrease in adhesion strength is not significant.
- Starting at 80 °C, the cohesion failure was predominant with major residues left on the substrate of both components (cf. Figure 2-8).
- A heavy binder migration occurred inside the films measured by EDS at the top and bottom of the samples.
- The results were then compared to values from publications of LIB electrodes, leading to the conclusions:
 - The mass loading of composite cathodes was higher than that of LIB cathodes at the same thicknesses because of the additional SE. However, the adhesion strength increased with higher mass loadings for ASSB components. This observation is contrary to LIBs and can be explained with either 1) the lower porosities for higher mass loadings, 2) the longer drying time for thicker samples so that particles have time to sink inside the pore structure, or 3) the initial particle size distribution of LPSCI inside the cathode is approx. 1 μm leading to a different rearrangement behavior inside the component and, therefore, different distribution of the binder.
 - No higher temperature than room temperature was beneficial for adhesion strength. In contrast, the adhesion strength was only decreasing. This effect was even more pronounced for SEs.

Contributions of the authors

Célestine Singer planned, coordinated, and executed the experiments. Lorenz Kopp and Milot Aruqaj supported the experimental execution within their master's and semester thesis, respectively (both theses were supervised by Célestine Singer). Célestine Singer analyzed the experimental data and discussed the findings with Lorenz Kopp and Milot Aruqaj. The manuscript was written by Célestine Singer and edited by Lorenz Kopp, Milot Aruqaj, and Rüdiger Daub. All authors commented on the results.

4.2.7 Publication VII: Insights Into Scalable Technologies and Process Chains for Sulfide-Based Solid-State Battery Production



Figure 4-8: Header of publication VII published in the Journal Batteries & Supercaps.

The last publication in this cumulative overview closes the frame to a scalable production of sulfide-based ASSBs. It focuses on transferring the results of Publications I-VI to create a novel production sequence and provide key enabling challenges to scale up the production. An essential comparison was made between LIBs and sulfide-based ASSBs to discuss the “drop-in” feasibility of the latter into existing Gigafactories. Therefore, a detailed analysis of every process step, including cell assembly, such as cutting, stacking, and laminating, was given. Newly generated data from experimental trials were presented to highlight the most important production aspects. Moreover, necessary changes to LIB machinery were detailed to support the future development of roll-to-roll processes. The key findings of the publication are summarized in the following:

- The terms single- and multi-component fabrication were introduced to break up the strict division of conventional electrode production and cell assembly from LIB production. Since innovative technologies can be used to fabricate the components, a novel production sequence is necessary. Two of the most promising production chains were presented, showing one continuous and one discontinuous process.
- The addition of SE as a new component and as part of the composite cathode led to significant changes in the process steps mixing, coating, and drying.
- A major challenge in the production will occur at the densification step due to higher densification pressures needed compared to LIB production. The technologies’ capability and material requirements must be evaluated to find a suitable process.
- Precise handling and stacking will be necessary to enable thin coating thicknesses for the SE separator.
- Applying pressure on the full cell during cycling will pose major challenges for the material, cell holders, and the application of sulfide-based ASSBs in electric vehicles.
- The SPACe⁻ (Sulfidic Cell Production Advancement Center) at the *iwb* was presented as one of the first laboratories with a roll-to-roll machinery for sulfide-based ASSBs to conduct academic research at an industry-relevant scale.

Contributions of the authors

Célestine Singer and Lovis Wach planned, coordinated, and executed the experiments. Elena Jaimez-Farnham supported the experimental execution. Célestine Singer and Lovis Wach analyzed the experimental data and discussed the findings with Elena Jaimez-Farnham. The manuscript was written by Célestine Singer and Lovis Wach. It was edited by Elena Jaimez-Farnham and Rüdiger Daub. All authors commented on the results.

4.3 Qualification of the Roll-To-Roll Coating Machinery

Together with the last publication of this thesis, this section supports the validation of gathered information within this dissertation. After the conceptualization and identification of material requirements, the design and installation of a roll-to-roll machinery for the new laboratory at *iwb* was conducted within a joint project between the institute *iwb* and the company TUMint. Energy Research GmbH. The goal of this project is to build sulfide-based ASSB cells with 1–5 Ah capacity using roll-to-roll processes. Concurrently, a calender was purchased within this project to complete the plants available for component manufacturing. Therefore, the machines were designed and constructed with the companies Mathis AG (Switzerland) and MBraun GmbH (Germany). The qualification of the machinery includes the aspects of concept and design, installation, and operation. The two latter points were verified during the site acceptance test at *iwb*. The following subsections detail the machinery and production concept.

4.3.1 Production Concept

The production concept in the SPACe⁻ was set up for the large-scale component manufacturing on roll-to-roll processes for sulfide-based ASSBs. For the slurry mixture, which is scalable up to 2 liters, the dry mixture is first weighed and produced in a Speedmixer© in a sealed container (mixing laboratory at *iwb*). Afterward, the dry mixture is transferred to the glovebox, where the binder solution is added to fabricate the wet mixture in a disperser (cf. Figure 4-9). The slurry is forwarded to the coating and drying machine. The coating is analyzed using x-ray radiation at three points (substrate, wet film, dry film) to track the mass loading and thickness using the Scantech© system. After the densification in the calender, the coil or sheets are transferred to another glovebox and assembled to full ASSBs. The composite cathode and SE separator are entirely produced in a microenvironment under a constant atmosphere. This coater and calender atmospheres are designed to flexibly change between argon, nitrogen, and compressed dry air (CDA). Therefore, the coater and dryer are only operated with gloves to separate the operator from the material. The insertion and extraction of material are conducted either through airlocks or by using the transportation cart, which was specially designed for this application.

Moreover, a safety concept was developed to prevent the formation of H₂S at any time and ensure the workers' safety by several sensors inside and outside the machinery, as well as safety protocols in case of machine malfunction or other error cases. Sensors are coupled with the machinery so that in case of exceeding the maximum limit of H₂S concentration, an automated extraction of the production environment via the exhaust air takes place. The coater and

calender are closed systems, connected with gas purifiers to clean the used gas and circulate it back to the production place. The entire layout of the SPACe⁺ is shown in Figure 4-10.

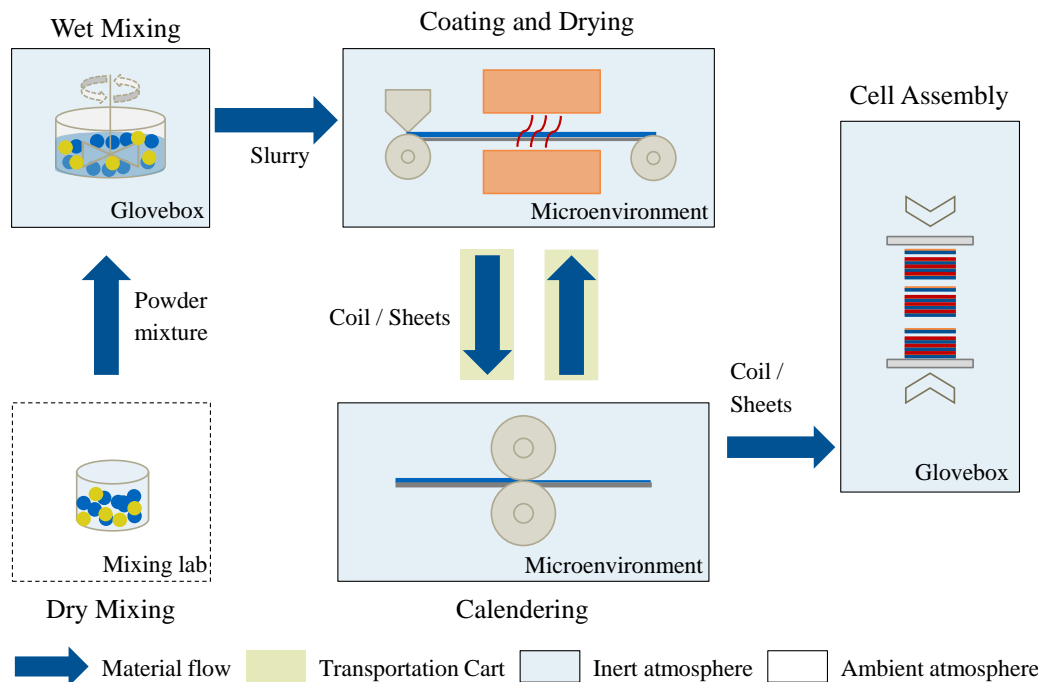


Figure 4-9: Production concept for the roll-to-roll fabrication of sulfide-based ASSBs in the SPACe⁺.

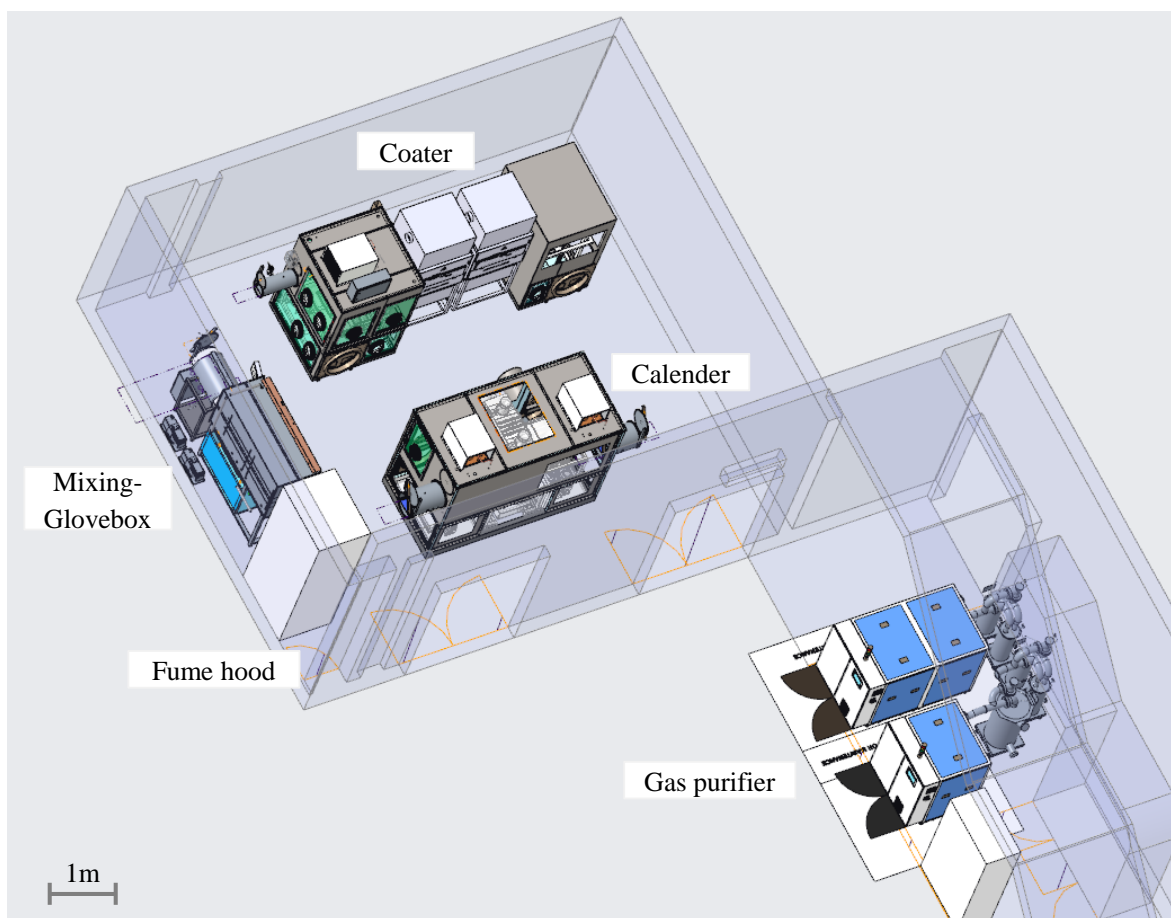


Figure 4-10: 3D-layout of the SPACe⁺ including a glovebox, fume hood, coater and dryer, calender and gas purifiers outside of the laboratory.

The anode is not included in this production concept since water-based silicon anodes can be produced on LIB machinery. LiM anodes can be laminated to the separator using the calender.

4.3.2 Machine Design

While the mixing glovebox consists of a standard glovebox and commercially available equipment, i.e., disperser, laboratory coater, or scales, inside it, the coater, dryer, and calender machinery are customized solutions. The microenvironments are designed to fit the roll-to-roll machinery with defined places for airlocks, the transportation cart, and glove positioning for operations. The scale of the machinery is chosen with the purpose of representing an industry-relevant process in the field of academic research. The most important machinery specifications are listed in Table 4-1.

Table 4-1: Specifications of the coater, dryer and calender machinery for sulfide-based ASSBs at *iwb*.

Coater and dryer	
Roll width	350 mm
Deflection roll diameter	Min. 110 mm
Support roll diameter	Min. 40 mm
Max. foil width	300 mm
Max. coating width	280 mm
Max. coating thickness	1000 μm
Machine velocity	0.1–4 m min^{-1}
Process velocity	0.2–2 m min^{-1}
Max. dryer temperature (convection)	160 °C, regulated at 120 °C
Web tension	5–50 N
Production atmosphere	Argon, nitrogen, CDA
Calender	
Roll width	350 mm
Roll diameter	350 mm
Max. material width	320 mm
Max. coating width	50–300 mm
Max. force	46 t
Max. line load	1500 N/mm at an electrode width of 300 mm 4500 N/mm at an electrode width of 100 mm
Gap height	0–1000 μm
Roll temperature	30 °C–200 °C
Process velocity	0.1–10 m min^{-1}
Web tension	30–400 N
Production atmosphere	Argon, nitrogen, CDA

The qualification of the plants was conducted and accordingly documented. Test material was used to simulate the production of sulfide-based ASSBs. The final set up and machine design is shown in Figure 4-11.



Figure 4-11: Photos of the machinery at *iwb* showing the microenvironments for the coater (right) and calender (left) machinery.

4.3.3 Initial Parameter Set for Pilot-Scale Experiments

As a guideline to initiate pilot-scale experiments, the final results of the presented publications are summarized, including the product and process parameters for the composite cathode and SE separator (cf. Table 4-2). These parameters shall function as a reference to have a starting point for recipes for the composite cathode and the SE, as well as an initial set of parameters for the settings on the machinery. In further experimental trials, the processes can be optimized on a role-to-role scale.

Table 4-2: Initial product and process parameters for the pilot scale production of sulfide-based composite cathodes and SE separators.

Product Parameters		Process parameters	
Composite cathode			
CAM material	NMC622	Dry mixing time	20 min
CAM share	67 wt%	Dry mixing speed	1000 rpm
SE material	LPSCI	Wet mixing time	40
SE share	27 wt%	Wet mixing speed	1250 rpm
Conductive carbon material	Super C65	Coating gap	600
Conductive carbon share	3 wt%	Coating velocity	2 cm s ⁻¹
Binder material	PIB	Drying time	5 min
Binder share	3 wt%	Drying temperature	30 °C

RESULTS

Binder share in the binder solution	5 wt%	Densification force (uniaxial press)	25 t
Solvent	Isobutylene:p-xylene (1:1 ratio)		
Solid content in slurry	55 wt%		
Substrate	Aluminum		
Solid Electrolyte Separator			
SE material	LPSCI	Dry mixing time	-
SE share	92 wt%	Dry mixing speed	-
Binder material	PIB	Wet mixing time	20 min
Binder share	8 wt%	Wet mixing speed	1250 rpm
Binder share in binder solution	5 wt%	Coating gap	800
Solvent	Isobutylene:p-xylene (1:1 ratio)	Coating velocity	2 cm s ⁻¹
Solid content in slurry	40 wt%	Drying time	5 min
Substrate	Mylar foil	Drying temperature	50 °C
		Densification force (uniaxial press)	25 t

5 Discussion of Results

In this chapter, a discussion of this dissertation's results and their contribution to the state of the art is provided. Herein, a critical reflection of the results presented in Chapter 4 with regard to the objective stated in Section 1.2, the derivation of need in Section 3.4, and the subgoals (cf. Section 4.1) is given.

5.1 Contribution to the Industrialization of Sulfide-Based All-Solid-State Batteries

To evaluate the novelty of the work, the state of the art is compared with the results on the processing strategies, the machine design, and the structure-product-process relations of sulfide-based ASSBs presented in Chapter 4. To categorize the publications content-wise, a matrix with the thematic scope and scale of fabrication is shown in Figure 5-1. The publications are sorted and classified according to their focus on either material, process, or machinery and the considered scale from laboratory over pilot to industrial.

The four introduced subgoals (cf. 1.3.1 and 4.1) of the thesis aimed to enable a scalable wet coating process for sulfide-based ASSBs. The novelty of the presented results is given by addressing the gap between laboratory scale and pilot scale, but also considering future scenarios for industrial scale, which was successfully realized in seven publications.

Process planning was the first subgoal, including developing a model and identifying characterization methods. As Publication I addresses possible process routes of sulfide-based ASSBs, offering an automatic tool to choose the technologies depending on the production task and cell design, the first part of Subgoal 1 was successfully researched and published. Therefore, the state-of-the-art literature (cf. Section 3.2) was broadened with specific knowledge on sulfide-based materials. The results of this publication are valuable in solving present challenges, e.g., choosing a suitable technology chain for battery producing companies. Moreover, the practical part of this subgoal contained the first evaluation and setup of characterization methods. Here, suitable analyzing techniques were chosen for sulfide-based material. Specifically, a rheometer, a z-tensile strength test, and an x-ray scanner were suitable characterization methods for these materials. As influencing environmental aspects, e.g., H₂S formation were not trivial to evaluate, this subgoal is closely connected with Subgoal 2.

Both first subgoals depend on identifying important material requirements to set up a production concept. The most significant influence in the further work was identified to be the H₂S formation. The state of the art presented first studies about the influence of water in contact with sulfides. However, the chemical reaction is material-specific and was not measured systematically in correlation with different material states. The concept in Publication II was still theoretical but contained different scenarios of the production environment and its costs.

Herein, the first machine design of a wet coating step was presented, exhibiting changes compared to a LIB coater. Publication III focused on the challenge of measuring H₂S formation to quantify the safety aspect. The current findings support further investigations on sulfide-based materials since only a few laboratories are set up for ASSBs on a pilot scale. Subgoal 2 was, therefore, successfully elaborated and formed the basis for Subgoal 3.

Based on the derived requirements, this dissertation's further experimental investigations focused on the gap between the laboratory and pilot scale to increase the produced batch size and investigate the applicability of the wet coating and drying processes. Subgoal 3 was defined to analyzing relevant parameters and characteristics of sulfide-based materials. Only a few further process studies in this range of detail are known in the field (cf. Section 3.1). However, to the best of the author's knowledge, no empirical data on the correlation of the composite cathode and SE separator recipes and the coating parameters, such as coating speed, are available to date. In addition, few data on the influence of the binder choice on the adhesion strength is available (cf. Subsection 3.3.3). The presented author's investigation of the drying behavior, both theoretically and empirically, is the first process-related experiment published on sulfide-based ASSBs so far. The reference and outlook on the pilot scale are, with respect to literature, unique in the authors' Publications IV, V, and VI, therefore giving access to new correlations between process parameters and the product quality of sulfide-based separators and composite cathodes. Therefore, these publications represent a high value for future research and the industrialization of ASSBs.

The conclusion and translation of the experiments are transferred and reflected in Publication VII and Section 4.3. Therein, novel process chains for the fabrication of sulfide-based ASSBs are presented and discussed, covering the complete production chain, focusing on component manufacturing and an outlook on cell assembly. Moreover, the realization of the new machinery at the SPACe⁺ was shown, and the production concept was described to complete Subgoal 4. This type of machinery is one of the first constructions dedicated to the pilot-scale fabrication of sulfide-based ASSBs.

Concluding, the defined subgoals were achieved by systematically addressing the lack of knowledge on processing sulfide-based ASSBs. This dissertation's gathered information and data are materials-specific and can be a starting point for future production research. Although the commercialization of ASSBs is still omitted in industry, the presented publications contribute to further industrialization, especially the acceleration of upscaled processes. An outlook on future topics is given in Section 6.2.

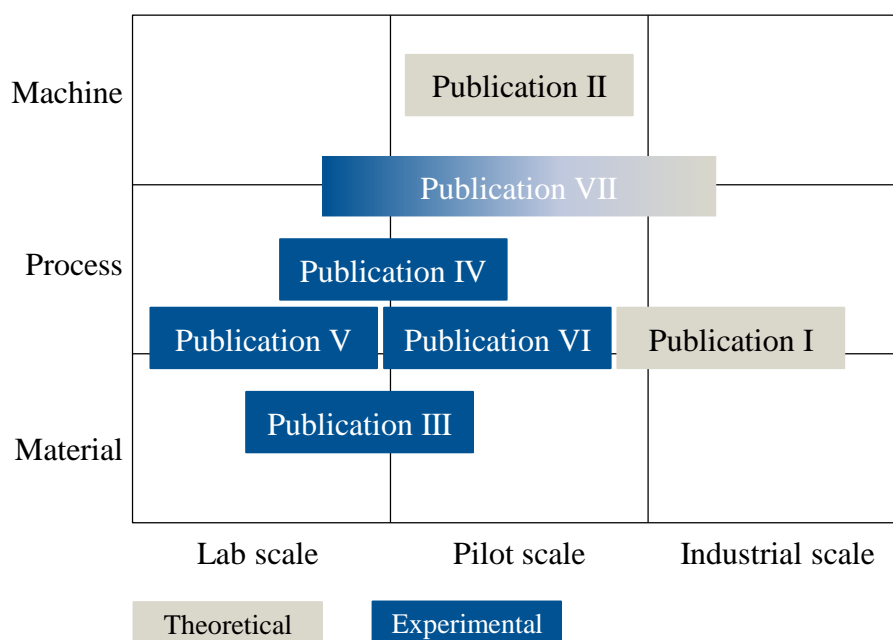


Figure 5-1: Classification of the presented Publications I-VII according to their thematic scope (material, process, machine) and production scale (laboratory, pilot, industrial).

5.2 Transferability of Results and Critical Reflection

Investigating the fabrication of a complex system, such as battery technology, exhibits the goal of solving very detailed and precise research questions. Therefore, the results presented in this dissertation aim to expand the publicly accessible knowledge on sulfide-based ASSBs focusing on the wet coating and drying processes.

The structure of this work is related to the close connection of the three fields: materials, process, and machinery. The general procedure behind this structure is easily transferable to any other product that shows the same level of development and requires an upscaling to be competitive in a commercial market. It can, therefore, be applied to other materials in battery storage systems, fuel cell applications, or other products with a comparable level of complexity.

However, the results obtained from this work are specifically valid for the sulfide-based materials LPSCl and LPS, as well as the composition of the respective slurries. Changing, for instance, the SE material would lead to different results in every process step due to the high dependence between the process parameters and the composition of the components. This behavior was also observed during this thesis, as a newly ordered batch of SE revealed a different morphology than the previous one, and the process had to be changed immediately. The same effect would apply if the solvent or binder were changed. Nevertheless, the developed methodology and sequence of research questions to be answered can be used as a general instruction or guide to follow.

Additionally, the upscaling process needs to be validated using the machinery. As the delivery of the machinery was delayed, the time frame of this work did not allow the building of ASSB cells with components manufactured on the roll-to-roll machinery. This step would be essential to compare the products' quality on two scales. Moreover, the number of process parameters

on the machinery is higher than on the laboratory scale, making it necessary to conduct further experimental investigations. Simulations should be conducted in the future to support the fast identification of process windows.

Retrospectively, the present dissertation implies fundamental knowledge of a scalable process of sulfide-based ASSBs. The material batch size was successfully upscaled from a scale of a few grams (1–5 g) up to 100 g, which is in a region of pilot-scale production processes. Essential characteristics of the material and its behavior during coating and drying were examined. Since the complexity of the process increases with higher amounts of slurry, a first step towards the industrialization of sulfide-based ASSBs was taken. The results represent the initiating phase to establish a roll-to-roll process. However, the correlations revealed between material, process, and machinery are only valid for the used material system.

6 Summary and Outlook

The last chapter summarizes the dissertation and provides an outlook on future topics that are highly relevant to continuing the upscaling process of sulfide-based ASSBs.

6.1 Summary

The urgent need for a sustainable future implies the development of innovative and cost-effective energy storage solutions. Conventional LIBs are limited regarding safety and energy density but highly developed regarding production knowledge. Knowledge about sulfide-based ASSBs, however, is limited regarding production-related behavior. To accelerate the development of ASSBs, close cooperation between academic research and industry will be required to find suitable long-term solutions. This work aims to contribute to this challenge by exploring scalable manufacturing processes to serve a more sustainable and safer future for electric mobility.

In order to achieve this goal, this dissertation is divided into six main chapters, which build the structure for this cumulative work. The objective and framework of this dissertation are set in Chapter 1, concluding with the definition of four subgoals (cf. Table 1-1). The development of the dissertation according to the design research methodology is presented in Subsection 1.3.2.

The fundamentals of this work are presented in Chapter 2 to complete the first literature-based research clarification, according to BLESSING & CHAKRABARTI (2009). The chapter includes an overview of the general functional principle of ASSBs and their materials. Further, basic knowledge about electrode processing is elaborated with a focus on mixing, wet coating, and drying. These research fields are the most relevant for this work and serve as a basis to present complex correlations later addressed in the publications on sulfide-based ASSBs.

In order to elaborate the four defined subgoals and the research gap, a descriptive study I is conducted. Therefore, the state of the art summarizes relevant literature in three fields (cf. Chapter 3). Picturing the current lab-scale fabrication of sulfide-based ASSBs highlights the need to upscale the production processes. Combined with the theoretical concepts on pilot or industrial production of ASSBs, the gap between laboratory and industry becomes apparent. The second part of this chapter focuses on studies conducted with materials from LIBs. Since the technology readiness level of LIBs is much higher, known correlations are studied to be later compared to the process behavior of sulfide-based ASSBs. Ultimately, the research need is derived, motivating this dissertation.

The cumulative overview of seven publications is presented according to their assignment on the research approach (cf. Figure 4-1). Following this structure, Publication I contains the system model and automated tool for a defined process planning (Subgoal 1) of industrial-scale

technologies for sulfide-based materials. The results in Publications II and III belong to the second subgoal, the production concept. Besides the design of a roll-to-roll wet coating machinery, special attention is paid to the implications for production. Within Publication III, a quantitative analysis of the sulfides' hydrolysis is given to identify critical production steps and derive safety aspects for future production planning. The results of this publication were also used to construct and evaluate the new laboratory for sulfide-based ASSBs at *iwb* (cf. Section 4.3). The summary of Publications IV, V, and VI reveals relevant structure-product-process correlations gained by experimentally investigating the behavior of sulfide-based materials during the processing of composite cathodes and SE separators. Chapter 4 closes with the validation part of this dissertation. Publication VII and Section 4.3 belong to the descriptive study II. Here, the transfer of experimental knowledge into the qualification of the roll-to-roll machinery is conducted. A summary and the key outcomes of every publication are given in Subsections 4.2.1 to 4.2.7.

The novelty of the results concerning the defined subgoals and the objective of this dissertation are discussed in the subsequent Chapter 5. The focus of the discussion is on the contribution to the industrialization of sulfide-based ASSBs. A following critical reflection of the author on the dissertation is conducted to elaborate on the transferability of results.

6.2 Outlook

The results presented in this work are an initial starting point to enable upscaling of the wet coating process of sulfide-based ASSBs. However, further research needs to be conducted to accelerate the industrialization of this energy storage in the future.

This dissertation provides first insights into the pilot-scale machinery of the wet coating process. To enable a roll-to-roll process, other production steps, such as calendaring and cell assembly, need to be addressed in the future. Machine suppliers depend on knowledge about the requirements of sulfide-based materials to design and build highly automated machines further.

The topic of H₂S formation was the focus of Publication III in this dissertation. Again, the focus was on the first processes within the component manufacturing. Processes used in the cell assembly should be considered in follow-up publications to define the required production atmosphere in every step and according to the intermediate products. Moreover, testing the material in desiccators gives first quantitative results on the behavior of the sulfide-based SEs. A study in an environment with the same conditions as an industrial dry room should be further conducted to emulate a production-near scenario.

The structure-product-process correlations in Publications IV to VI were gathered with samples fabricated on a laboratory scale. Further studies on process research with pilot machinery are needed to investigate suitable technologies and produce high-quality components. Moreover, rethinking the process routes for sulfide-based ASSBs should take place. Innovative routes and technologies should be considered to enhance the material's properties and guarantee cost-efficient production. Future investigations should also contain experimental, analytical, and

simulation results to thoroughly analyze prevailing mechanisms and phenomena of sulfide-based components. Additionally, no publication on cell assembly and processes such as cutting, stacking, and welding was found in the literature. Studies on the required process parameters and machinery are highly relevant to completing the production steps and gaining insights into the different possibilities of cell design.

In summary, the process research of sulfide-based ASSBs is at the beginning of development. Therefore, industrial research departments need to address various essential topics to gain more knowledge on the materials and their production. Finding the right combination of materials will be a trade-off between electrochemically ideal compositions and materials that can be processed on industrial machines. The need for interdisciplinary cooperation becomes apparent and will be required to make further steps toward commercializing sulfide-based ASSBs and facilitate their market integration.

7 Bibliography

- BAEHR, H. D.; STEPHAN, K. (2008): Wärme- und Stoffübertragung. 6., re-edit ed. Berlin, Heidelberg: Springer. ISBN: 978-3-540-87688-5. (Springer Reference).
- BAEK, S.-W.; LEE, J.-M.; KIM, T. Y.; SONG, M.-S.; PARK, Y. (2014): Garnet related lithium ion conductor processed by spark plasma sintering for all-solid-state batteries. *Journal of Power Sources* 249., pp. 197–206. DOI: 10.1016/j.jpowsour.2013.10.089.
- BANERJEE, A.; WANG, X.; FANG, C.; WU, E. A.; MENG, Y. S. (2020): Interfaces and Interphases in All-Solid-State Batteries with Inorganic Solid Electrolytes. *Chemical Reviews* 120. 14, pp. 6878–6933. DOI: 10.1021/acs.chemrev.0c00101.
- BATZER, M.; HECK, C.; MICHALOWSKI, P.; KWADE, A. (2022a): Current Status of Formulations and Scalable Processes for Producing Sulfidic Solid-State Batteries. *Batteries & Supercaps* 5. 12, pp. 1–22. DOI: 10.1002/batt.202200328.
- BATZER, M.; VOGES, K.; WANG, W.; MICHALOWSKI, P.; KWADE, A. (2022b): Systematic evaluation of materials and recipe for scalable processing of sulfide-based solid-state batteries. *Materials Today Communications* 30. 103189, pp. 1–13. DOI: 10.1016/j.mtcomm.2022.103189.
- BAUER, W.; NÖTZEL, D. (2014): Rheological properties and stability of NMP based cathode slurries for lithium ion batteries. *Ceramics International* 40. 3, pp. 4591–4598. DOI: 10.1016/j.ceramint.2013.08.137.
- BERNI, A.; MENNIG, M.; SCHMIDT, H. (2004): Doctor Blade. In: AEGERTER, M. A. et al. (Ed.): Sol-Gel Technologies for Glass Producers and Users. Boston, MA, s.l.: Springer US, pp. 89–92. DOI: 10.1007/978-0-387-88953-5_10. ISBN: 978-1-4419-5455-8.
- BIELEFELD, A.; WEBER, D. A.; JANEK, J. (2020): Modeling Effective Ionic Conductivity and Binder Influence in Composite Cathodes for All-Solid-State Batteries. *ACS Applied Materials & Interfaces* 12. 11, pp. 12821–12833. DOI: 10.1021/acsami.9b22788.
- BILLOT, N.; BEYER, M.; KOCH, N.; IHLE, C.; REINHART, G. (2021): Development of an adhesion model for graphite-based lithium-ion battery anodes. *Journal of Manufacturing Systems* 58., pp. 131–142. DOI: 10.1016/j.jmsy.2020.10.016.
- BILLOT, N.; GÜNTHER, T.; SCHREINER, D.; STAHL, R.; KRANNER, J.; BEYER, M.; REINHART, G. (2020): Investigation of the Adhesion Strength along the Electrode Manufacturing Process for Improved Lithium-Ion Anodes. *Energy Technology* 8. 2, pp. 1–7. DOI: 10.1002/ente.201801136.
- BINNEWIES, M.; FINZE, M.; JÄCKEL, M.; SCHMIDT, P.; WILLNER, H.; RAYNER-CANHAM, G. (2016): Allgemeine und anorganische Chemie. 3rd completely revised edition. Berlin: Springer Spektrum. ISBN: 978-3-662-45066-6.

- BIRKE, P.; WEEBER, M.; OBERLE, M. (ED.) (2022): Handbook on smart battery cell manufacturing. The power of digitalization. New Jersey, London, Singapore, Beijing, Shanghai, Hong Kong, Taipei, Chennai, Tokyo: World Scientific. ISBN: 978-981-12-4561-9.
- BITSCH, B.; DITTMANN, J.; SCHMITT, M.; SCHARFER, P.; SCHABEL, W.; WILLENBACHER, N. (2014): A novel slurry concept for the fabrication of lithium-ion battery electrodes with beneficial properties. *Journal of Power Sources* 265., pp. 81–90. DOI: 10.1016/j.jpowsour.2014.04.115.
- BLESSING, L. T. M.; CHAKRABARTI, A. (ED.) (2009): DRM, a design research methodology. Dordrecht, Heidelberg: Springer. ISBN: 978-1-84882-586-4.
- BMWK: Batterien „made in Germany“ – ein Beitrag zu nachhaltigem Wachstum und klimafreundlicher Mobilität. URL: <https://www.bmwk.de/Redaktion/DE/Dossier/batteriezellfertigung.html> (visited on 16.11.2023).
- BOLLORE GROUP: Battery Technology. URL: <https://www.blue-solutions.com/en/> (visited on 23.10.2023).
- BONNICK, P.; MULDOON, J. (2022): The quest for the holy grail of solid-state lithium batteries. *Energy Environ. Sci.* 15. 5, pp. 1840–1860. DOI: 10.1039/D2EE00842D.
- CAO, D.; SUN, X.; WANG, Y.; ZHU, H. (2022): Bipolar stackings high voltage and high cell level energy density sulfide based all-solid-state batteries. *Energy Storage Materials* 48., pp. 458–465. DOI: 10.1016/j.ensm.2022.03.012.
- CAO, D.; ZHAO, Y.; SUN, X.; NATAN, A.; WANG, Y.; XIANG, P.; WANG, W.; ZHU, H. (2020): Processing Strategies to Improve Cell-Level Energy Density of Metal Sulfide Electrolyte-Based All-Solid-State Li Metal Batteries and Beyond. *ACS Energy Letters* 5. 11, pp. 3468–3489. DOI: 10.1021/acsenerylett.0c01905.
- CARVALHO, M. S.; KHESHGI, H. S. (2000): Low-flow limit in slot coating: Theory and experiments. *AIChE Journal* 46. 10, pp. 1907–1917. DOI: 10.1002/aic.690461003.
- CHEN, C.; EICHEL, R.-A.; NOTTEN, P. H. (2017): Metal-organic chemical vapor deposition enabling all-solid-state Li-ion microbatteries: A short review. *Journal of Electroceramics* 38. 2-4, pp. 230–247. DOI: 10.1007/s10832-017-0090-1.
- CHEN, S.; WEN, K.; FAN, J.; BANDO, Y.; GOLBERG, D. (2018a): Progress and future prospects of high-voltage and high-safety electrolytes in advanced lithium batteries: from liquid to solid electrolytes. *J. Mater. Chem. A* 6. 25, pp. 11631–11663. DOI: 10.1039/C8TA03358G.
- CHEN, S.; XIE, D.; LIU, G.; MWIZERWA, J. P.; ZHANG, Q.; ZHAO, Y.; XU, X.; YAO, X. (2018b): Sulfide solid electrolytes for all-solid-state lithium batteries: Structure, conductivity, stability and application. *Energy Storage Materials* 14., pp. 58–74. DOI: 10.1016/j.ensm.2018.02.020.

- CHEN, Y.-T.; MARPLE, M. A.; TAN, D. H.; HAM, S.-Y.; SAYAHPOUR, B.; LI, W.-K.; YANG, H.; LEE, J. B.; HAH, H. J.; WU, E. A.; DOUX, J.-M.; JANG, J.; RIDLEY, P.; CRONK, A.; DEYSHER, G.; CHEN, Z.; MENG, Y. S. (2022): Investigating dry room compatibility of sulfide solid-state electrolytes for scalable manufacturing. *J. Mater. Chem. A* 10. 13, pp. 7155–7164. DOI: 10.1039/D1TA09846B.
- CHOI, S.; LEE, S.; YU, J.; DOH, C.-H.; HA, Y.-C. (2017): Slurry-Processed Glass-Ceramic Li₂S-P₂S₅-LiI Electrolyte for All-Solid-State Li-Ion Batteries. *ECS Transactions* 77. 1, pp. 65–70. DOI: 10.1149/07701.0065ecst.
- CHOU, S.-L.; PAN, Y.; WANG, J.-Z.; LIU, H.-K.; DOU, S.-X. (2014): Small things make a big difference: binder effects on the performance of Li and Na batteries. *Physical Chemistry Chemical Physics* 16. 38, pp. 20347–20359. DOI: 10.1039/c4cp02475c.
- DA SILVA, L. FILIPE MARTINS; ÖCHSNER, A.; ADAMS, R. D. (ED.) (2011): Handbook of adhesion technology. Berlin, Heidelberg, Cham: Springer. ISBN: 978-3-642-01168-9. (Springer Reference).
- DA SILVA, L. FILIPE MARTINS; ÖCHSNER, A.; ADAMS, R. D. (ED.) (2018): Handbook of adhesion technology. Second edition. Cham: Springer. ISBN: 978-3-319-55411-2.
- DAVID, L.; RUTHER, R. E.; MOHANTY, D.; MEYER, H. M.; SHENG, Y.; KALNAUS, S.; DANIEL, C.; WOOD, D. L. (2018): Identifying degradation mechanisms in lithium-ion batteries with coating defects at the cathode. *Applied Energy* 231., pp. 446–455. DOI: 10.1016/j.apenergy.2018.09.073.
- DEVIANNAPOORANI, C.; DHIVYA, L.; RAMAKUMAR, S.; MURUGAN, R. (2013): Lithium ion transport properties of high conductive tellurium substituted Li₇La₃Zr₂O₁₂ cubic lithium garnets. *Journal of Power Sources* 240., pp. 18–25. DOI: 10.1016/j.jpowsour.2013.03.166.
- DIEHM, R.; KUMBERG, J.; DÖRRER, C.; MÜLLER, M.; BAUER, W.; SCHARFER, P.; SCHABEL, W. (2020a): In Situ Investigations of Simultaneous Two-Layer Slot Die Coating of Component-Graded Anodes for Improved High-Energy Li-Ion Batteries. *Energy Technology* 8. 5, pp. 1–7. DOI: 10.1002/ente.201901251.
- DIEHM, R.; WEINMANN, H.; KUMBERG, J.; SCHMITT, M.; FLEISCHER, J.; SCHARFER, P.; SCHABEL, W. (2020b): Edge Formation in High-Speed Intermittent Slot-Die Coating of Disruptively Stacked Thick Battery Electrodes. *Energy Technology* 8. 2, pp. 1–8. DOI: 10.1002/ente.201900137.
- DING, X.; LIU, J.; HARRIS, T. A. (2016): A review of the operating limits in slot die coating processes. *AIChE Journal* 62. 7, pp. 2508–2524. DOI: 10.1002/aic.15268.
- DIRICAN, M.; YAN, C.; ZHU, P.; ZHANG, X. (2019): Composite solid electrolytes for all-solid-state lithium batteries. *Materials Science and Engineering: R: Reports* 136., pp. 27–46. DOI: 10.1016/j.mser.2018.10.004.
- DOPPELBAUER, M. (2020): Grundlagen der Elektromobilität. Wiesbaden: Springer Fachmedien Wiesbaden.

- DOUX, J.-M.; NGUYEN, H.; TAN, D. H.; BANERJEE, A.; WANG, X.; WU, E. A.; JO, C.; YANG, H.; MENG, YING SHIRLEY (2020a): Stack Pressure Considerations for Room-Temperature All-Solid-State Lithium Metal Batteries. *Advanced Energy Materials* 10. 1, p. 1903253–1903253. DOI: 10.1002/aenm.201903253.
- DOUX, J.-M.; YANG, Y.; TAN, D. H.; NGUYEN, H.; WU, E. A.; WANG, X.; BANERJEE, A.; MENG, Y. S. (2020b): Pressure effects on sulfide electrolytes for all solid-state batteries. *J. Mater. Chem. A* 8. 10, pp. 5049–5055. DOI: 10.1039/C9TA12889A.
- DRAKOPOULOS, S. X.; GHOLAMIPOUR-SHIRAZI, A.; MACDONALD, P.; PARINI, R. C.; REYNOLDS, C. D.; BURNETT, D. L.; PYE, B.; O'REGAN, K. B.; WANG, G.; WHITEHEAD, T. M.; CONDUIT, G. J.; CAZACU, A.; KENDRICK, E. (2021): Formulation and manufacturing optimization of lithium-ion graphite-based electrodes via machine learning. *Cell Reports Physical Science* 2. 12, p. 100683–100683. DOI: 10.1016/j.xcrp.2021.100683.
- DUAN, H.; ZHENG, H.; ZHOU, Y.; XU, B.; LIU, H. (2018): Stability of garnet-type Li ion conductors: An overview. *Solid State Ionics* 318., pp. 45–53. DOI: 10.1016/j.ssi.2017.09.018.
- DUFFNER, F.; KRONEMEYER, N.; TÜBKE, J.; LEKER, J.; WINTER, M.; SCHMUCH, R. (2021): Post-lithium-ion battery cell production and its compatibility with lithium-ion cell production infrastructure. *Nature Energy* 6. 2, pp. 123–134. DOI: 10.1038/s41560-020-00748-8.
- FAMPRIKIS, T.; CANEPA, P.; DAWSON, J. A.; ISLAM, M. S.; MASQUELIER, C. (2019): Fundamentals of inorganic solid-state electrolytes for batteries. *Nature materials* 18. 12, pp. 1278–1291. DOI: 10.1038/s41563-019-0431-3.
- FAN, L.; WEI, S.; LI, S.; LI, Q.; LU, Y. (2018): Recent Progress of the Solid-State Electrolytes for High-Energy Metal-Based Batteries. *Advanced Energy Materials* 8. 11, pp. 1–31. DOI: 10.1002/aenm.201702657.
- FERGUS, J. W. (2010): Ceramic and polymeric solid electrolytes for lithium-ion batteries. *Journal of Power Sources* 195. 15, pp. 4554–4569. DOI: 10.1016/j.jpowsour.2010.01.076.
- FONT, F.; PROTAS, B.; RICHARDSON, G.; FOSTER, J. M. (2018): Binder migration during drying of lithium-ion battery electrodes: Modelling and comparison to experiment. *Journal of Power Sources* 393., pp. 177–185. DOI: 10.1016/j.jpowsour.2018.04.097.
- FRANCO GONZALEZ, A.; YANG, N.-H.; LIU, R.-S. (2017): Silicon Anode Design for Lithium-Ion Batteries: Progress and Perspectives. *The Journal of Physical Chemistry C* 121. 50, pp. 27775–27787. DOI: 10.1021/acs.jpcc.7b07793.
- FRENKEL, J. (1926): Über die Wärmebewegung in festen und flüssigen Körpern. *Zeitschrift für Physik* 35.8-9., pp. 625–669.
- FRITH, J. T.; LACEY, M. J.; ULISSI, U. (2023): A non-academic perspective on the future of lithium-based batteries. *Nature Communications* 14. 1, p. 420–420. DOI: 10.1038/s41467-023-35933-2.

- GAMBE, Y.; SUN, Y.; HONMA, I. (2015): Development of bipolar all-solid-state lithium battery based on quasi-solid-state electrolyte containing tetraglyme-LiTFSa equimolar complex. *Scientific reports* 5., p. 8869–8869. DOI: 10.1038/srep08869.
- GAO, Z.; SUN, H.; FU, L.; YE, F.; ZHANG, Y.; LUO, W.; HUANG, Y. (2018): Promises, Challenges, and Recent Progress of Inorganic Solid-State Electrolytes for All-Solid-State Lithium Batteries. *Advanced materials* 30. 1705702, pp. 1. DOI: 10.1002/adma.201705702.
- GRAF, C. (2018): Cathode materials for lithium-ion batteries. In: KORTHAUER, R. (ED.): Lithium-ion batteries. Basics and applications. Berlin, Heidelberg: Springer, pp. 29–41. DOI: 10.1007/978-3-662-53071-9_4. ISBN: 978-3-662-53069-6.
- GRUNDMANN, M. (2016): The Physics of Semiconductors. Cham: Springer International Publishing.
- GÜNTHER, T.; BILLOT, N.; SCHUSTER, J.; SCHNELL, J.; SPINGLER, F. B.; GASTEIGER, H. A. (2016): The Manufacturing of Electrodes: Key Process for the Future Success of Lithium-Ion Batteries. *Advanced Materials Research* 1140., pp. 304–311. DOI: 10.4028/www.scientific.net/AMR.1140.304.
- GUO, R.; ZHANG, K.; ZHAO, W.; HU, Z.; LI, S.; ZHONG, Y.; YANG, R.; WANG, X.; WANG, JIANTAO; WU, CHUAN; BAI, YING (2023): Interfacial Challenges and Strategies toward Practical Sulfide-Based Solid-State Lithium Batteries. *Energy Material Advances* 4., pp. 1–31. DOI: 10.34133/energymatadv.0022.
- GUTOFF, E. B.; COHEN, E. D.; KHEBOIAN, G. I. (2006): Coating and Drying Defects // Coating and drying defects. Troubleshooting operating problems. ebrary, Inc. 2nd ed. New Jersey: John Wiley & Sons; Wiley-Interscience. ISBN: 978-0-471-71368-5.
- HAN, J.; ZHU, J.; LI, Y.; YU, X.; WANG, S.; WU, G.; XIE, H.; VOGEL, S. C.; IZUMI, F.; MOMMA, K.; KAWAMURA, Y.; HUANG, Y.; GOODENOUGH, J. B.; ZHAO, Y. (2012): Experimental visualization of lithium conduction pathways in garnet-type $\text{Li}_7\text{La}_3\text{Zr}_2\text{O}_{12}$. *Chemical communications (Cambridge, England)* 48. 79, pp. 9840–9842. DOI: 10.1039/c2cc35089k.
- HASELRIEDER, W.; WESTPHAL, B.; BOCKHOLT, H.; DIENER, A.; HÖFT, S.; KWADÉ, A. (2015): Measuring the coating adhesion strength of electrodes for lithium-ion batteries. *International Journal of Adhesion and Adhesives* 60., pp. 1–8. DOI: 10.1016/j.ijadhadh.2015.03.002.
- HATZELL, K. B.; ZHENG, Y. (2021): Prospects on large-scale manufacturing of solid state batteries. *MRS Energy & Sustainability* 8. 1, pp. 33–39. DOI: 10.1557/s43581-021-00004-w.
- HIGGINS, B. G.; SCRIVEN, L. E. (1980): Capillary pressure and viscous pressure drop set bounds on coating bead operability. *Chemical Engineering Science* 35. 3, pp. 673–682. DOI: 10.1016/0009-2509(80)80018-2.

- HOMANN, G.; MEISTER, P.; STOLZ, L.; BRINKMANN, J. P.; KULISCH, J.; ADERMANN, T.; WINTER, M.; KASNATSCHEEW, J. (2020): High-Voltage All-Solid-State Lithium Battery with Sulfide-Based Electrolyte: Challenges for the Construction of a Bipolar Multicell Stack and How to Overcome Them. *ACS Applied Energy Materials* 3. 4, pp. 3162–3168. DOI: 10.1021/acsaem.0c00041.
- HU, Y.-S. (2016): Batteries: Getting solid. *Nature Energy* 1. 4, pp. 1–2. DOI: 10.1038/nenergy.2016.42.
- HUANG, K. J.; CEDER, G.; OLIVETTI, E. A. (2021): Manufacturing scalability implications of materials choice in inorganic solid-state batteries. *Joule* 5. 3, pp. 564–580. DOI: 10.1016/j.joule.2020.12.001.
- HUO, H.; JANEK, J. (2022): Silicon as Emerging Anode in Solid-State Batteries. *ACS Energy Letters* 7. 11, pp. 4005–4016. DOI: 10.1021/acsenerylett.2c01950.
- HWANG, A. (2017): Fabrication and Electrochemical Properties of $\text{Li}_4\text{Ti}_5\text{O}_{12}@\text{Li}_6\text{PS}_5\text{Cl}$ for All-solid-state Lithium Batteries using Simple Mechanical Method. *International Journal of Electrochemical Science*, pp. 7795–7806. DOI: 10.20964/2017.08.29.
- INAGUMA, Y.; LIQUAN, C.; ITOH, M.; NAKAMURA, T.; UCHIDA, T.; IKUTA, H.; WAKIHARA, M. (1993): High ionic conductivity in lithium lanthanum titanate. *Solid State Communications* 86. 10, pp. 689–693. DOI: 10.1016/0038-1098(93)90841-A.
- JAISER, S.; FUNK, L.; BAUNACH, M.; SCHARFER, P.; SCHABEL, W. (2017): Experimental investigation into battery electrode surfaces: The distribution of liquid at the surface and the emptying of pores during drying. *Journal of colloid and interface science* 494., pp. 22–31. DOI: 10.1016/j.jcis.2017.01.063.
- JAISER, S.; MÜLLER, M.; BAUNACH, M.; BAUER, W.; SCHARFER, P.; SCHABEL, W. (2016): Investigation of film solidification and binder migration during drying of Li-Ion battery anodes. *Journal of Power Sources* 318., pp. 210–219. DOI: 10.1016/j.jpowsour.2016.04.018.
- JANEK, J.; ZEIER, W. G. (2016): A solid future for battery development. *Nature Energy* 1. 9, pp. 1–4. DOI: 10.1038/nenergy.2016.141.
- JANEK, J.; ZEIER, W. G. (2023): Challenges in speeding up solid-state battery development. *Nature Energy* 8. 3, pp. 230–240. DOI: 10.1038/s41560-023-01208-9.
- JIA, M.; ZHAO, N.; HUO, H.; GUO, X. (2020): Comprehensive Investigation into Garnet Electrolytes Toward Application-Oriented Solid Lithium Batteries. *Electrochemical Energy Reviews*, pp. 1–34. DOI: 10.1007/s41918-020-00076-1.
- JIMÉNEZ, R.; DEL CAMPO, A.; CALZADA, M. L.; SANZ, J.; KOBLYLIANSKA, S. D.; SOLOPAN, S. O.; BELOUS, A. G. (2016): Lithium $\text{La}_{0.57}\text{Li}_{0.33}\text{TiO}_3$ Perovskite and $\text{Li}_{1.3}\text{Al}_{0.3}\text{Ti}_{1.7}(\text{PO}_4)_3$ Li-NASICON Supported Thick Films Electrolytes Prepared by Tape Casting Method. *Journal of The Electrochemical Society* 163. 8, pp. A1653-A1659. DOI: 10.1149/2.0881608jes.

- JUNG, K.-N.; SHIN, H.-S.; PARK, M.-S.; LEE, J.-W. (2019): Solid-State Lithium Batteries: Bipolar Design, Fabrication, and Electrochemistry. *ChemElectroChem* 6. 15, pp. 3842–3859. DOI: 10.1002/celec.201900736.
- JUNG, Y. S.; OH, D. Y.; NAM, Y. J.; PARK, K. H. (2015): Issues and Challenges for Bulk-Type All-Solid-State Rechargeable Lithium Batteries using Sulfide Solid Electrolytes. *Israel Journal of Chemistry* 55. 5, pp. 472–485. DOI: 10.1002/ijch.201400112.
- KAISER, J.; WENZEL, V.; NIRSCHL, H.; BITSCH, B.; WILLENBACHER, N.; BAUNACH, M.; SCHMITT, M.; JAISER, S.; SCHARFER, PHILIP; SCHABEL, WILHELM (2014): Prozess- und Produktentwicklung von Elektroden für Li-Ionen-Zellen. *Chemie Ingenieur Technik* 86. 5, pp. 695–706. DOI: 10.1002/cite.201300085.
- KAMMAMPATA, S. P.; THANGADURAI, V. (2018): Cruising in ceramics—discovering new structures for all-solid-state batteries—fundamentals, materials, and performances. *Ionics* 24. 3, pp. 639–660. DOI: 10.1007/s11581-017-2372-7.
- KARABELLI, D.; BIRKE, K. P. (2021): Feasible Energy Density Pushes of Li-Metal vs. Li-Ion Cells. *Applied Sciences* 11. 16, p. 7592–7592. DOI: 10.3390/app11167592.
- KARABELLI, D.; BIRKE, K. P. (2022): Beyond Lithium Ion: All Solid-State Batteries. In: BIRKE, P. et al. (Ed.): Handbook on smart battery cell manufacturing. The power of digitalization. New Jersey, London, Singapore, Beijing, Shanghai, Hong Kong, Taipei, Chennai, Tokyo: World Scientific, pp. 411–423. DOI: 10.1142/9789811245626_0022. ISBN: 978-981-12-4561-9.
- KASEMCHAINAN, J.; BRUCE, P. G. (2018): All-Solid-State Batteries and their Remaining Challenges. *Johnson Matthey Technology Review* 62. 2, pp. 177–180. DOI: 10.1595/205651318X696747.
- KATO, Y.; HORI, S.; SAITO, T.; SUZUKI, K.; HIRAYAMA, M.; MITSUI, A.; YONEMURA, M.; IBA, H.; KANNO, R. (2016): High-power all-solid-state batteries using sulfide superionic conductors. *Nature Energy* 30, pp. 1–7.
- KAZYAK, E.; CHEN, K.-H.; DAVIS, A. L.; YU, S.; SANCHEZ, A. J.; LASSO, J.; BIELINSKI, A. R.; THOMPSON, T.; SAKAMOTO, JEFF; SIEGEL, DONALD J.; DASGUPTA, NEIL P. (2018): Atomic layer deposition and first principles modeling of glassy Li₃BO₃–Li₂CO₃ electrolytes for solid-state Li metal batteries. *Journal of Materials Chemistry A* 6. 40, pp. 19425–19437. DOI: 10.1039/C8TA08761J.
- KERMAN, K.; LUNTZ, A.; VISWANATHAN, V.; CHIANG, Y.-M.; CHEN, Z. (2017): Review—Practical Challenges Hindering the Development of Solid State Li Ion Batteries. *Journal of The Electrochemical Society* 164. 7, pp. A1731–A1744. DOI: 10.1149/2.1571707jes.
- KIM, A.-Y.; STRAUSS, F.; BARTSCH, T.; TEO, J. H.; HATSUKADE, T.; MAZILKIN, A.; JANEK, J.; HARTMANN, P.; BREZESINSKI, TORSTEN (2019a): Stabilizing Effect of a Hybrid Surface Coating on a Ni-Rich NCM Cathode Material in All-Solid-State Batteries. *Chemistry of Materials* 31. 23, pp. 9664–9672. DOI: 10.1021/acs.chemmater.9b02947.

- KIM, D. H.; LEE, H. A.; SONG, Y. B.; PARK, J. W.; LEE, S.-M.; JUNG, Y. S. (2019b): Sheet-type Li₆PS₅Cl-infiltrated Si anodes fabricated by solution process for all-solid-state lithium-ion batteries. *Journal of Power Sources* 426., pp. 143–150. DOI: 10.1016/j.jpowsour.2019.04.028.
- KIM, D. H.; LEE, Y.-H.; SONG, Y. B.; KWAK, H.; LEE, S.-Y.; JUNG, Y. S. (2020): Thin and Flexible Solid Electrolyte Membranes with Ultrahigh Thermal Stability Derived from Solution-Processable Li Argyrodites for All-Solid-State Li-Ion Batteries. *ACS Energy Letters* 5. 3, pp. 718–727. DOI: 10.1021/acseenergylett.0c00251.
- KIM, D. H.; OH, D. Y.; PARK, K. H.; CHOI, Y. E.; NAM, Y. J.; LEE, H. A.; LEE, S.-M.; JUNG, Y. S. (2017): Infiltration of Solution-Processable Solid Electrolytes into Conventional Li-Ion-Battery Electrodes for All-Solid-State Li-Ion Batteries. *Nano letters* 17. 5, pp. 3013–3020. DOI: 10.1021/acs.nanolett.7b00330.
- KIM, J. G.; SON, B.; MUKHERJEE, S.; SCHUPPERT, N.; BATES, A.; KWON, O.; CHOI, M. J.; CHUNG, H. Y.; PARK, SAM (2015): A review of lithium and non-lithium based solid state batteries. *Journal of Power Sources* 282., pp. 299–322. DOI: 10.1016/j.jpowsour.2015.02.054.
- KIM, K. J.; BALAISH, M.; WADAGUCHI, M.; KONG, L.; RUPP, J. L. (2021): Solid-State Li–Metal Batteries: Challenges and Horizons of Oxide and Sulfide Solid Electrolytes and Their Interfaces. *Advanced Energy Materials* 11. 1, p. 2002689–2002689. DOI: 10.1002/aenm.202002689.
- KIM, K. T.; KWON, T. Y.; JUNG, Y. S. (2022): Scalable fabrication of sheet-type electrodes for practical all-solid-state batteries employing sulfide solid electrolytes. *Current Opinion in Electrochemistry* 34., p. 101026–101026. DOI: 10.1016/j.coelec.2022.101026.
- KORTHAUER, R. (2019): Lithium-ion batteries. Basics and applications. Berlin: Springer. ISBN: 9783662530719.
- KRAUSKOPF, T.; HARTMANN, H.; ZEIER, W. G.; JANEK, J. (2019): Toward a Fundamental Understanding of the Lithium Metal Anode in Solid-State Batteries-An Electrochemo-Mechanical Study on the Garnet-Type Solid Electrolyte Li_{6.25}Al_{0.25}La₃Zr₂O₁₂. *ACS applied materials & interfaces* 11. 15, pp. 14463–14477. DOI: 10.1021/acscami.9b02537.
- KRAUSKOPF, T.; RICHTER, F. H.; ZEIER, W. G.; JANEK, J. (2020): Physicochemical Concepts of the Lithium Metal Anode in Solid-State Batteries. *Chemical reviews* 120. 15, pp. 7745–7794. DOI: 10.1021/acs.chemrev.0c00431.
- KRAYTSBERG, A.; EIN-ELI, Y. (2016): Conveying Advanced Li-ion Battery Materials into Practice The Impact of Electrode Slurry Preparation Skills. *Advanced Energy Materials* 6. 21, pp. 1–23. DOI: 10.1002/aenm.201600655.
- KUMAR, P. P.; YASHONATH, S. (2006): Ionic conduction in the solid state. *Journal of Chemical Sciences* 118. 1, pp. 135–154. DOI: 10.1007/BF02708775.
- KUMBERG, J.; MÜLLER, M.; DIEHM, R.; SPIEGEL, S.; WACHSMANN, C.; BAUER, W.; SCHARFER, P.; SCHABEL, W. (2019): Drying of Lithium-Ion Battery Anodes for Use in High-Energy Cells:

- Influence of Electrode Thickness on Drying Time, Adhesion, and Crack Formation. *Energy Technology* 7. 11, pp. 1–11. DOI: 10.1002/ente.201900722.
- KURZWEIL, P.; DIETLMEIER, O. (ED.) (2018): Elektrochemische Speicher. Superkondensatoren, Batterien, Elektrolyse-Wasserstoff, rechtliche Rahmenbedingungen. 2. aktualisierte und erweiterte Auflage; Springer Fachmedien Wiesbaden. Wiesbaden, Heidelberg: Springer Vieweg. ISBN: 978-3-658-21828-7. (Lehrbuch).
- LAN, T.; MA, Q.; TIETZ, F.; GUILLON, O.: Deutschland US11417870B2: Solid state battery and method for producing same.
- LEE, H.; OH, P.; KIM, J.; CHA, H.; CHAE, S.; LEE, S.; CHO, J. (2019): Advances and Prospects of Sulfide All-Solid-State Lithium Batteries via One-to-One Comparison with Conventional Liquid Lithium Ion Batteries. *Advanced materials (Deerfield Beach, Fla.)* 31. 29, pp. e1900376. DOI: 10.1002/adma.201900376.
- LEE, J.; LEE, T.; CHAR, K.; KIM, K. J.; CHOI, J. W. (2021): Issues and Advances in Scaling up Sulfide-Based All-Solid-State Batteries. *Accounts of chemical research* 54. 17, pp. 3390–3402. DOI: 10.1021/acs.accounts.1c00333.
- LEE, K.; KIM, S.; PARK, J.; PARK, S. H.; COSKUN, A.; JUNG, D. S.; CHO, W.; CHOI, J. W. (2017): Selection of Binder and Solvent for Solution-Processed All-Solid-State Battery. *Journal of The Electrochemical Society* 164. 9, pp. A2075–A2081. DOI: 10.1149/2.1341709jes.
- LIM, S.; AHN, K. H.; YAMAMURA, M. (2013): Latex migration in battery slurries during drying. *Langmuir: the ACS journal of surfaces and colloids* 29. 26, pp. 8233–8244. DOI: 10.1021/la4013685.
- LIN, D.; LIU, Y.; CUI, Y. (2017): Reviving the lithium metal anode for high-energy batteries. *Nature nanotechnology* 12. 3, pp. 194–206. DOI: 10.1038/nnano.2017.16.
- LIU, D.; CHEN, L.-C.; LIU, T.-J.; FAN, T.; TSOU, E.-Y.; TIU, C. (2014): An Effective Mixing for Lithium Ion Battery Slurries. *Advances in Chemical Engineering and Science* 04. 04, pp. 515–528. DOI: 10.4236/aces.2014.44053.
- LUNTZ, A. C.; VOSS, J.; REUTER, K. (2015): Interfacial challenges in solid-state Li ion batteries. *The journal of physical chemistry letters* 6. 22, pp. 4599–4604. DOI: 10.1021/acs.jpcllett.5b02352.
- MANTHIRAM, A.; YU, X.; WANG, S. (2017): Lithium battery chemistries enabled by solid-state electrolytes. *Nature Reviews Materials* 2., pp. 1–16. DOI: 10.1038/natrevmats.2016.103.
- MAUGER, A.; JULIEN, C. M.; PAOLELLA, A.; ARMAND, M.; ZAGHIB, K. (2019): Building Better Batteries in the Solid State: A Review. *Materials (Basel, Switzerland)* 12. 23, pp. 1–86. DOI: 10.3390/ma12233892.
- MCCLOSKEY, B. D. (2015): Attainable gravimetric and volumetric energy density of Li-S and li ion battery cells with solid separator-protected Li metal anodes. *The journal of physical chemistry letters* 6. 22, pp. 4581–4588. DOI: 10.1021/acs.jpcllett.5b01814.

- MCGROGAN, F. P.; SWAMY, T.; BISHOP, S. R.; EGGLETON, E.; PORZ, L.; CHEN, X.; CHIANG, Y.-M.; VAN VLIET, K. J. (2017): Compliant Yet Brittle Mechanical Behavior of Li₂S–P₂S₅ Lithium-Ion-Conducting Solid Electrolyte. *Advanced Energy Materials* 7. 12, pp. 1–5. DOI: 10.1002/aenm.201602011.
- MEWIS, J.; WAGNER, N. J. (2012): Colloidal suspension rheology. Cambridge: Cambridge Univ. Press. ISBN: 9780521515993. (Cambridge series in chemical engineering).
- MEYER, C.; WEYHE, M.; HASELRIEDER, W.; KWAD, A. (2020): Heated Calendering of Cathodes for Lithium-Ion Batteries with Varied Carbon Black and Binder Contents. *Energy Technology* 8. 2, pp. 1–12. DOI: 10.1002/ente.201900175.
- MEZGER, T. (2020): The rheology handbook. For users of rotational and oscillatory rheometers. Vincentz Network GmbH & Co. KG. 5th revised edition. Hannover: Vincentz. ISBN: 9783866305328. (European coatings library).
- MITTAL, K. L. (1976): Adhesion measurements of thin films. *Electrocomponent Science and Technology* 3., pp. 21–42.
- MOHANTY, D.; HOCKADAY, E.; LI, J.; HENSLEY, D. K.; DANIEL, C.; WOOD, D. L. (2016): Effect of electrode manufacturing defects on electrochemical performance of lithium-ion batteries: Cognizance of the battery failure sources. *Journal of Power Sources* 312., pp. 70–79. DOI: 10.1016/j.jpowsour.2016.02.007.
- MÜLLER, M.; PFAFFMANN, L.; JAISER, S.; BAUNACH, M.; TROUILLET, V.; SCHEIBA, F.; SCHARFER, P.; SCHABEL, W.; BAUER, WERNER (2017): Investigation of binder distribution in graphite anodes for lithium-ion batteries. *Journal of Power Sources* 340., pp. 1–5. DOI: 10.1016/j.jpowsour.2016.11.051.
- MURUGAN, R.; THANGADURAI, V.; WEPPNER, W. (2007): Fast lithium ion conduction in garnet-type Li₇La₃Zr₂O₁₂. *Angewandte Chemie (International ed. in English)* 46. 41, pp. 7778–7781. DOI: 10.1002/anie.200701144.
- NAM, Y. J.; CHO, S.-J.; OH, D. Y.; LIM, J.-M.; KIM, S. Y.; SONG, J. H.; LEE, Y.-G.; LEE, S.-Y.; JUNG, YOON SEOK (2015): Bendable and thin sulfide solid electrolyte film: a new electrolyte opportunity for free-standing and stackable high-energy all-solid-state lithium-ion batteries. *Nano letters* 15. 5, pp. 3317–3323. DOI: 10.1021/acs.nanolett.5b00538.
- NAM, Y. J.; OH, D. Y.; JUNG, S. H.; JUNG, Y. S. (2018): Toward practical all-solid-state lithium-ion batteries with high energy density and safety: Comparative study for electrodes fabricated by dry- and slurry-mixing processes. *Journal of Power Sources* 375., pp. 93–101. DOI: 10.1016/j.jpowsour.2017.11.031.
- NIKODIMOS, Y.; HUANG, C.-J.; TAKLU, B. W.; SU, W.-N.; HWANG, B. J. (2022): Chemical stability of sulfide solid-state electrolytes: stability toward humid air and compatibility with solvents and binders. *Energy & Environmental Science* 15. 3, pp. 991–1033. DOI: 10.1039/D1EE03032A.

- OH, D. Y.; KIM, D. H.; JUNG, S. H.; HAN, J.-G.; CHOI, N.-S.; JUNG, Y. S. (2017): Single-step wet-chemical fabrication of sheet-type electrodes from solid-electrolyte precursors for all-solid-state lithium-ion batteries. *J. Mater. Chem. A* 5. 39, pp. 20771–20779. DOI: 10.1039/C7TA06873E.
- OH, D. Y.; NAM, Y. J.; PARK, K. H.; JUNG, S. H.; KIM, K. T.; HA, A. R.; JUNG, Y. S. (2019): Slurry-Fabricable Li⁺-Conductive Polymeric Binders for Practical All-Solid-State Lithium-Ion Batteries Enabled by Solvate Ionic Liquids. *Advanced Energy Materials* 9. 16, p. 1802927–1802927. DOI: 10.1002/aenm.201802927.
- PERVEZ, S. A.; GANJEH-ANZABI, P.; FAROOQ, U.; TRIFKOVIC, M.; ROBERTS, E. P.; THANGADURAI, V. (2019): Fabrication of a Dendrite-Free all Solid-State Li Metal Battery via Polymer Composite/Garnet/Polymer Composite Layered Electrolyte. *Advanced Materials Interfaces* 334., p. 1900186–1900186. DOI: 10.1002/admi.201900186.
- PLACKE, T.; KLOEPSCH, R.; DÜHNEN, S.; WINTER, M. (2017): Lithium ion, lithium metal, and alternative rechargeable battery technologies: the odyssey for high energy density. *Journal of Solid State Electrochemistry* 21. 7, pp. 1939–1964. DOI: 10.1007/s10008-017-3610-7.
- RANDAU, S.; WEBER, D. A.; KÖTZ, O.; KOERVER, R.; BRAUN, P.; WEBER, A.; IVERS-TIFFÉE, E.; ADERMANN, T.; KULISCH, JÖRN; ZEIER, WOLFGANG G.; RICHTER, FELIX H.; JANEK, JÜRGEN (2020): Benchmarking the performance of all-solid-state lithium batteries. *Nature Energy*, . DOI: 10.1038/s41560-020-0565-1.
- REYNOLDS, C. D.; HARE, S. D.; SLATER, P. R.; SIMMONS, M. J.; KENDRICK, E. (2022): Rheology and Structure of Lithium-Ion Battery Electrode Slurries. *Energy Technology* 10. 10, p. 2200545–2200545. DOI: 10.1002/ente.202200545.
- REYNOLDS, C. D.; SLATER, P. R.; HARE, S. D.; SIMMONS, M. J.; KENDRICK, E. (2021): A review of metrology in lithium-ion electrode coating processes. *Materials & Design* 209., p. 109971–109971. DOI: 10.1016/j.matdes.2021.109971.
- RICKERBY, D. S. (1988): A review of the methods for the measurement of coating-substrate adhesion. *Surface and Coating Technology* 36., pp. 541–557.
- RICKERT, H. (1978): Feste Ionenleiter — Grundlagen und Anwendungen. *Angewandte Chemie* 90. 1, pp. 38–48. DOI: 10.1002/ange.19780900107.
- RIPHAUS, N.; STROBL, P.; STIASZNY, B.; ZINKEVICH, M. Y.; SCHNELL, J.; INDRIS, S.; GASTEIGER, H. A.; SEDLMAIER, S. J. (2018): Slurry-Base Processing of Solid Electrolytes: A Comparative Binder Study. *Journal of The Electrochemical Society* 165. 16, pp. A3993–A3999. DOI: 10.1149/2.0961816jes.
- SAKUDA, A.; KURATANI, K.; YAMAMOTO, M.; TAKAHASHI, M.; TAKEUCHI, T.; KOBAYASHI, H. (2017): All-Solid-State Battery Electrode Sheets Prepared by a Slurry Coating Process. *Journal of The Electrochemical Society* 164. 12, pp. A2474–A2478. DOI: 10.1149/2.0951712jes.
- SATOU, A. (2017): US 20170/263981 A1. (07.03.2017) 15/451,676: Bipolar Laminated All-Solid-State Lithium-Ion Rechargeable Battery and Method for Manufacturing Same.

- SCHETZ, J. A.; FUHS, A. E. (1999): Fundamentals of fluid mechanics. New York, Weinheim: Wiley. ISBN: 0471348562. (A Wiley-Interscience publication).
- SCHMITT, M.; BAUNACH, M.; WENGELER, L.; PETERS, K.; JUNGES, P.; SCHARFER, P.; SCHABEL, W. (2013): Slot-die processing of lithium-ion battery electrodes—Coating window characterization. *Chemical Engineering and Processing: Process Intensification* 68., pp. 32–37. DOI: 10.1016/j.cep.2012.10.011.
- SCHMITT, M.; SCHARFER, P.; SCHABEL, W. (2014): Slot die coating of lithium-ion battery electrodes: investigations on edge effect issues for stripe and pattern coatings. *Journal of Coatings Technology and Research* 11. 1, pp. 57–63. DOI: 10.1007/s11998-013-9498-y.
- SCHNELL, J. (03.09.2020): Strategic Technology Planning for the Production of All-Solid-State Batteries. Institut für Werkzeugmaschinen und Betriebswissenschaften, TU München. München.
- SCHNELL, J.; GÜNTHER, T.; KNOCH, T.; VIEIDER, C.; KÖHLER, L.; JUST, A.; KELLER, M.; PASSERINI, S.; REINHART, G. (2018): All-solid-state lithium-ion and lithium metal batteries – paving the way to large-scale production. *Journal of Power Sources* 382., pp. 160–175. DOI: 10.1016/j.jpowsour.2018.02.062.
- SCHNELL, J.; KNÖRZER, H.; IMBSWEILER, A. J.; REINHART, G. (2020): Solid versus Liquid—A Bottom-Up Calculation Model to Analyze the Manufacturing Cost of Future High-Energy Batteries. *Energy Technology* 8. 3, p. 1901237–1901237. DOI: 10.1002/ente.201901237.
- SCHNELL, J.; TIETZ, F.; SINGER, C.; HOFER, A.; BILLOT, N.; REINHART, G. (2019): Prospects of production technologies and manufacturing costs of oxide-based all-solid-state lithium batteries. *Energy & Environmental Science* 12. 6, pp. 1818–1833. DOI: 10.1039/C8EE02692K.
- SEINO, Y.; OTA, T.; TAKADA, K.; HAYASHI, A.; TATSUMISAGO, M. (2014): A sulphide lithium super ion conductor is superior to liquid ion conductors for use in rechargeable batteries. *Energy Environ. Sci.* 7. 2, pp. 627–631. DOI: 10.1039/C3EE41655K.
- SHIN, D. O.; KIM, H.; JUNG, S.; BYUN, S.; CHOI, J.; KIM, M. P.; KIM, J. Y.; KANG, S. H.; PARK, YOUNG-SAM; HONG, SUNG YOU; CHO, MAENGHYO; LEE, YOUNG-GI; CHO, KYEONGJAE; LEE, YONG MIN (2022): Electrolyte-free graphite electrode with enhanced interfacial conduction using Li⁺-conductive binder for high-performance all-solid-state batteries. *Energy Storage Materials* 49., pp. 481–492. DOI: 10.1016/j.ensm.2022.04.029.
- SINGER, C.; KOPP, L.; ARUQAJ, M.; DAUB, R. (2023a): Drying Process of Sulfide-Based All-Solid-State Battery Components—Investigation on Adhesion Strength and Microstructural Changes. *Energy Technology*, p. 2300098–2300098. DOI: 10.1002/ente.202300098.
- SINGER, C.; KOPP, L.; DAUB, R. (2023b): Fundamental investigation on drying rates of cathodes and separators for sulfide-based all-solid-state batteries. *Drying Technology*, pp. 1–7. DOI: 10.1080/07373937.2023.2189943.

- SINGER, C.; SCHMALZBAUER, S.; DAUB, R. (2023c): Influence of the slurry composition on thin-film components for the wet coating process of sulfide-based all-solid-state batteries. *Journal of Energy Storage* 68., p. 107703–107703. DOI: 10.1016/j.est.2023.107703.
- SINGER, C.; SCHNELL, J.; REINHART, G. (2020): Scalable Processing Routes for the Production of All-Solid-State Batteries—Modeling Interdependencies of Product and Process. *Energy Technology*, p. 2000665–2000665. DOI: 10.1002/ente.202000665.
- SINGER, C.; TÖPPER, H.-C.; GÜNTER, F. J.; REINHART, G. (2021): Plant Technology for the Industrial Coating Process for Sulfide-Based All-Solid-State Batteries. *Procedia CIRP* 104., pp. 56–61. DOI: 10.1016/j.procir.2021.11.010.
- SINGER, C.; TÖPPER, H.-C.; KUTSCH, T.; SCHUSTER, R.; KOERVER, R.; DAUB, R. (2022): Hydrolysis of Argyrodite Sulfide-Based Separator Sheets for Industrial All-Solid-State Battery Production. *ACS Applied Materials & Interfaces*. DOI: 10.1021/acsami.2c01099.
- SINGER, C.; WACH, L.; JAIMEZ FARNHAM, E.; DAUB, R. (2024): Insights Into Scalable Technologies and Process Chains for Sulfide-Based Solid-State Battery Production. *Batteries & Supercaps*, pp. e202400142. DOI: 10.1002/batt.202400142.
- SONG, S.; CHEN, B.; RUAN, Y.; SUN, J.; YU, L.; WANG, Y.; THOKCHOM, J. (2018): Gd-doped Li₇La₃Zr₂O₁₂ garnet-type solid electrolytes for all-solid-state Li-Ion batteries. *Electrochimica Acta* 270., pp. 501–508. DOI: 10.1016/j.electacta.2018.03.101.
- STAMPATORI, D.; RAIMONDI, P. P.; NOUSSAN, M. (2020): Li-Ion Batteries: A Review of a Key Technology for Transport Decarbonization. *Energies* 13. 10, p. 2638–2638. DOI: 10.3390/en13102638.
- STRAUSS, F.; BARTSCH, T.; BIASI, L. DE; KIM, A.-Y.; JANEK, J.; HARTMANN, P.; BREZESINSKI, T. (2018): Impact of Cathode Material Particle Size on the Capacity of Bulk-Type All-Solid-State Batteries. *ACS Energy Letters* 3. 4, pp. 992–996. DOI: 10.1021/acsenergylett.8b00275.
- STRAUSS, F.; TEO, J. H.; MAIBACH, J.; KIM, A.-Y.; MAZILKIN, A.; JANEK, J.; BREZESINSKI, T. (2020): Li₂ZrO₃-Coated NCM622 for Application in Inorganic Solid-State Batteries: Role of Surface Carbonates in the Cycling Performance. *ACS Applied Materials & Interfaces* 12. 51, pp. 57146–57154. DOI: 10.1021/acsami.0c18590.
- SUN, C.; LIU, J.; GONG, Y.; WILKINSON, D. P.; ZHANG, J. (2017): Recent advances in all-solid-state rechargeable lithium batteries. *Nano Energy* 33., pp. 363–386. DOI: 10.1016/j.nanoen.2017.01.028.
- TAKADA, K. (2013): Progress and prospective of solid-state lithium batteries. *Acta Materialia* 61. 3, pp. 759–770. DOI: 10.1016/j.actamat.2012.10.034.
- TAN, D. H.; BANERJEE, A.; DENG, Z.; WU, E. A.; NGUYEN, H.; DOUX, J.-M.; WANG, X.; CHENG, J.; ONG, SHYUE PING; MENG, YING SHIRLEY; CHEN, ZHENG (2019): Enabling Thin and Flexible Solid-State Composite Electrolytes by the Scalable Solution Process. *ACS Applied Energy Materials* 2. 9, pp. 6542–6550. DOI: 10.1021/acsaem.9b01111.

- TAN, D. H.; CHEN, Y.-T.; YANG, H.; BAO, W.; SREENARAYANAN, B.; DOUX, J.-M.; LI, W.; LU, B.; HAM, SO-YEON; SAYAHPOUR, BAHARAK; SCHARF, JONATHAN; WU, ERIK A.; DEYSHER, GRAYSON; HAN, HYEAE EUN; HAH, HOE JIN; JEONG, HYERI; LEE, JEONG BEOM; CHEN, ZHENG; MENG, YING SHIRLEY (2021): Carbon-free high-loading silicon anodes enabled by sulfide solid electrolytes. *Science* 373. 6562, pp. 1494–1499. DOI: 10.1126/science.abg7217.
- TAN, D. H.; MENG, Y. S.; JANG, J. (2022): Scaling up high-energy-density sulfidic solid-state batteries: A lab-to-pilot perspective. *Joule* 6. 8, pp. 1755–1769. DOI: 10.1016/j.joule.2022.07.002.
- TATSUMISAGO, M.; NAGAO, M.; HAYASHI, A. (2013): Recent development of sulfide solid electrolytes and interfacial modification for all-solid-state rechargeable lithium batteries. *Journal of Asian Ceramic Societies* 1. 1, pp. 17–25. DOI: 10.1016/j.jascer.2013.03.005.
- THANGADURAI, V.; WEPPNER, W. (2006): Recent progress in solid oxide and lithium ion conducting electrolytes research. *Ionics* 12. 1, pp. 81–92. DOI: 10.1007/s11581-006-0013-7.
- THIELMANN, A.; NEEF, C.; HETTESHEIMER, T.; DÖSCHER, H.; WIETSCHER, M.; TÜBKE, J.: Energiespeicher-Roadmap (Update 2017). Karlsruhe (12/2017).
- TIKEKAR, M. D.; CHOUDHURY, S.; TU, Z.; ARCHER, L. A. (2016): Design principles for electrolytes and interfaces for stable lithium-metal batteries. *Nature Energy* 1. 9. DOI: 10.1038/nenergy.2016.114.
- UMWELTBUNDESAMT: Treibhausgas-minderungsziele Deutschlands. URL: <https://www.umweltbundesamt.de/daten/klima/treibhausgas-minderungsziele-deutschlands> (visited on 16.11.2023).
- VARZI, A.; RACCICHINI, R.; PASSERINI, S.; SCROSATI, B. (2016): Challenges and prospects of the role of solid electrolytes in the revitalization of lithium metal batteries. *Journal of Materials Chemistry A* 4. 44, pp. 17251–17259. DOI: 10.1039/C6TA07384K.
- VARZI, A.; THANNER, K.; SCIPIONI, R.; DI LECCE, D.; HASSOUN, J.; DÖRFLER, S.; ALTHEUS, H.; KASKEL, S.; PREHAL, CHRISTIAN; FREUNBERGER, STEFAN A. (2020): Current status and future perspectives of lithium metal batteries. *Journal of Power Sources* 480., p. 228803–228803. DOI: 10.1016/j.jpowsour.2020.228803.
- VDI E.V. (ED.) (2013): VDI-Wärmeatlas. 11., edit and exp. ed. VDI-Gesellschaft Verfahrenstechnik und Chemieingenieurwesen. Berlin, Heidelberg: Springer Vieweg. ISBN: 978-3-642-19980-6. (VDI/-Buch).
- WANG, C.; LIANG, J.; ZHAO, Y.; ZHENG, M.; LI, X.; SUN, X. (2021): All-solid-state lithium batteries enabled by sulfide electrolytes: from fundamental research to practical engineering design. *Energy Environ. Sci.* 14. 5, pp. 2577–2619. DOI: 10.1039/D1EE00551K.

- WANG, L.; ZHOU, Z.; YAN, X.; HOU, F.; WEN, L.; LUO, W.; LIANG, J.; DOU, S. X. (2018): Engineering of lithium-metal anodes towards a safe and stable battery. *Energy Storage Materials* 14., pp. 1–82. DOI: 10.1016/j.ensm.2018.02.014.
- WANG, M. J.; CARMONA, E.; GUPTA, A.; ALBERTUS, P.; SAKAMOTO, J. (2020): Enabling "lithium-free" manufacturing of pure lithium metal solid-state batteries through in situ plating. *Nature Communications* 11. 1, p. 5201–5201. DOI: 10.1038/s41467-020-19004-4.
- WANG, X.; HE, K.; LI, S.; ZHANG, J.; LU, Y. (2023): Realizing high-performance all-solid-state batteries with sulfide solid electrolyte and silicon anode: A review. *Nano Research* 16. 3, pp. 3741–3765. DOI: 10.1007/s12274-022-4526-9.
- WENZEL, S.; SEDLMAIER, S. J.; DIETRICH, C.; ZEIER, W. G.; JANEK, J. (2018): Interfacial reactivity and interphase growth of argyrodite solid electrolytes at lithium metal electrodes. *Solid State Ionics* 318., pp. 102–112. DOI: 10.1016/j.ssi.2017.07.005.
- WESTPHAL, B.; BOCKHOLT, H.; KWADE, A. (2014): Influence of Convective Drying Parameters on Electrode Performance and Physical Electrode Properties. *ECS Meeting Abstracts* MA2014-02. 5, p. 328–328. DOI: 10.1149/MA2014-02/5/328.
- WESTPHAL, B. G.; KWADE, A. (2018): Critical electrode properties and drying conditions causing component segregation in graphitic anodes for lithium-ion batteries. *Journal of Energy Storage* 18., pp. 509–517. DOI: 10.1016/j.est.2018.06.009.
- WEYMANN, L.; LEIDERBERGER, J.: Europäische Batteriezellfertigung: Verzehnfachung der Produktionskapazitäten bis 2030. URL: <https://www.isi.fraunhofer.de/de/presse/2022/presseinfo-17-Batteriezellfertigung-Verzehnfachung-2030.html> (visited on 06.01.2024).
- WOLFENSTINE, J.; ALLEN, J. L.; SAKAMOTO, J.; SIEGEL, D. J.; CHOE, H. (2018): Mechanical behavior of Li-ion-conducting crystalline oxide-based solid electrolytes: a brief review. *Ionics* 24. 5, pp. 1271–1276. DOI: 10.1007/s11581-017-2314-4.
- WURM, C.; OETTINGER, O.; WITTKAEMPER, S.; ZAUTER, R.; VUORILEHTO, K. (2018): Anode materials for lithium-ion batteries. In: KORTHAUER, R. (ED.): *Lithium-ion batteries. Basics and applications*. Berlin, Heidelberg: Springer, pp. 43–58. DOI: 10.1007/978-3-662-53071-9_5. ISBN: 978-3-662-53069-6.
- XIAO, Y.; WANG, Y.; BO, S.-H.; KIM, J. C.; MIARA, L. J.; CEDER, G. (2020): Understanding interface stability in solid-state batteries. *Nature Reviews Materials* 5. 2, pp. 105–126. DOI: 10.1038/s41578-019-0157-5.
- XU, L.; LU, Y.; ZHAO, C.-Z.; YUAN, H.; ZHU, G.-L.; HOU, L.-P.; ZHANG, Q.; HUANG, J.-Q. (2021): Toward the Scale-Up of Solid-State Lithium Metal Batteries: The Gaps between Lab-Level Cells and Practical Large-Format Batteries. *Advanced Energy Materials* 11. 4, p. 2002360–2002360. DOI: 10.1002/aenm.202002360.
- XU, R.; ZHANG, S.; WANG, X.; XIA, Y.; XIA, X.; WU, J.; GU, C.; TU, J. (2018): Recent Developments of All-Solid-State Lithium Secondary Batteries with Sulfide Inorganic Electrolytes. *Chemistry* 24. 23, pp. 6007–6018. DOI: 10.1002/chem.201704568.

- XU, R. C.; XIA, X. H.; YAO, Z. J.; WANG, X. L.; GU, C. D.; TU, J. P. (2016): Preparation of Li₇P₃S₁₁ glass-ceramic electrolyte by dissolution-evaporation method for all-solid-state lithium ion batteries. *Electrochimica Acta* 219., pp. 235–240. DOI: 10.1016/j.electacta.2016.09.155.
- YAMAMOTO, M.; TERAUCHI, Y.; SAKUDA, A.; TAKAHASHI, M. (2018): Binder-free sheet-type all-solid-state batteries with enhanced rate capabilities and high energy densities. *Scientific reports* 8. 1, pp. 1–10. DOI: 10.1038/s41598-018-19398-8.
- YAO, X.; HUANG, B.; YIN, J.; PENG, G.; HUANG, Z.; GAO, C.; LIU, D.; XU, X. (2016): All-solid-state lithium batteries with inorganic solid electrolytes: Review of fundamental science. *Chinese Physics B* 25. 1, pp. 1–14. DOI: 10.1088/1674-1056/25/1/018802.
- YE, L.; LI, X. (2021): A dynamic stability design strategy for lithium metal solid state batteries. *Nature* 593. 7858, pp. 218–222. DOI: 10.1038/s41586-021-03486-3.
- YU, C.; GANAPATHY, S.; VAN ECK, ERNST R. H.; WANG, H.; BASAK, S.; LI, Z.; WAGEMAKER, M. (2017): Accessing the bottleneck in all-solid state batteries, lithium-ion transport over the solid-electrolyte-electrode interface. *Nature Communications* 8. 1086, pp. 1–9.
- ZHANG, J.; ZHONG, H.; ZHENG, C.; XIA, Y.; LIANG, C.; HUANG, H.; GAN, Y.; TAO, X.; ZHANG, WENKUI (2018): All-solid-state batteries with slurry coated LiNi_{0.8}Co_{0.1}Mn_{0.1}O₂ composite cathode and Li₆PS₅Cl electrolyte: Effect of binder content. *Journal of Power Sources* 391., pp. 73–79. DOI: 10.1016/j.jpowsour.2018.04.069.
- ZHANG, S.; ERVIN, M.; XU, K.; JOW, T. (2004): Microporous poly(acrylonitrile-methyl methacrylate) membrane as a separator of rechargeable lithium battery. *Electrochimica Acta* 49. 20, pp. 3339–3345. DOI: 10.1016/j.electacta.2004.02.045.
- ZHANG, Y.; CHEN, R.; LIU, T.; SHEN, Y.; LIN, Y.; NAN, C.-W. (2017): High Capacity, Superior Cyclic Performances in All-Solid-State Lithium-Ion Batteries Based on 78Li₂S-22P₂S₅ Glass-Ceramic Electrolytes Prepared via Simple Heat Treatment. *ACS applied materials & interfaces* 9. 34, pp. 28542–28548. DOI: 10.1021/acsami.7b06038.
- ZHAO, X.; XIANG, P.; WU, J.; LIU, Z.; SHEN, L.; LIU, G.; TIAN, Z.; CHEN, L.; YAO, XIAYIN (2023): Toluene Tolerated Li_{9.88}GeP_{1.96}Sb_{0.04}S_{11.88}Cl_{0.12} Solid Electrolyte toward Ultrathin Membranes for All-Solid-State Lithium Batteries. *Nano letters* 23. 1, pp. 227–234. DOI: 10.1021/acs.nanolett.2c04140.
- ZHENG, J.; WANG, P.; LIU, H.; HU, Y.-Y. (2019): Interface-Enabled Ion Conduction in Li₁₀GeP₂S₁₂-Poly(ethylene Oxide) Hybrid Electrolytes. *ACS Applied Energy Materials* 2. 2, pp. 1452–1459. DOI: 10.1021/acsaeem.8b02008.
- ZHOU, Y.; DOERRER, C.; KASEMCHAINAN, J.; BRUCE, P. G.; PASTA, M.; HARDWICK, L. J. (2020): Observation of Interfacial Degradation of Li₆PS₅Cl against Lithium Metal and LiCoO₂ via In Situ Electrochemical Raman Microscopy. *Batteries & Supercaps* 3. 7, pp. 647–652. DOI: 10.1002/batt.201900218.

8 Appendix

A. Publication List

SINGER ET AL. 2020

Singer, C.; Schnell, J.; Reinhart, G.: Scalable Processing Routes for the Production of All-Solid-State Batteries – Modeling Interdependencies of Product and Process. *Energy Technology* (2020), p. 2000665.

DOI: 10.1002/ente.202000665

Publication I in this dissertation.

SINGER ET AL. 2021

Singer, C.; Töpfer, H.-C.; Günter, F. J.; Reinhart, G.: Plant Technology for the Industrial Coating Process for Sulfide-Based All-Solid-State Batteries. *Procedia CIRP* 104 (2021), p. 56.

DOI: 10.1016/j.procir.2021.11.010

Publication II in this dissertation.

SINGER ET AL. 2022

Singer, C.; Töpfer, H.-C.; Kutsch, T.; Schuster, R.; Koerver, R.; Daub, R.: Hydrolysis of Argyrodite Sulfide-Based Separator Sheets for Industrial All-Solid-State Battery Production. *ACS Applied Materials & Interfaces* (2022), p. 24245.

DOI: 10.1021/acsami.2c01099

Publication III in this dissertation.

SINGER ET AL. 2023c

Singer, C.; Schmalzbauer, S.; Daub, R.: Influence of the slurry composition on thin-film components for the wet coating process of sulfide-based all-solid-state batteries. *Journal of Energy Storage* 68 (2023), p. 107703.

DOI: 10.1016/j.est.2023.107703

Publication IV in this dissertation.

SINGER ET AL. 2023b

Singer, C.; Kopp, L.; Daub, R.: Fundamental investigation on drying rates of cathodes and separators for sulfide-based all-solid-state batteries. *Drying Technology* (2023), p. 1010.

DOI: 10.1080/07373937.2023.2189943

Publication V in this dissertation.

SINGER ET AL. 2023a

Singer, C.; Kopp, L.; Aruqaj, M.; Daub, R.: Drying Process of Sulfide-Based All-Solid-State Battery Components—Investigation on Adhesion Strength and Microstructural Changes. *Energy Technology* (2023), p. 2300098.

DOI: 10.1002/ente.202300098

Publication VI in this dissertation.

SINGER ET AL. 2024

Singer, C.; Wach, L.; Jaimez Farnham, E.; Daub, R. (2024): Insights Into Scalable Technologies and Process Chains for Sulfide-Based Solid-State Battery Production. *Batteries & Supercaps*, pp. e202400142.

DOI: 10.1002/batt.202400142.

Publication VII in this dissertation.

B. Overview of Supervised Student Theses

Within the framework of this dissertation, the student work listed below in chronological order was carried out at the *iwb* of the TUM under the essential scientific, technical and content-related guidance of the author of this work. In them, various questions in the field of ASSB production were addressed. Some of their results have been incorporated into the present work and cited in the relevant places. The author would like to take this opportunity to thank all students for their commitment in supporting this scientific work.

FELIX WERNER

Prozesskettenanalyse in der Herstellung von prismatischen Hardcase-Gehäusen für Lithium-Ionen-Batterien, 2020.

CHRISTIAN GEIGER

Herstellung und Analyse polymerer Festkörperbatterien, 2020.

PHILIPP KAISER

Prozessentwicklung und -analyse zur Herstellung großformatiger polymerer Festelektrolytschichten für den Einsatz in Festkörperbatterien, 2020.

LORENZ KOPP

Prozesscharakterisierung der Schichtherstellung sulfidischer Festelektrolyte für den industriellen Einsatz, 2020.

ARMIN SUMMER

Analytische Untersuchung zur Übertragbarkeit der Schichtherstellung von Lithium-Ionen-Batterien auf Festkörperbatterien, 2020.

MILOT ARUQAJ

Einfluss des Trocknungsvorgangs auf die Festelektrolytschicht in sulfidischen Festkörperbatterien, 2021.

LEONI PUTZE

Prozessentwicklung für die Schichtherstellung von Kathodenkomposite in der Festkörperbatterie, 2021.

STEFAN SCHMALZBAUER

Analyse von Defekten im Beschichtungs- und Trocknungsprozess der Festkörperbatterieproduktion, 2021.

HEIKO SEEL-MAYER

Untersuchung des Trocknungsprozesses sulfid-basierter Kompositkathoden von Festkörperbatterien, 2021.

MILOT ARUQAJ

Einfluss der Adhäsionskräfte in sulfidischen Festkörperbatterien auf die Auswahl einer Prozessroute zur Herstellung des Verbundes aus Kompositkathode und Festelektrolyt, 2022.

LORENZ KOPP

Characterization of the adhesion strength of components in all-solid-state batteries with respect to industrial scaling, 2022.

STEFAN SCHMALZBAUER

Wet coating of large-scale separator and composite cathode for sulfide-based all-solid-state batteries, 2022.

LENA STÜCKL

Entwicklung von Prozessstrategien zur Zellausbaubereitung einer sulfidischen Festkörperbatterie mit Lithium-Metall-Anode, 2022.

SHICHEN GUO

Untersuchung des Mischprozesses in der Produktion von Komponente sulfidischer Festkörperbatterien, 2022.

SHU-WEI CHEN

Neuartiges Herstellungsverfahren für die Produktion von Separatoren für sulfidischen Festkörperbatterien, 2023.

LORENZ KOPP

Synthesis of organic passivation layers on lithium metal anodes and characterization of their material properties with an outlook on scaling in lithium-ion battery production, 2023.

GENTIAN BALLGJINI

Entwicklung von Assemblierungsstrategien für kleinformatige sulfidischen Festkörperbatterie-Pouchzellen, 2023.